



Comparison of Calibration Strategies for Mixture Components

A DEM study of pellet and sinter

by

Sabine van Epen

in partial fulfillment of the requirements for the degree of

Master of Science

in Mechanical Engineering

at the Department Maritime and Transport Technology of Faculty Mechanical Engineering of Delft University of Technology

Student number: 4686144

MSc track: Multi-Machine Engineering

Report number: 2025.MME.9050

Daily Supervisor: Ir. Raïsa Roeplal

Supervisor: Prof.dr.ir. Dingena Schott
Institution: Delft University of Technology

Location: Faculty of Mechanical Engineering in Delft

Date: April 2025

Cover: Sinter by Fe Techno Engineering and Power Solutions (Modified)



Preface

This thesis represents my final work of my master degree, Multi-Machine Engineering at Delft University of Technology. It has been an incredibly enriching journey, and I am deeply grateful to those who have supported and guided me along the way.

First and foremost, I would like to express my sincere gratitude to my daily supervisor, Raïsa Roeplal, for your continuous guidance, dedication, and approachability. Your insights have taught me to look critically at my work and helped create the substantiations for my work. To my supervisor Dingena for the motivation, insightful discussions, and helping me create a well-structured thesis. I would also like to express my appreciation to Ahmed for your assistance with the technical specifics of DEM model calibration. This team made my thesis an enjoyable experience.

A special thank you to my friends in Delft, you have made my time in Delft truly memorable. Like my parents said, your student-time is the best time of your life (let's hope not, now that it is over) and that was definitely because of the people I have met in Delft. Thank you Pim, Coen and Frederiek for the amazing coffee breaks in the train and support throughout this thesis. Lastly, thank you to my family, without you, I would not have come this far.

Sabine van Epen Delft, April 2025

Summary

The blast furnace is used for the production of steel, the most widely used construction material world-wide. Engineers want to make this process as efficient as possible by getting insight in the segregation of different raw materials, in this case pellet and sinter. However, placing sensors in this furnace to get insight in the dynamics is difficult due to the harsh conditions. To improve the efficiency of the blast furnace, digital simulations are a useful tool for optimizing the process in a cost-effective and efficient manner. Discrete Element Method (DEM), in particular, is very useful for this purpose. Small changes can easily be made to the system to check the effect of these changes. However, the accuracy of these simulations is critical for reliable results. One of the main challenges in using DEM simulations lies in determining the correct values for the input parameters, as these directly affect the simulation's validity. Input values, such as the interaction between different particles, the particle shape, particle shape, are a few examples of the many input parameters necessary for a DEM simulation. Consequently, calibrating these input parameters is an important step.

Methods for finding input values of DEM simulations are broadly categorized into two approaches: direct measurement and bulk calibration. Direct measurement involves the use of specific equipment to measure the physical properties of materials directly. While effective, this method is not always feasible due to limitations in accuracy or practicality. Bulk calibration, on the other hand, adjusts the input parameter values to ensure that the Key Performance Indicators (KPIs) obtained from simulations align with those obtained from laboratory experiments. This method is particularly useful when direct measurement is not viable.

The calibration process is complex when dealing with materials, such as sinter and pellet, due to the amount of input parameters. To maintain the viability of the calibration process, a fundamental principle must be followed: the number of input parameters should match the number of outputs. If this is not achieved, multiple combinations of parameter values could result in identical KPIs, leading to ambiguity.

To address this challenge, a sensitivity analysis is conducted to identify the parameters that significantly influence the outputs (KPIs). In this study, the Plackett-Burman design was employed to simulations of pellet, to determine the parameters that account for 90% of the effect on the KPIs. This analysis narrowed down the amount of parameters to five dominant parameters. These selected parameters were then used to develop fitting models through a central composite design. Polynomial regression is used as a fitting model in this study.

These models were initially optimized using a local optimization technique. Although this method is computationally efficient, it demonstrated a high dependency on the initial guesses for the parameter values, which makes it unsuitable for most applications. To overcome this limitation, global optimization methods were employed, these algorithms avoids being trapped in local minima in early iterations and are able to explore globally for better solutions. Specifically, two techniques were used: genetic algorithm, and particle swarm optimization. These methods provided a more robust optimization process, capable of exploring a wider range of parameter values and giving reliable results regardless of initial conditions unlike local optimization.

With the optimal parameter set found using these optimization techniques, the DEM model calibration for both pellet and sinter was successfully completed. The results demonstrated that PSO required fewer computational runs than GA in order to converge to a objective function value, making it the most computationally efficient method. Most of the KPIs of the DEM simulations with the optimal parameter set were sufficiently close to the experimental values for the KPIs. The validation further showed that the optimal parameter set found for pellet was accurate. The validation for sinter showed less accurate results meaning the optimal parameter set found could be inaccurate.

Lastly, a mixture of pellet and sinter was created using the optimal parameter set found for the individual components. The interaction parameters between sinter and pellet were taken as an average between

the interaction parameters of the individual materials. This yielded accurate results for the segregation of the materials when compared to the experimental values. Most of the KPIs are also very close to the experimental values except for the shape of the heap KPIs. This could be because of the inaccurate sinter input parameters.

Overall, the combination of sensitivity analysis, central composite design, and global optimization methods forms a calibration framework. This framework ensures the accuracy of DEM simulations for pellet, ultimately leading to more efficient and reliable blast furnace operations. Future research could include an in depth sensitivity analysis, different sampling techniques, different regression techniques and the effect of the performance of GA and PSO with different regression techniques.

Contents

Pr	reface	i
Su	ummary	ii
No	omenclature	vi
1	Introduction 1.1 Literature Gap 1.2 Research Objectives 1.3 Methodology 1.4 Thesis Outline	1 3 4 4 5
2	Framework Calibration Procedure 2.1 Introduction to DEM: Contact Model and Input Parameters 2.2 Direct Measurement and Literature Sourcing 2.3 Calibration of Interaction Parameters 2.4 Sensitivity Analysis 2.5 Experiments in Laboratory 2.6 Experiments in DEM 2.7 Design of Experiments: Central Composite Design 2.8 Model Relations between Input and Output 2.9 Optimization Polynomials 2.9.1 Objective Function 2.9.2 Local Optimization 2.9.3 Global Optimization 2.9.4 Stopping Criteria 2.9.5 Evaluation Metrics for Optimization Algorithms 2.10 Validation	6 7 8 9 10 13 15 16 17 18 18 19 19 20
	, and the state of	20 21
3	3.1 Contact Model 3.2 Direct Measurement & Literature 3.3 Sensitivity Analysis 3.3.1 Rayleigh Time Step 3.3.2 Amount of Runs 3.3.3 Sinter Particle Shape 3.4 Dominant DEM Parameters using Plackett-Burman	22 23 23 23 25 26 29 29 31
4	4.1 Polynomial Regression using CCD 4.2 Optimization Setup and Results 4.3 Local Optimization 4.3.1 Effect of Initial Guess 4.3.2 Results Local Optimization 4.4 Global Optimization Methods 4.4.1 Effect of Swarm and Population Size	32 33 34 34 35 35 36 37

<u>Contents</u> v

	4.5 Comparison Performance of the Optimization Techniques 4.6 Simulation Results Pellet 4.7 Validation Pellet Simulations 4.8 Simulation Results Sinter 4.9 Validation Sinter Simulations 4.10 Discussion Results 4.10.1 Sensitivity Analysis 4.10.2 Objective Function Value 4.10.3 Fitting Model 4.11 Conclusion	40 41 42 43 44 44 44
5	Case Study: Mixture Simulation 5.1 Results Mixture Simulation	48
6	Conclusion and Recommendations 6.1 Conclusion	52
Re	ferences	53
Α	Scientific Paper	58
В	System Inputs B.1 Sinter particle shape in EDEM	74 74
С	Results Plackett-Burmann C.1 Levels of PB and resulting KPIs	
D	MATLAB Codes D.1 Local Optimization and polynomial regression	80
E	Results CCD and RSM E.1 Results CCD	
F	Results	90
G	Optimization results G.1 Sensitivity of the Local Optimization	
Н	Results of optimal parameter inputs H.1 At 4.665 m	95
I	Results of Processed Heaps of the Mixture 1.1 Experimental runs	

Nomenclature

Abbreviations

Abbreviation	Definition
CCD	Central composite design
DEM	Discrete Element Method
DoE	Design of Experiments
DtR	Rayleigh time step
GA	Genetic Algorithm
KPI	Key Performance Indicator
LO	Local optimization
LHS	Latin hypercube sampling
PB	Plackett-Burman
PSD	Particle Size Distribution
PSO	Particle Swarm Optimization
R^2	Coefficient of determination
RSD	Relative standard deviation
RSM	Response Surface Modeling
SF	Scaling factor

Symbols

Symbol	Definition	Unit
Α	Area	$[m^2]$
C	Coefficient of restitution	
E	Pellet pixels	[px]
G	Shear modulus	[Pa]
Н	Hopper height	[m]
Р	Parameters	
S	Sinter pixels	[px]
$ar{R}$	Average pixels	[px]
w	Weighting factor	
β	Linear coefficients	
δ	Interaction coefficients	
γ	Quadratic coefficients	
μ	Friction coefficient	
ho	Density	$[kg/m^3]$
σ	Standard deviation	
ν	Poisson's ratio	
y	Target KPI	
$ar{y}$	Mean KPI	
$ar{y} \ \hat{y}$	Predicted KPI	

Contents

Subscripts

Subscript	Definition
\overline{e}	Pellet
i, j	Refers to tile i, j
k	KPI number
g	Geometry
p	Particle
s	Sinter
s-	Static
r-	Rolling

Introduction

Steel production begins with the extraction of molten iron from raw iron ores, a ferrous material, and the blast furnace is the primary tool for this step. It is a vertical shaft furnace that uses heat, pressure, and chemical reactions to extract iron from a mixture of ferrous materials and fuel. The ferrous material consist of pellets (small, rounded particles made from iron ore fines), and sinter (clumps of iron-rich dust heated until they partially fuse). Coke is added to the furnace as fuel and helps drive the necessary reactions.

Steel is the most widely used engineering and construction material worldwide [1]. Figure 1.1 shows the role of the blast furnace in the overall steel production process. As can be seen in this figure, the blast furnace is one of the first steps. After iron is extracted, the molten material is transported to the steel factory for further processing into steel products.

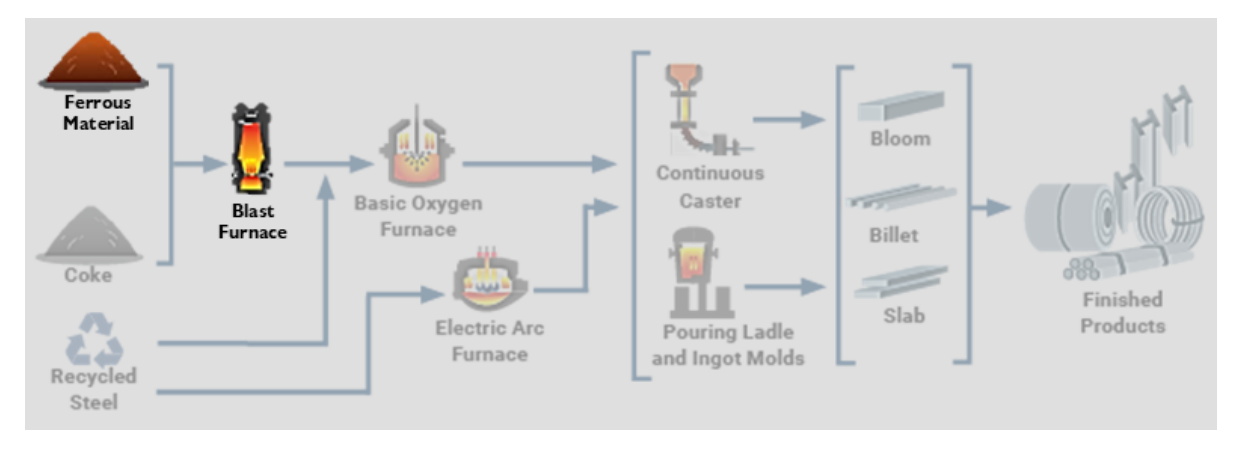


Figure 1.1: This study focuses on the ferrous material fed into the blast furnace, this figure highlights its position within steel making. Modified from [2].

The blast furnace process begins as follows: the mixture of the ferrous material and coke are charged into the top of the blast furnace forming a layer. This layer forms a packed bed of the different materials. A powerful blast of hot, pressurized gas is then injected from below, forcing its way upward through the bed and reacting with the particles along the way. This reaction gradually melts the iron within the ferrous material, and the molten iron collects at the bottom, ready for further processing.

A crucial aspect of this process is the initial arrangement of the ferrous material, which consists of pellet and sinter. This is known as the bed configuration. This configuration directly impacts gas flow through the furnace, which in turn affects permeability, a key factor in the efficiency of iron extraction [3, 4, 5, 6, 7], it is the ability of a substance to allow gases or liquids to go through it. Since the configuration of materials influences permeability, understanding and optimizing their configuration is interesting. It is

found that when pellet and sinter are mixed well, the permeability increases [1]. Figure 1.2 provides a schematic view of the top of the blast furnace, where the pellet-sinter mixture and coke is loaded.

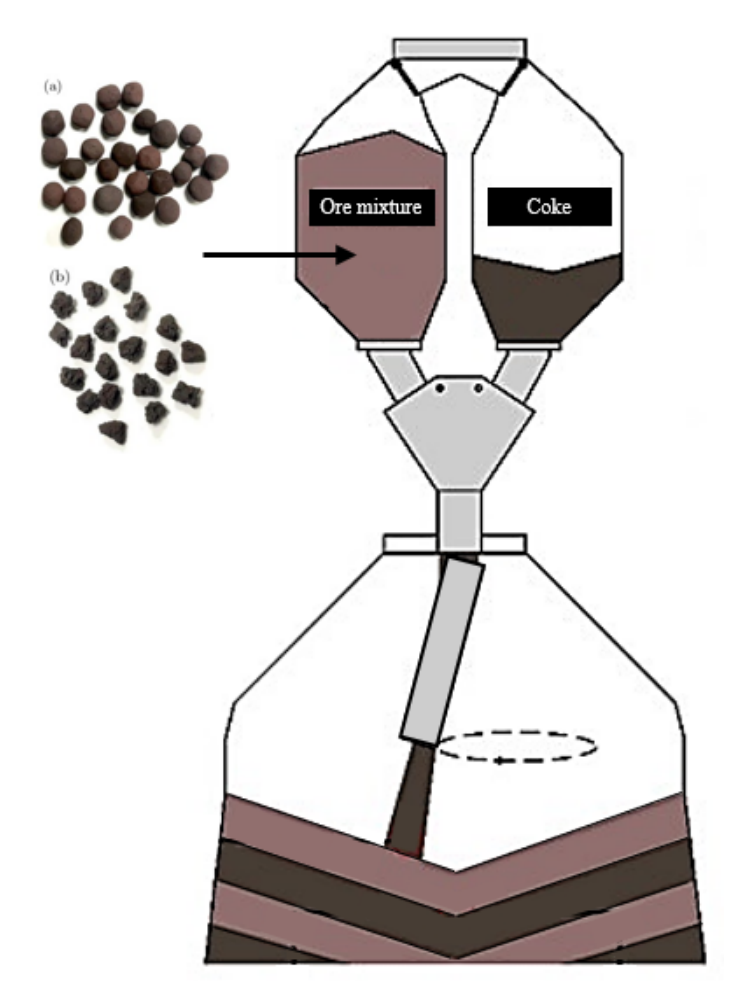


Figure 1.2: Top of the blast furnace, a) pellets, b) sinter. Modified from [8, 9].

Segregation of pellet and sinter, also known as de-mixing, is undesirable because it reduces gas permeability and makes the furnace less efficient. However, monitoring this distribution in real time is difficult. The extreme conditions inside the furnace make it challenging to place sensors directly. To gain more insight into the behavior of these materials, engineers often use computer simulations. One method that helps with understanding the behavior of granular material mixtures is the discrete element method (DEM), developed by Cundall and Strack [10]. DEM provides detailed, particle-level information that is difficult and expensive to obtain through experiments. This makes it a useful tool for improving the design of production processes where bulk materials are involved, as well as for the design of the equipment used to handle them.

DEM is a computational method that simulates the behavior of granular materials. It was developed in the 1970s, but it has only started gaining popularity in recent years, which makes it a relatively modern approach [11]. In DEM, the flow of particles is simulated by calculating the forces acting on each particle and using numerical integration to predict how they move over time. These particle interactions are governed by contact models, each of which has a variety of different parameters that must be quantified. The values of these parameters affect both the overall and the particle-level behavior of the material.

Finding the values to these parameters is the main difficulty for the application of DEM [12]. For most parameters, direct measurement cannot directly determine the values, and thus, the model requires calibration. This is due to the stochastic nature of the particles; the particles are not identical. The goal

1.1. Literature Gap 3

of the calibration process is to identify a parameter set whose resulting system response corresponds as closely as possible to the real physical behavior. This is an optimization problem and there are different ways to come up with the values for the parameters. A method often used by researchers is trial and error, this is a straightforward technique which is usually very inefficient, requires an experienced user and rarely leads to an optimal parameter set [11].

That is why the calibration process in DEM has been a topic of scientific research for years and will be the focus of this study. Different approaches for the calibration process have been suggested [11, 13, 12], however, this research on the calibration of DEM models focuses mainly on single-component materials. The studies focused on the calibration of multi-component mixtures remain scarce. There are studies which investigate pellet-sinter mixtures [14, 15, 16, 17, 18], however, these studies are lacking because of one or more of the following reasons: the study **assumes** the interaction parameter values from literature, **leaves out** sinter-pellet interactions, or calibrates for only **one** Key Performance Indicator (KPI). There are several short-comings in this approach as will be described in the next section, including the resulting problem statement.

1.1. Literature Gap

To summarize from the previous section, there are three main short-comings in the DEM calibration of materials in general: assuming values, leaving out values or only using one KPI which creates ambiguity. This section explains why this is problematic and what has been done in literature.

Assuming interaction parameter values from literature can be insufficient because the parameters obtained from these resources also have not conducted calibration. Furthermore, the material should be similar or exactly the same as the resource to be usable [1]. Also **leaving out** sinter-pellet interaction can be inaccurate because as shown by Hadi *et al.* [19] these have an effect on the heap.

Generally when an effort is made to experimentally find the values for the input parameters, there are two approaches to obtaining input values accurately, referred to as direct measurement approach and bulk calibration approach [20]. The first approach is measuring the particle or contact properties directly to obtain the input values. In this study, the particle size distribution (PSD) and density of sinter and pellet were collected from Roeplal *et al.* [21]. There are many methods to determine additional parameter values, however they are not possible for all parameters and do not account for the stochastic nature of the parameters. These are the main disadvantages of direct of measurement. This is why many researchers use a combination of both [20, 22, 23, 24, 25, 26, 27].

The second approach is the determination of DEM simulation parameters by comparing simulation results with bulk experiments and calibrating the input parameters to achieve a combination thereof such that the simulation and experiments give comparable KPIs. This approach will be the focus of this study. For bulk calibration it is important the amount of KPIs is the same as the amount of unknown input parameters. When there are not enough KPIs the model is underdetermined. In an underdetermined system, there are more unknown parameters than there are KPIs, leading to ambiguity and multiple possible combinations of parameter values. This lack of sufficient KPIs means that the system does not have a *unique* combination of parameter values and additional information is required to resolve the ambiguity. This is one of the main gaps in research, where often only **one** KPI is used to calibrate, often the angle of repose (a metric which describes the steepness of the heap) in bulk calibration of sinter and pellet, while several input parameters are being determined [17, 15, 28, 29, 30]. Using multiple KPIs to find the optimal input parameter set, multi-objective optimization, has not been performed in studies with sinter and pellet, even though it is necessary to prevent ambiguity.

Additionally, a specific research gap for blast furnace DEM calibration should be mentioned. Most blast furnace research performed using DEM calibration have done so by using the ledge test or the pouring test according to the review of Hadi *et al.* [1]. This leads to static experiments and this does not account for the effects of high velocities in the blast furnace. This is taken into account in the experiments of Roeplal *et al.* [21] where the material velocities reach up to 10 m/s.

Lastly, little research has been done on the calibration of multi-component mixtures. Despite the growing interest in DEM calibration, there is a lack of established strategies for accurately calibrating individual components within multi-component systems such as sinter-pellet mixtures. Existing studies

often overlook parameter interactions, rely on assumed parameter values, or focus on only a single KPI, resulting in underdetermined and potentially inaccurate models. As such, there is a clear need to investigate systematic and comparative calibration approaches for the individual components as a foundation for reliable multi-component simulations. This literature gap leads to the following research objective, as posed in the following section.

1.2. Research Objectives

The aim of this study is twofold. The primary objective is to evaluate how different multi-objective optimization algorithms influence the calibration outcomes of DEM simulations for sinter and pellet materials. This means assessing their performance when multiple KPIs are simultaneously considered.

As a secondary objective, this study investigates a practical case: whether the input parameters obtained from calibrating sinter and pellet materials individually can be applied directly to simulate a mixture of both. The interaction parameters between sinter and pellet are then taken as the average of the individual interaction parameters, following the successful method applied by Chakrabarty *et al.* [8].

To guide this research, the following main question and subquestions are posed.

Main Research Question:

"In the context of DEM calibration for sinter and pellet, how do different multi-objective optimization algorithms compare during the parameter optimization step?"

Subquestions:

- 1. What are the key steps in determining input parameters for a DEM simulation, and which techniques are suitable for each step?
- 2. What are the most significant input parameters affecting KPIs in DEM simulations of sinter and pellet?
- 3. Which optimization techniques be used to accurately determine DEM input parameters for sinter and pellet with multiple KPIs and how can the calibrated parameter values and simulation results be validated against experimental data?
- 4. Can an accurate multi-component mixture be created using interaction parameters derived from individually calibrated materials?

To answer these research questions and achieve the aim of this study the following methodology is applied in this study, as described in the following section.

1.3. Methodology

This study follows a step-by-step approach to calibrating a simulation model that can accurately represent how pellet and sinter behave. The simulation technique used is called the Discrete Element Method, which models how individual particles move and interact with each other and with their surroundings. To do this, a contact model is selected that describes how forces act between the particles when they touch.

Some of these input values, such as particle size, density, and stiffness, are known from earlier experiments or available from literature. Others, such as the shape of the particles and the time interval between simulation steps, must be selected based on a balance between accuracy and computational time. Once these values are set, the required number of simulations can be determined to account for the variability of the results.

Other input values define how particles behave when they collide or slide against each other. These are more difficult to determine directly and are therefore estimated through calibration. Before calibration, it is important to identify which input values have the most significant influence on the simulation results. This is done through a sensitivity analysis, which determines the parameters that most strongly affect the key performance indicators (KPIs).

To further reduce the number of simulations, a structured sampling method is used. Instead of testing every possible combination of input parameter values, a selection is chosen. The results of these

1.4. Thesis Outline 5

simulations are used to create polynomials that describe the relationship between input parameter values and KPIs.

Once these polynomials are determined, different optimization methods are used to find the input parameter values that produce the most similar simulation results to the experimental results. These input parameter values are validated using additional experiments.

The final step of this study is to assess whether the calibrated input values for the individual components can be applied effectively to a multi-component mixture. Upon completion of these steps, the main research question and subquestions can be addressed. A visual representation of these steps is presented in the next figure, Figure 1.3.

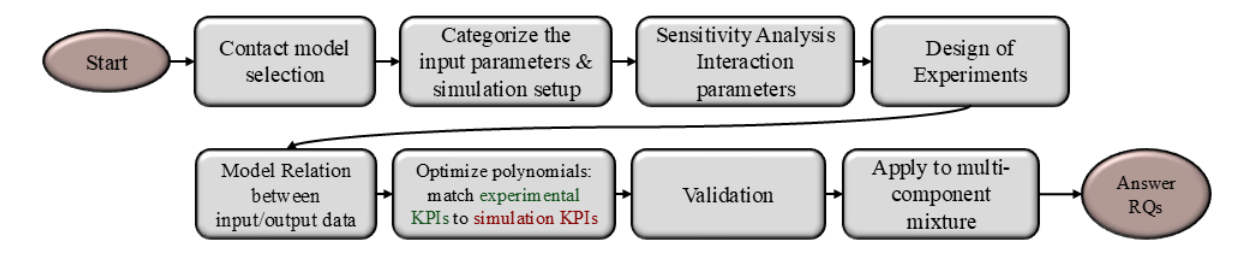


Figure 1.3: Visual representation of the steps performed in this study. The steps are from left to right and after DoE the next step is the setting up the model relation.

The next chapter outlines the structure of this thesis, detailing the content and focus of each chapter.

1.4. Thesis Outline

Chapter 2 presents the framework for calibration techniques in DEM simulations. It introduces the challenges of parameter selection in multi-component mixtures and reviews existing calibration methodologies. The concepts of bulk calibration, direct measurement, and optimization techniques are discussed in detail. This section establishes the methodology for the following calibration procedures and will answer subquestion 1.

Chapter 3 details the experimental setup and methodology used for data collection. It describes the experiments, focusing on the measurement of the KPIs. The technical aspects of DEM modeling are covered, including material parameter selection, and simulation setup. Additionally, the parameter sensitivity analysis is explained which is used to identify dominant factors influencing DEM simulations. This section provides an answer to subquestion 2.

Chapter 4 focuses on the calibration procedure for single-component materials, sinter and pellet. The implementation of CCD for response surface analysis is discussed, alongside various optimization techniques used to determine parameter values. The effectiveness of local and global optimization methods is compared to ensure robust parameter estimation. This section explains the answer to subquestion 3 and 4. This chapter also reflects on the results of the experiments and touches upon specific challenges encountered during the study.

Chapter 5 investigates the feasibility of deriving interaction parameters for multi-component mixtures from individually calibrated materials. Instead of performing direct calibration, the interaction parameters for sinter-pellet contacts are determined by averaging the individually calibrated values of sinter and pellet. The accuracy of this approach is evaluated by analyzing simulation results and comparing them to experimental observations. This section will answer subquestion 5.

Chapter 6 concludes the thesis, summarizing key findings and assessing the extent to which the research objectives have been met. Finally, recommendations are given for further refining the calibration process and expanding its use in systems with multi-component mixtures.

Framework Calibration Procedure

In Figure 2.1 all the steps are shown in the gray boxes, under each step the techniques are presented, except for the second gray box, here the parameters are sorted and the techniques are shown in bold. It is important to note that selecting and representing particle shape in the DEM simulation involves a more nuanced process than direct measurement alone; this is discussed in greater detail in Chapter 3. This chapter describes the substantiation for every technique chosen for each calibration step, and can be seen as a methodology chapter. In the following chapters, the results are described.

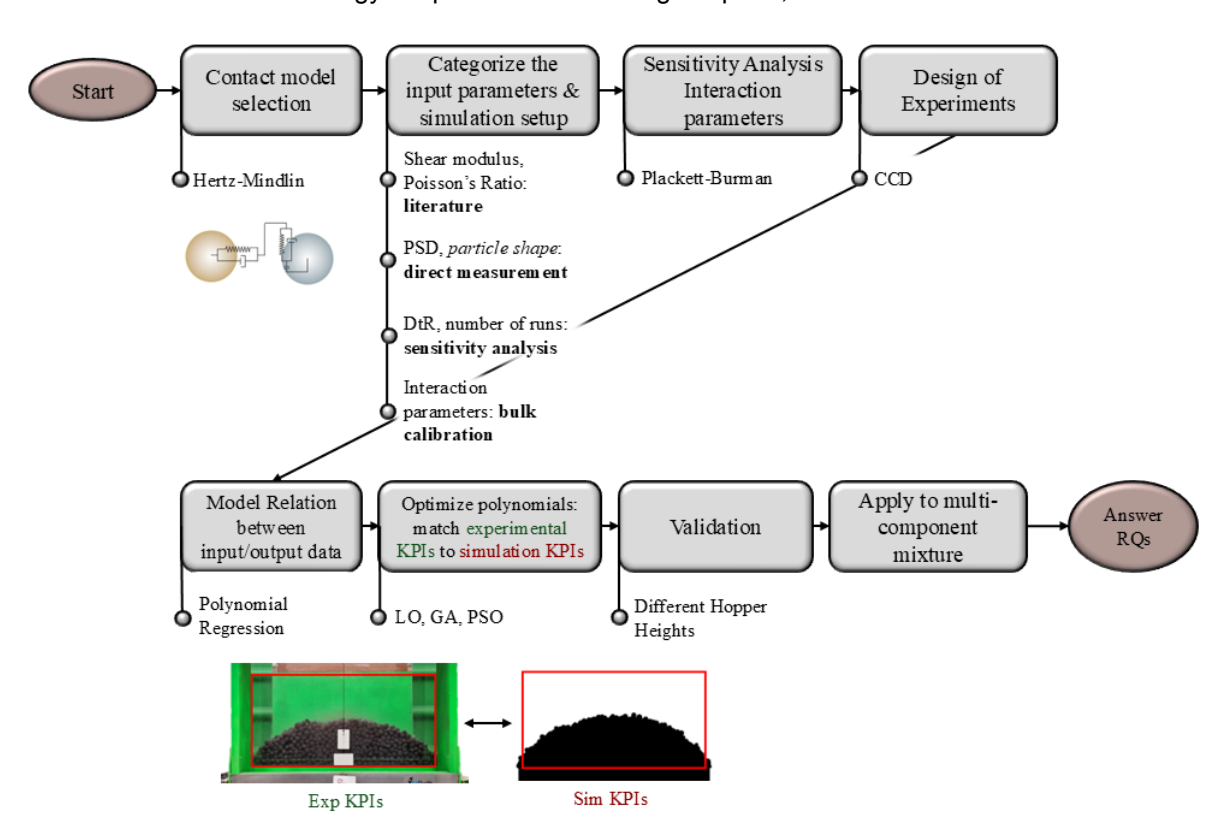


Figure 2.1: Visual representation of the steps performed in this study. The steps are from left to right and after DoE the next step is the setting up the model relation.

2.1. Introduction to DEM: Contact Model and Input Parameters

DEM is a technique used to simulate the behavior of particles in a flow by tracking each particle's movement over time. DEM works by calculating the forces and torques on each particle at every step of the simulation. Using these forces, the method applies Newton's second law to predict how each particle will move. In simpler terms, DEM determines all the pushes and pulls on a particle and then uses these to figure out the particle's trajectory. This process is repeated for each particle in the simulation to model how they all interact and move together. Contact models are used in the DEM to define the physical collision between particle materials or particles and geometries. The contact model should be selected according to its application.

Forces that act on particles can come from a few different sources: short-range interactions like collisions between particles or between particles and walls, body forces, and long-range interactions. While body forces and torques can be calculated using basic physics principles, figuring out the forces and torques from short and long-range interactions is a bit more complicated.

When particles come into contact, the normal forces are crucial because, without them, particles would simply pass through each other. For tangential movements, there are three types of interaction laws to think about: friction (which resists sliding), rolling resistance, and torsion resistance. A diagram showing how sliding, spring, and dashpot forces are represented in two interacting particles, is shown in Figure 2.2. This is why contact models necessary, for example, the Hertz-Mindlin model calculates the normal force based on Hertzian contact theory [31].

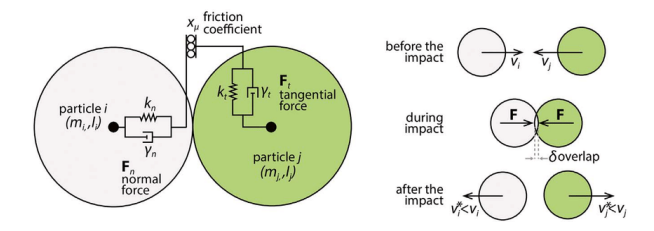


Figure 2.2: Schematic of general contact model between two particles according to Capozzi et al [32]

We want to simulate three materials; sinter, pellet and a mixture of sinter and pellet. There are several DEM parameters which need to be determined. In this chapter the methodology of finding these parameters is described, in the next chapter, the results are presented. The model inputs can generally be divided into three categories: morphological parameters, material parameters and interaction parameters [1]. An overview of the parameters, each in their respective category, can be found in Table 2.1 below.

DEM Parameter	Pellet	Sinter	Sinter-Pellet
Morphological Parameters			
Particle shape	Sphere	Clumped Sphere	N/A
Size distribution	Direct Measurement	Direct Measurement	N/A
Material Parameters			
Density (ρ)	Direct Measurement	Direct Measurement	N/A
Shear modulus (G)	Literature	Literature	N/A
Poisson's ratio (v)	Literature	Literature	N/A
Particle-Particle Interaction			
Coefficient of restitution (C_{pp})	Bulk Calibration	Bulk Calibration	Average
Coefficient of rolling friction (μ_{r-pp})	Bulk Calibration	Bulk Calibration	Average
Coefficient of static friction (μ_{s-pp})	Bulk Calibration	Bulk Calibration	Average
Particle-Geometry Interaction			
Coefficient of restitution (C_{pq})	Bulk Calibration	Bulk Calibration	N/A
Coefficient of rolling friction (μ_{r-pq})	N/A	N/A	N/A
Coefficient of static friction (μ_{s-pg})	Bulk Calibration	Bulk Calibration	N/A

Table 2.1: Overview of parameters associated with Hertz-Mindlin and rolling model C, including their determination method and corresponding symbol.

What is not shown in Table 2.1, is the Rayleigh time step (DtR), which is a simulation-specific parameter rather than a material property [33].

2.2. Direct Measurement and Literature Sourcing

Before beginning the calibration steps, a subset of the input parameters was determined using direct measurements or values sourced from literature. These include:

- · Particle size distribution (PSD)
- · Particle shape (initial classification)
- Density (ρ)
- Shear modulus (G)
- Poisson's ratio (ν)

Using direct measurement and sourcing from literature for these input parameters is very suitable because these properties are fundamental and not typically influenced by bulk behavior or particle interactions, so direct measurement is preferred [34]. The particle shape, although initially categorized here, requires further substantiation due to its effect on simulation outcomes and its complexity; this is explained further in Section 2.4.

2.3. Calibration of Interaction Parameters

The remaining parameters which are not found using literature or direct measurement, are calibrated based on bulk material behavior. These parameters include:

- Coefficients of restitution (C_{pp}, C_{pg})
- Coefficients of static friction (μ_{s-pp}, μ_{s-pg})
- Coefficients of rolling friction (μ_{r-pp}, μ_{r-pg})

The calibration process to find these interaction parameters is structured as follows: a sensitivity analysis to identify dominant parameters, and a design of experiments (DoE) approach to construct and optimize polynomial models. Each of these steps lead to numerical input values for the remaining parameters. These steps are elaborated in the sections that follow.

2.4. Sensitivity Analysis

As mentioned earlier, there are several input parameters that still need to be determined but cannot be found using direct measurement. The first being the time-step. In DEM simulations, the time-step is defined as the time between each iteration. A simulation is stable only if the time-step employed is lower than a critical time-step which in the DEM simulation is defined as a percentage of the Rayleigh time-step (DtR). The DtR is determined by the following formula [9]:

$$DtR = \frac{\pi r \sqrt{\frac{\rho}{G}}}{0.1631v + 0.8766} \tag{2.1}$$

As can be seen in the formula for the Rayleigh time-step, it is dependent on the characteristic dimension of the particle (such as the radius of the smallest particle, r), the density of the particle material (ρ), the shear modulus of the particle material (G) and the Poisson's ratio of the material (V). The time-step is set to 20 % of DtR by default [33]. According to literature, a value between 10 and 40 % of DtR should be used for the time step [9] and the selected value depends on the coordination number and energy in the system. If the time-step is too small, the simulation will take a long time to run. If the time-step is too large, particles can behave erratically [33]. Research has demonstrated that the percentage of DtR taken affects the KPIs, the stability of the simulation, and if optimized, can reduce the computational cost [35, 36, 9].

The shape of the particles is another characteristic that will be evaluated. It is not a continuous variable, making it challenging to evaluate. In most DEM calibrations the particle shape is simulated as spherical or the particle shape is based on previous studies [37]. It is seldomly calibrated, and if it is looked at, the common conclusion is to use fewer spheres to reduce computational costs.

Since pellets are almost spherical, single spheres work well for the particle shape of pellets, this has often been done in previous studies as shown by the review by Hadi *et al* [1]. However, as shown in Figure 2.3, sinter particles have a highly irregular form, meaning a non-spherical representation is needed for DEM modeling. Different studies have different approaches to modeling the sinter particle shape.

It is known that the segregation of a mixture is dependent on the particle shape [38, 39, 40, 41, 42, 19, 43, 44], making it a factor to take into account. One method that avoids the high computational cost associated with using multiple spheres to represent particle shapes is the rolling model, which introduces 'shape-like' behavior [45]. However, the rolling friction approach underestimates the segregation tendency even when it is calibrated to predict the repose angle. This is most likely because of the effect of particle-particle mechanical interlocking as well as the particle's different aspect ratios and moment of inertia, which only occurs in the real system and the clumped sphere approach [46].

Therefore, we used a clumped sphere approach to depict the irregular shape of sinter particles. A total of 285 different sinter particles scans were available. Ideally, these shapes would be directly replicated in the DEM simulation; however, increasing the number of spheres in each clump to closely match the real particle shape leads to a significantly increased computational cost. Due to these reasons, the sinter particle shape is simplified in this study. The method of simplification is presented in Section 3.3.3, along with the sensitivity analysis of the way it is simulated in the DEM simulation.



Figure 2.3: Sinter and pellet shape [19]

Finally, the remaining input parameters are interaction parameters. These consist of friction coefficients and coefficients of restitution between particles and between particle and geometry. To reduce the complexity of the calibration task, it first needs to be tested which interaction parameters are useful to calibrate. Therefore, a sensitivity analysis is applied, to find out which interaction parameters have a dominant effect on the KPIs. Plackett-Burman (PB) is employed to efficiently explore the relationship between certain input variables and one or more outputs (or KPIs).

PB is chosen because it is computationally the least expensive DoE, it is sufficient for the sensitivity analysis, and it is available in Altair Hyperstudy. Once the parameters which have an influence on the KPIs have been determined the dominant parameters can be calibrated.

2.5. Experiments in Laboratory

To measure the dominant input parameters found during the sensitivity analysis the simulation needs to be calibrated. This is done by comparing the experiments in the laboratory to the simulation experiments in DEM. The experiments are taken from the experiments performed by Roeplal *et al.* [21]. This study performs hopper experiments with pellet, sinter and a mixture of sinter and pellet. The discharge time is measured, images are extracted and mass measurements are performed from which the following KPIs can be extracted:

- 1. KPI 1: The discharge **time** of the material flowing from the hopper.
- 2. KPI 2: The mass of material that falls to the left side of the scale.
- 3. KPI 3: The mass of material that falls to the right side of the scale.
- 4. KPI 4: The mass of material that remains on the scale.
- KPI 5: The x-coordinate of the highest point of the heap (the peak), indicating its position along the horizontal axis. The MATLAB code used for identifying this coordinate can also be found in Appendix D.
- 6. KPI 6: The **y-coordinate** of the highest point of the heap, representing the height of the heap's peak.
- 7. KPI 7, 8, 9: The y-coordinate is taken of the heap at a **quarter**, **halfway** and **three quarters** of the width, which represent KPI 7, 8, and 9 respectively.

The experimental setup developed by Roeplal *et al.* [21], which forms the basis for this study, is shown in Figure 2.4. In their work, experiments were carried out to investigate the bulk behavior of sinter and pellet materials. In these experiments, the material was placed into a hopper; once the gate was opened, it flowed out onto a scale positioned below. Tests were performed using sinter, pellet, and a mixture of both. In this study, the raw experimental data generated by Roeplal *et al.* [21] was used to evaluate KPIs. The methodology used to extract these KPIs from the data is described in the following section, while the results are presented and compared with simulation outcomes in Chapter 4.

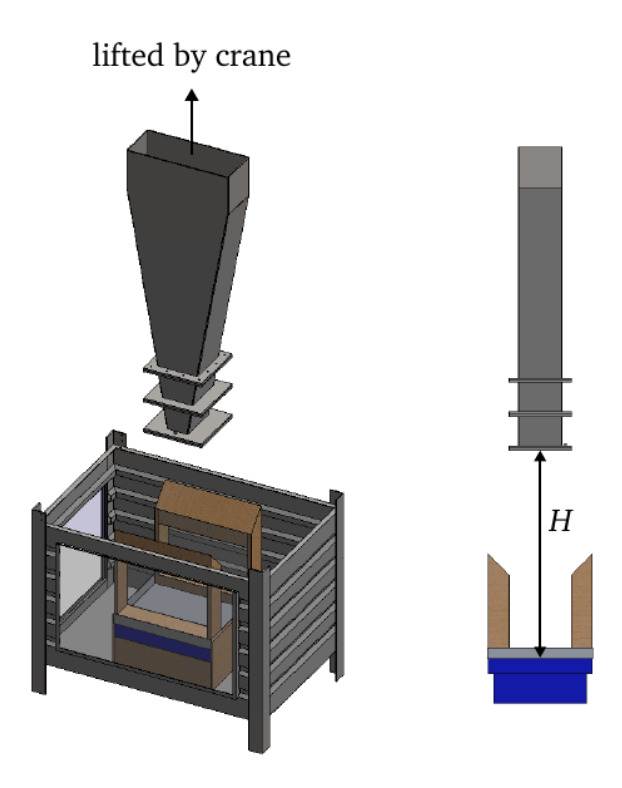


Figure 2.4: The experimental setup in the laboratory performed by Roeplal et al [21].

A camera was positioned at the of the bottom of the hopper to record the opening of the gate. This footage gave a view of the material's flow at the opening of the hopper and the dynamics of the hopper gate. Taking the moment when the last particles flows out of the hopper gives us the discharge time, KPI 1. The discharge times for the different materials were given as raw data by Roeplal *et al.* [21]



Figure 2.5: Video recording of the hopper gate.

The mass is measured at three different locations after the hopper is emptied. The mass that falls directly on the scale, and the mass which flows over onto the left and right side of the scale is measured. In front of the scale, at the bottom of the container a partition is placed to have a clear division between the left and right side. These measurements provide the values for KPI 2, 3 and 4. These values were also given by Roeplal et al. [21]

Images of the heap, formed on the scale, were taken at the scale's level after the hopper was emptied. To obtain images suitable for analysis, a green background was used to create contrast to enhance the visibility of the heap's shape. The angle of repose, a commonly used KPI in DEM studies, is challenging to measure due to this varying heap shape. To address this, the highest point of the heap is analyzed instead. The pixel height is taken at three set locations (at a quarter, halfway and three guarters) and

the x and y coordinate of the peak of the heap are taken. For a more accurate image analysis of the experimental results, the background is made completely green and the image of the heap is edited so that it consists entirely of pellets or sinter. The images are provided by Roeplal *et al.* [21]

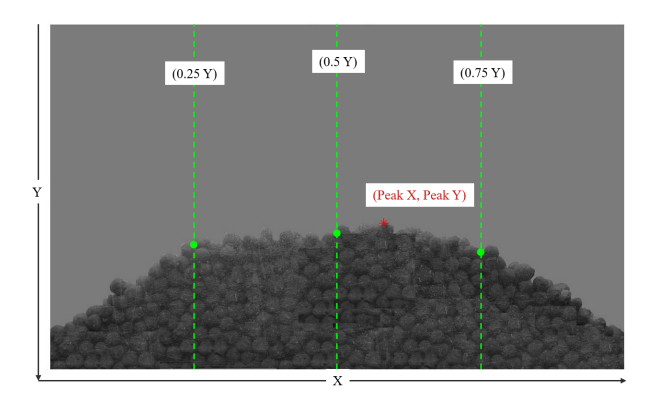


Figure 2.6: Five KPIs found using the image of the heap.

To be able to compare it to the DEM simulation, both images are cropped and scaled so that they have the same pixel dimensions, as shown in Figure 2.7. The width of both should be the same, it is the same container, so it is scaled accordingly. The height is not scaled in order not to effect the heap properties, a green box has been added to the top of the experimental image to match the height of the simulation image so as not to interfere with the experimental results.

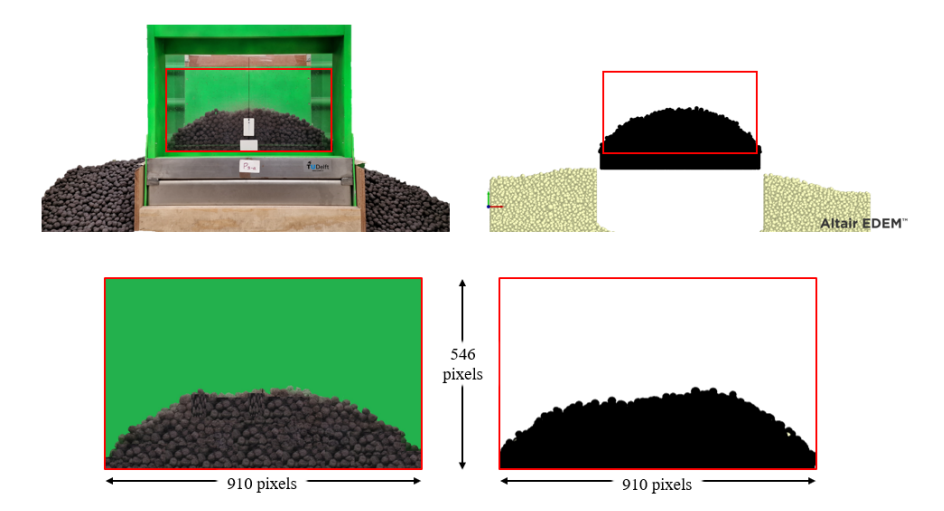


Figure 2.7: Dimensions of the images of the heaps.

These measurements give us the values for KPI 5, 6, 7, 8, and 9.

2.6. Experiments in DEM

The experimental setup was designed by Roeplal *et al.* [21] to closely replicate the laboratory environment. For the purpose of this study, the STL files of the experimental geometries were obtained directly from their work and used to reconstruct the setup in the simulation environment. Figure 2.8 illustrates the geometries as implemented in the simulations of this study.

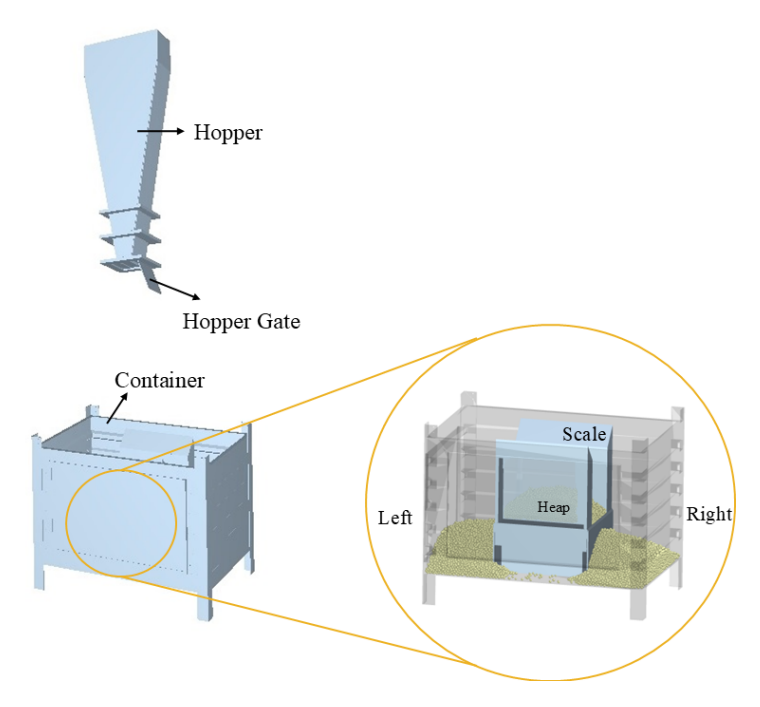


Figure 2.8: The geometries used in the simulations, imported from [21]. Note that in this image the scale is made partly transparent to show the heap but the imported scale is made of one material (steel) in the simulations.

The KPIs taken from the simulations need to be as similar as possible as the KPIs taken from the physical experiments. These include an image of the heap, the masses of the heap (scale, left side, and right side), and the discharge of the material at the hopper gate.

The time of the simulation and maximum y-coordinate of all particles is exported from the DEM simulation. When the maximum y-coordinate is below that of the hopper gate for the first time, the corresponding time is taken as the discharge time, KPI 1. The particle locations and masses are extracted from the simulations. Using MatLab the masses at different locations are extracted, to find KPI 2, 3, and 4. The shape of the heap is very sensitive to the input parameters as can be seen in Figure 2.9.

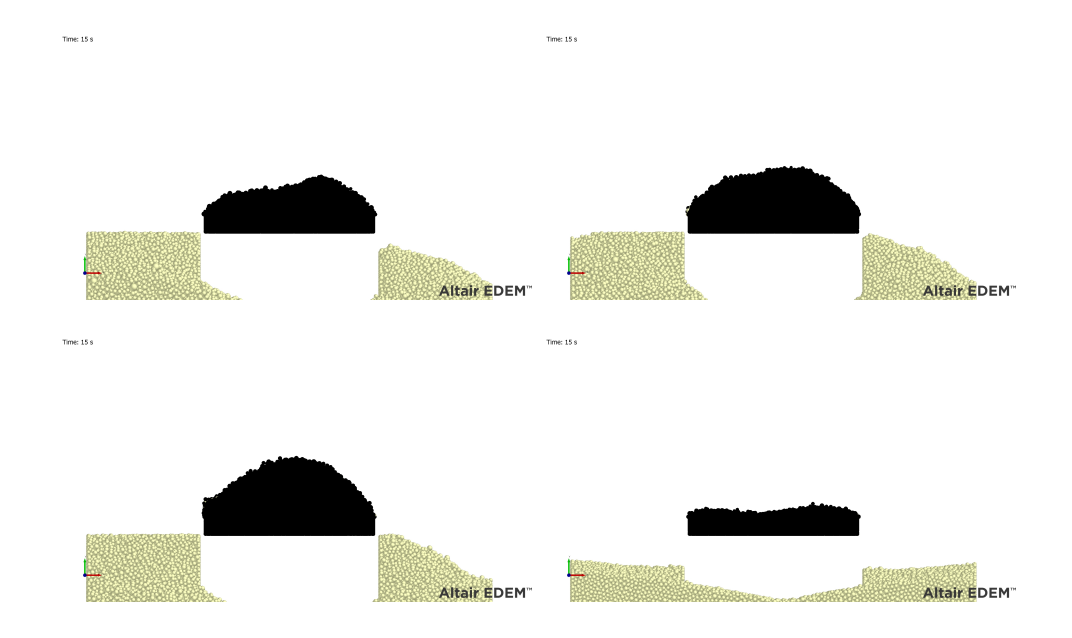


Figure 2.9: Different heap shapes due to variation of the interaction parameters.

The x-coordinate of this point indicates the position of the highest point, while the y-coordinate provides information about its height. Combined with the height at set positions in the heap (at a quarter, halfway and three quarters), this approach provides an analysis of the heap shape, the remaining KPIs, 5 to 9.

For this calibration procedure 12 interaction parameters are studied, each with their respective upper and lower bounds as can be seen in Table 2.2. They are taken as broadly as possible to maximize the likelihood of finding accurate parameter values.

Parameter	Lower Bound	Upper Bound
C_{pp}	0.0001	0.9
μ_{s-pp}	0	0.9
μ_{r-pp}	0	0.9
C_{pg}	0.0001	0.9
μ_{s-pq}	0	0.9
μ_{r-pg}	0	0.9
C_{ss}	0.0001	0.9
μ_{s-ss}	0	0.9
μ_{r-ss}	0	0.9
C_{sg}	0.0001	0.9
μ_{s-sg}	0	0.9
μ_{r-sg}	0	0.9

 Table 2.2: Simulation parameters with corresponding ranges.

To accurately calibrate the DEM model, it is necessary to understand how changes in input parameters affect the simulation outputs. However, running exhaustive simulations for every possible parameter combination would be computationally infeasible. Therefore, a Design of Experiments (DoE) approach is used to strategically sample the design space with a limited number of simulations. These samples are used to construct polynomial models that describe the relationships between input parameters and outputs. This modeling process, known as response surface methodology (RSM), allows for efficient exploration of the parameter space.

2.7. Design of Experiments: Central Composite Design

KPIs can be expressed as a function of multiple independent parameters and can often be represented as a linear combination of these parameters. However, to accurately predict responses, experiments must be structured to capture interaction effects and even quadratic relationships among the parameters. To achieve this, the Central Composite Design (CCD) method is applied which is capable of estimating interaction and quadratic effects [47]. This technique provides high-quality predictions of response surfaces, accounting for linear, quadratic, and interaction effects across the entire design space. Alternative DoE techniques commonly used in DEM calibration include Latin Hypercube Sampling, Full Factorial Design, Box-Behnken Design, and Fractional Factorial Design. However, CCD was chosen because it provides a balance between accuracy and efficiency, requiring fewer simulations while still covering a wide range of input variables [47].

CCD is a widely used experimental design method that combines an embedded factorial or fractional factorial design with center points, augmented by points to estimate curvature. It comes in three variations as can be seen in Figure 2.10: Circumscribed (CCC), Inscribed (CCI), and Face-Centered (CCF). CCC designs are the original form, with star points located at a distance beyond the factorial space, creating circular, spherical, or hyperspherical symmetry. These designs require five levels per variable and allow the exploration of extended variable ranges. CCI designs, on the other hand, scale the CCC design to fit entirely within the specified variable limits, using those limits as the pink square points. This makes them ideal for situations where the variable settings are strictly constrained, like this case. Lastly, CCF designs place the pink square points at the center of each face of the factorial space, requiring only three levels per variable.

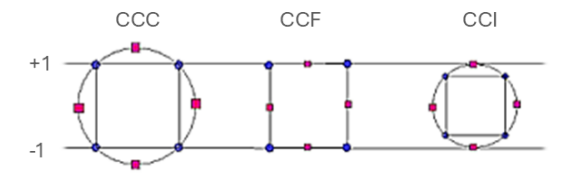


Figure 2.10: Three types of CCD [33].

For this study, the CCI design was chosen due to the strict limits of the parameter ranges, it is impossible to have a negative coefficients or a coefficient of restitution that is larger than 1. The specific CCD used for this thesis is described in Figure 2.11, showing an example with two factors.

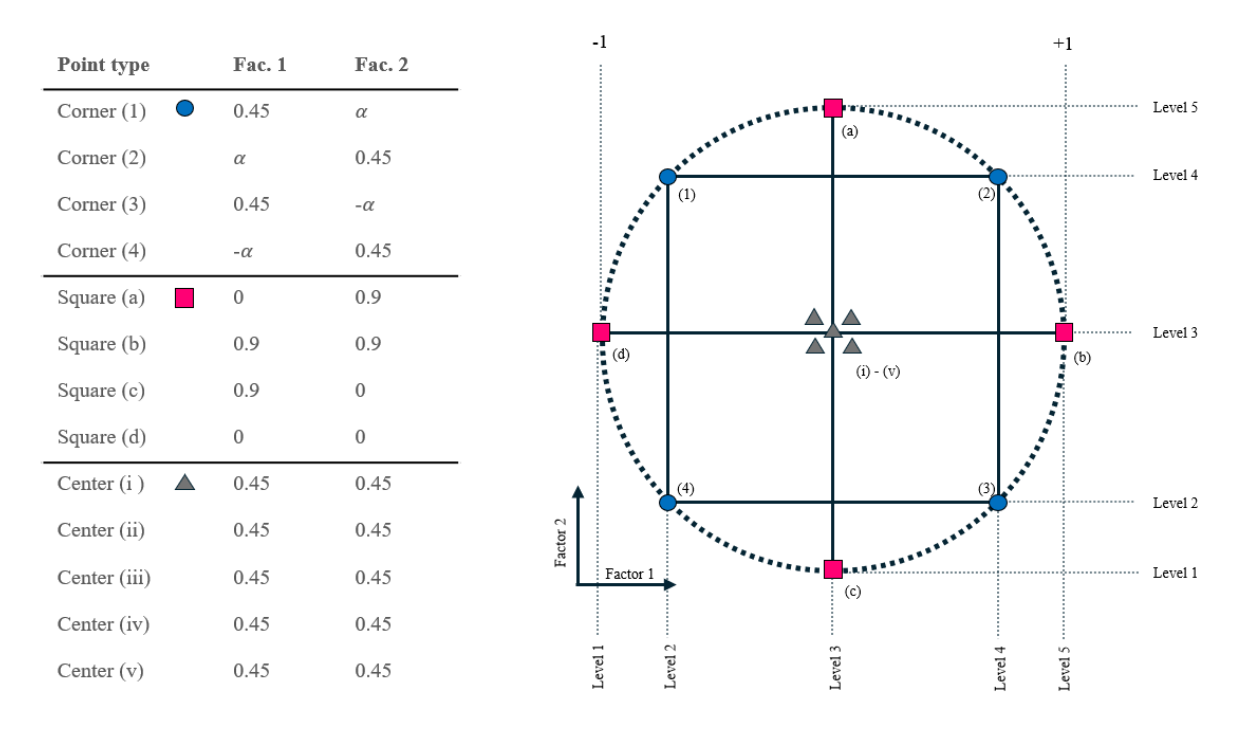


Figure 2.11: Complete design matrix for Central Composite Design inspired from [47].

The middle point is repeated five times to account for the variability of the KPIs. The α of the corner points can be found using scaling factor, and in the case of a rotatable design, it is found using the following formula, where k is amount of parameters:

$$SF = (2^k)^{\frac{1}{4}}$$
 (2.2)

The amount of runs are dependent on the amount of parameters which are used for the calibration. From those runs the KPIs are extracted and used for the polynomials, which model the relationship between the inputs and KPIs, as described in the next section.

2.8. Model Relations between Input and Output

Once the results of the CCD have been evaluated, they can be used to fit a model which relates the KPIs to the inputs. Using the results of the simulations, a polynomial can be created, one for every KPI. These polynomials contain a constant, a linear variable, a squared variable and interaction variables. It is a widely used and easy to understand statistical tool [48], and has been used in combination with CCD [47]. Using MATLAB's built-in function "fitlm", a second-order polynomial model was fitted using the least squares method. The model minimizes the sum of squared errors between predicted values and actual values.

The predicted KPI value is calculated as follows:

Predicted KPI = Constant +
$$\sum_{i=1}^{m} \beta_i P_i + \sum_{i=1}^{m} \gamma_i P_i^2 + \sum_{i=1}^{m} \sum_{j=i+1}^{m} \delta_{ij} P_i P_j$$
 (2.3)

Where:

- β_i : Linear coefficients.
- γ_i : Quadratic coefficients.
- δ_{ij}: Interaction coefficients.
- P_i: Parameters

Note: Indices i and j, in this case, refer to the parameters in the ordered list $\{C_{pp}, \mu_{r-pp}, \mu_{s-pp}, C_{pq}, \mu_{s-pq}\}$.

To compare the fitting of different models and measure their accuracy, R^2 can be used. The coefficient of determination (R^2) as shown in equation 2.8 measures how well a model explains the variance in the data, with values closer to one indicating a better fit.

$$R^{2} = 1 - \frac{\sum_{k=1}^{n} (y_{k} - \hat{y_{k}})^{2}}{\sum_{k=1}^{n} (y_{k} - \bar{y_{k}})^{2}}$$
 (2.4)

The fitting model is also verified first by using a parameter set which was not used during CCD. Once the polynomials have been established they can be used in the next step. Here the parameter set which gives the predicted KPIs closest to the experimental values is found.

2.9. Optimization Polynomials

Using the KPIs from the experiments (the target KPIs), the optimal values can be found for the parameters. Optimizing the polynomials can be done in different ways, different techniques and how often they appear in literature are shown in Figure 2.12. Several techniques are compared in this thesis, and are described below.

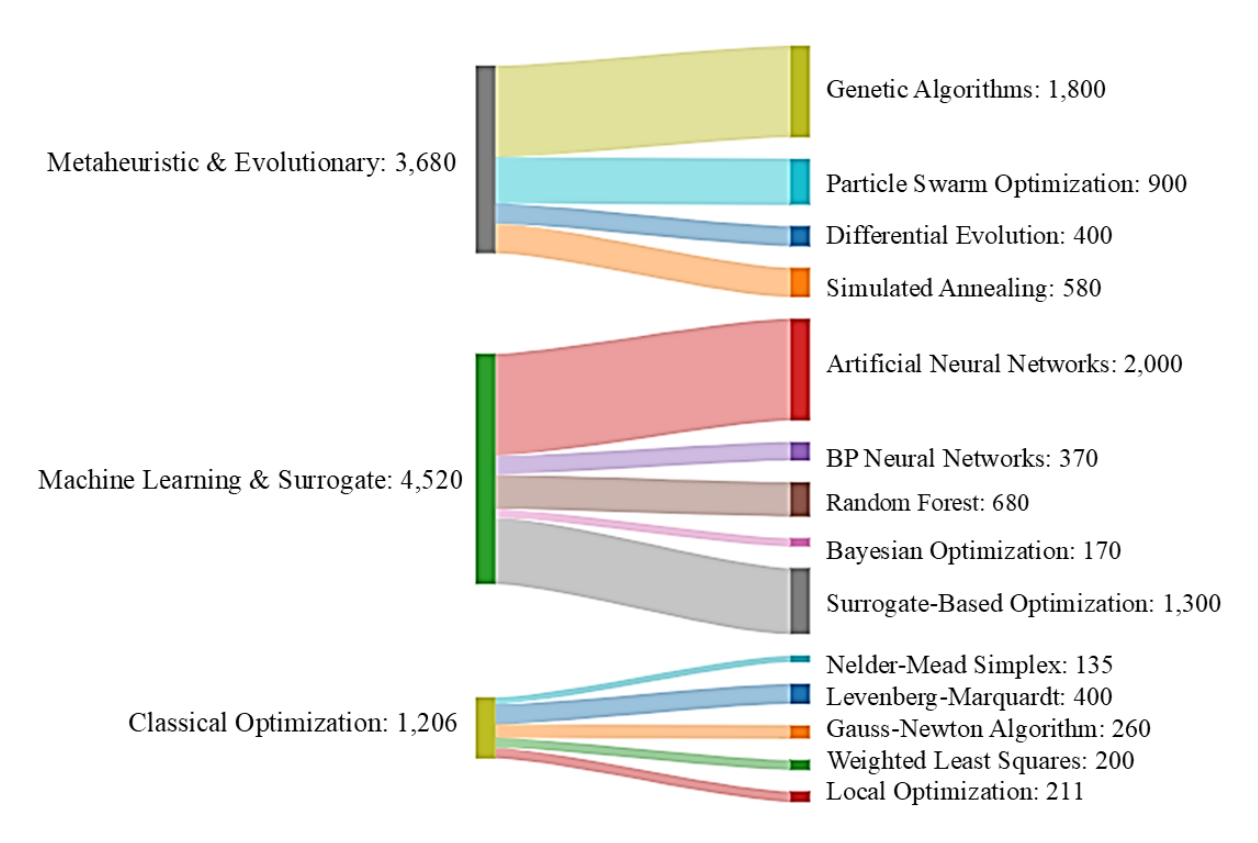


Figure 2.12: A Sankey chart of the optimization techniques used for finding the optimal parameter values in DEM simulations. The values represent the number of papers found when the following keywords are applied: "discrete element method" AND "calibration" AND "technique". Year: 1970-2025.

From this figure, it can be seen that Genetic Algorithm (GA) and Particle Swarm Optimization (PSO) are among the most commonly used optimization techniques, apart from Artificial Neural Networks (ANN). Although ANN is widely used in DEM calibration, it was not considered in this study due to its complexity and potential challenges in comparison with other techniques. Instead, GA and PSO were chosen because they are both well-established metaheuristic methods capable of handling non-linearities, and high-dimensional search spaces, which are some of the main challenges in DEM calibration [11]. Additionally, a local optimization method was included as a baseline comparison due to its simplicity and

ease of implementation. These optimization techniques are described in the rest of the section, including the objective function, upper and lower bounds, and stopping criteria.

2.9.1. Objective Function

The objective is to make the absolute value of the difference between all KPI values, one from the physical test and the other from the simulation, close to zero. To prevent larger KPI values from disproportionately influencing the optimization process, the objective function is normalized. The error is also squared to give a balanced outcome between the parameter values. This objective function combines the errors of *all* KPIs and can be written as follows:

$$Error = \sum_{k=1}^{n} \left(\frac{\text{Target KPI}_{k} - \text{Predicted KPI}_{k}}{\text{Target KPI}_{k}} \right)^{2}$$
(2.5)

The parameter bounds in which the optimal solution is allowed, are defined in Table 2.3.

Parameter	Lower Bound	Upper Bound
$\overline{C_{pp}}$	0.0001	0.9
μ_{r-pp}	0	0.9
μ_{s-pp}	0	0.9
C_{pq}	0.0001	0.9
μ_{s-pg}	0	0.9

Table 2.3: Bounds for the optimization parameters.

Local optimization, GA and PSO use the same objective function and parameter bounds.

2.9.2. Local Optimization

The "Fmin" function in MATLAB represents a calculus-based optimization (CBO) method. CBO relies on the gradients (or derivatives) of the objective function to identify optimal values [49]. The optimization process starts from an initial guess and iteratively moves in the direction of the negative gradient to minimize the objective function. This approach assumes that is differentiable across the search space. The method continues until it converges to a local minimum.

Key aspects for local optimization:

- · Initial guess for the optimization.
- Convergence criteria (e.g., maximum iterations, tolerance).

2.9.3. Global Optimization

Global optimization has several techniques, in this thesis, genetic algorithm, and particle swarm optimization are compared. These techniques are readily available in the Global Optimization Toolbox in MatLab [50]. These two methods belong to the category of metaheuristic approaches and they are population-based techniques.

Genetic Algorithm

Genetic Algorithms (GAs) are population-based metaheuristic optimization techniques that simulate natural evolutionary processes [51]. The algorithm starts with an initial population of candidate solutions (referred to as elements or chromosomes). Each element represents a potential solution, a set of parameter values.

GAs employ genetic operators like crossover, mutation, and elitism to evolve the population over successive generations. These operators iteratively refine the population, improving the solutions based on their fitness (the objective function value). The algorithm continues until a predefined stopping condition is reached, such as a maximum runtime, a certain objective function value, or a fixed number of generations.

Key aspects for Genetic Algorithm:

- · Population size and initialization strategy.
- · Genetic operators: crossover, mutation, and elitism.
- · Fitness function for evaluating solutions.
- Stopping criteria (e.g., max number of generations, fitness threshold).

Particle Swarm Optimization

Particle Swarm Optimization (PSO), is another population-based metaheuristic method inspired by the collective behavior observed in animal groups, such as bird flocks or fish schools [52, 53]. In this algorithm, a group of particles (potential solution sets) is initialized with random positions and velocities within the design space.

Each particle evaluates the objective function and remembers both its best position and the global best position found by the entire swarm. The velocity of each particle is updated based on its current velocity, its best-known position, and the global best position. This update ensures that particles move toward promising regions of the search space while maintaining diversity. The process continues until a stopping condition is reached, such as a maximum computational time or a desired solution.

Key aspects for Particle Swarm Optimization:

- Swarm size and initialization of particles' positions and velocities.
- · Fitness evaluation of particles.
- Stopping criteria (e.g., number of iterations, fitness threshold).

2.9.4. Stopping Criteria

In this study, the optimization algorithms, GA and PSO, were configured to prioritize convergence as the stopping criteria. Rather than relying on fixed limits for the number of generations or iterations, the focus was placed on allowing each algorithm to run until meaningful improvements in the objective function ceased. For the GA, stopping occurred when the average change in the fitness values across the population fell below the specified 'FunctionTolerance', indicating that the population had effectively converged to a stable solution. Similarly, the PSO algorithm was set to stop when the relative change in the objective value over the course of several iterations 'MaxStallIterations' dropped below the same tolerance threshold. This approach ensured that optimization was driven by solution stability rather than arbitrary computational limits, allowing each run to naturally converge to a minimal error.

2.9.5. Evaluation Metrics for Optimization Algorithms

When assessing the efficacy of optimization algorithms, there are several factors that are taken into consideration. Most importantly, the value of the objective function that the optimization can find, in this the 'quality of the solution', the difference between the target KPIs from the experiments and the predicted KPIs. A lower value is preferable, as it indicates a stronger alignment between the predicted KPIs and the target KPIs. Secondly, the variability in the objective function value is important. Specifically, it is important to determine whether the optimization algorithm consistently identifies the same optimal value or if the results exhibit significant variability. Consistency is desirable because it ensures reliability and reduces the necessity for multiple runs.

Another comparison metric is the computational speed; the faster an optimizer can find an optimal solution, the better, as this minimizes computational costs and speeds up decision-making. This includes the number of function evaluations needed to find the solution. Finally, the complexity of user-defined parameters plays a role in usability. If an optimization algorithm requires a large number of key inputs, it can be more challenging to fine-tune and less user-friendly. Additionally, high sensitivity to these user inputs can increase the risk of selecting suboptimal parameter sets, making the optimization process more error-prone.

2.10. Validation 20

Overview of evaluation metrics:

- 1. Objective function value
- 2. Variability in the objective function value
- 3. Amount of necessary iterations
- 4. Sensitivity to user-inputs

From these optimization algorithms, several 'optimal' parameter inputs will be found. These input parameters will be tested in the DEM simulations to check if they provide the predicted KPIs. If they are similar, the input parameters need to be validated as described in the next section.

2.10. Validation

Once the optimal parameter values have been found, it is important to check if these are accurate and make sure that these values are not only exclusively accurate for this specific situation. The physical experiments have been conducted with the hopper at varying heights, as shown in Section 2.5 and displayed in Figure 2.13 shown below. The KPIs for sinter and pellet have been measured at hopper heights of 1 meter, 3 meter, and 4.665 meter. The experimental KPIs change when the hopper height varies and this study checks if this same change occurs in the DEM simulation. The mixture has been measured at a hopper height of 4.665 meters. Therefore, the experimental results of hopper heights 1 and 3 meters will be used as validation experiments for sinter and pellet.

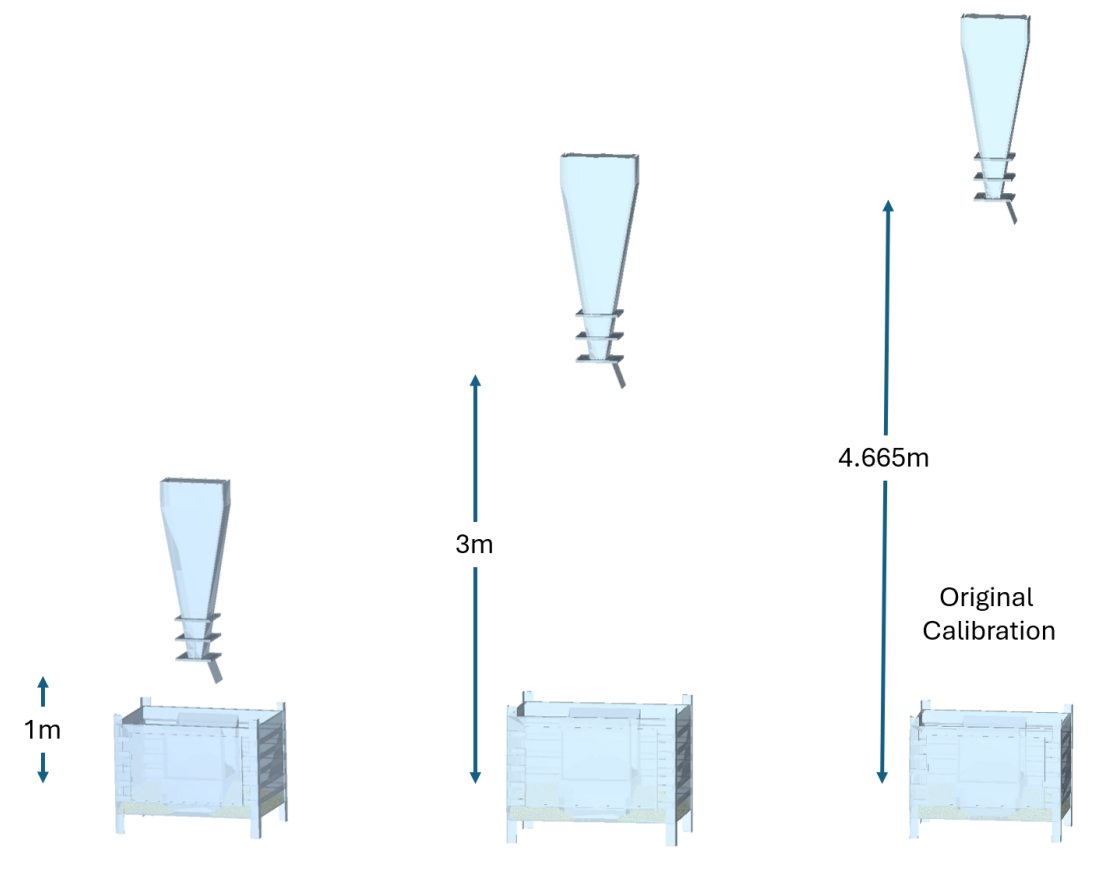


Figure 2.13: Different hopper heights in the DEM simulation.

2.11. Case Study: Mixture

As described in Table 2.1, the interaction parameters for the mixture of sinter and pellet will be taken as an average of the individual material's interaction parameters. This was applied successfully by Chakrabarty *et al.* [8] and is tested in this study.

2.12. Summary 21

2.12. Summary

To answer subquestion one, bulk calibration is a process involving several steps, starting with the experimental setup and proceeding to DEM model configuration, parameter determination, and optimization. In this study, the experimental setup included measuring the mass distribution of the material, analyze the heap shape using images, and record the mass flow at the hopper gate. These experiments provided 9 KPIs that are sensitive to DEM input parameters, allowing for bulk calibration.

To establish relationships between input parameters and KPIs, Central Composite Design is chosen. CCD is chosen due to its ability to capture interaction effects and quadratic relationships, making it well-suited for developing accurate response surface models. Polynomial regression is chosen as the regression technique, with model evaluation metric, \mathbb{R}^2 , which will be used to test the fit.

Subsequently, optimization techniques which are going to be applied to determine the best parameter values which minimize the difference between the experimental results and the simulation. Local optimization and global optimization methods such as genetic algorithm, and particle swarm optimization are chosen to be compared.

Finally, validation will be performed to ensure that the optimized parameters are not overfitted to a specific scenario and can be accurately used in different situations. This is done using different hopper heights.

Configuration DEM Model and Sensitivity Analysis

This chapter describes the setup of the DEM model. It describes the model inputs, the set parameters, and determines the interaction parameters which have an influence on the KPIs. The steps in the flowchart which are discussed in this chapter are highlighted by an orange box, in Figure 3.1.

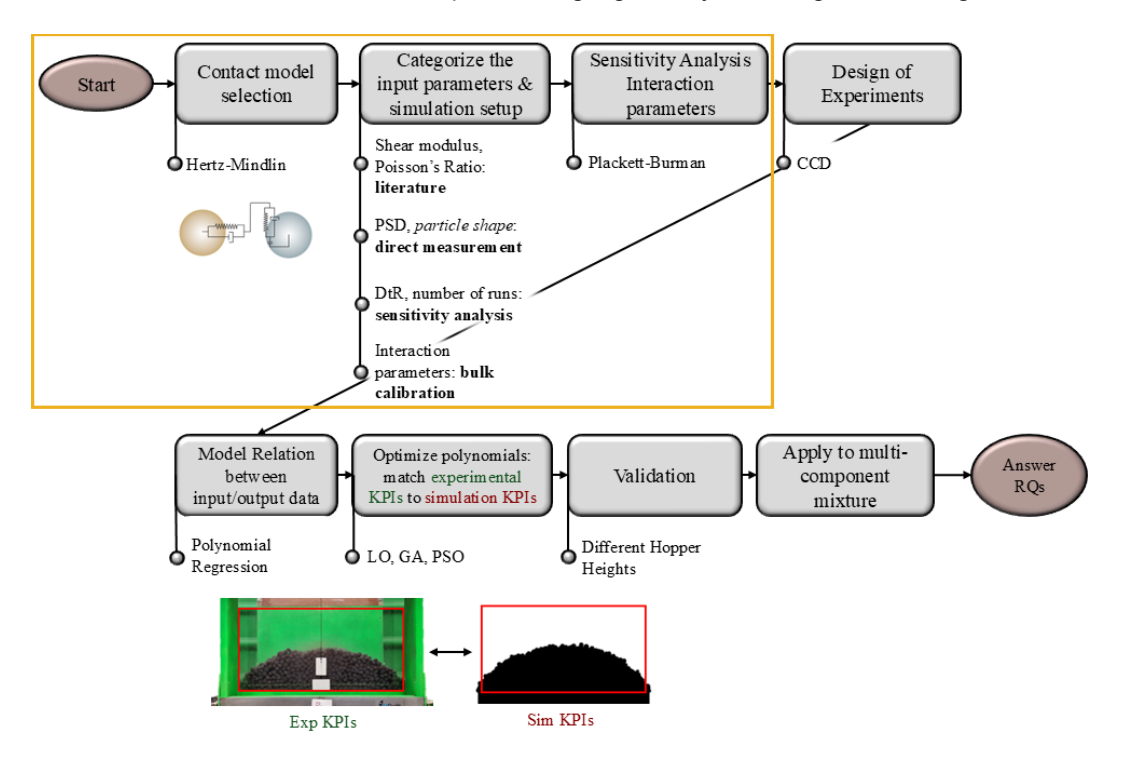


Figure 3.1: Steps described in this chapter.

3.1. Contact Model 23

3.1. Contact Model

We use Hertz-Mindlin (no-slip) [54] contact model and rolling friction model C, an elastic-plastic spring-dashpot model, according to Ai et al. [55]. For more information, EDEM theory reference guide should be referred to [33]. This contact model is widely used in blast furnace research, making it relevant for our study [1].

We used commercial software EDEM version 2024.1 to develop the DEM model and we conducted all simulations on the DelftBlue high performance cluster [56].

3.2. Direct Measurement & Literature

Three materials are simulated; sinter, pellet and a mixture of sinter and pellet. For those materials there are several material properties which will have a fixed value in this calibration process and will not be adjusted during this study, these are summarized in Table 3.1.

DEM Parameter	Pellet	Sinter	Geometry
Shear modulus (G)	2.5e+8 Pa [57, 8]	2.5e+8 Pa [57, 8]	2e+11 Pa [58]
Poisson's ratio (v)	0.25 [57, 8]	0.25 [57, 8]	0.3 [58]
Solid density (ρ_s)	3602 (kg/m ³) [57, 8]	3449 (kg/m ³) [57, 8]	7800 (kg/m ³) [58]

Table 3.1: Material properties used in DEM simulations

Available data was used for the particle shape distribution. This was scaled by volume and every volume was given as a percentage of the total mass.

3.3. Sensitivity Analysis

The remaining parameters include the sinter particle shape, the DtR and the interaction parameters of both materials. In this section the results of the sensitivity analysis for these parameters are described.

3.3.1. Rayleigh Time Step

To optimize computational efficiency while ensuring simulation stability and accuracy, a time step analysis was conducted using Rayleigh time step percentages of 5%, 10%, 20%, 30%, and 40%.

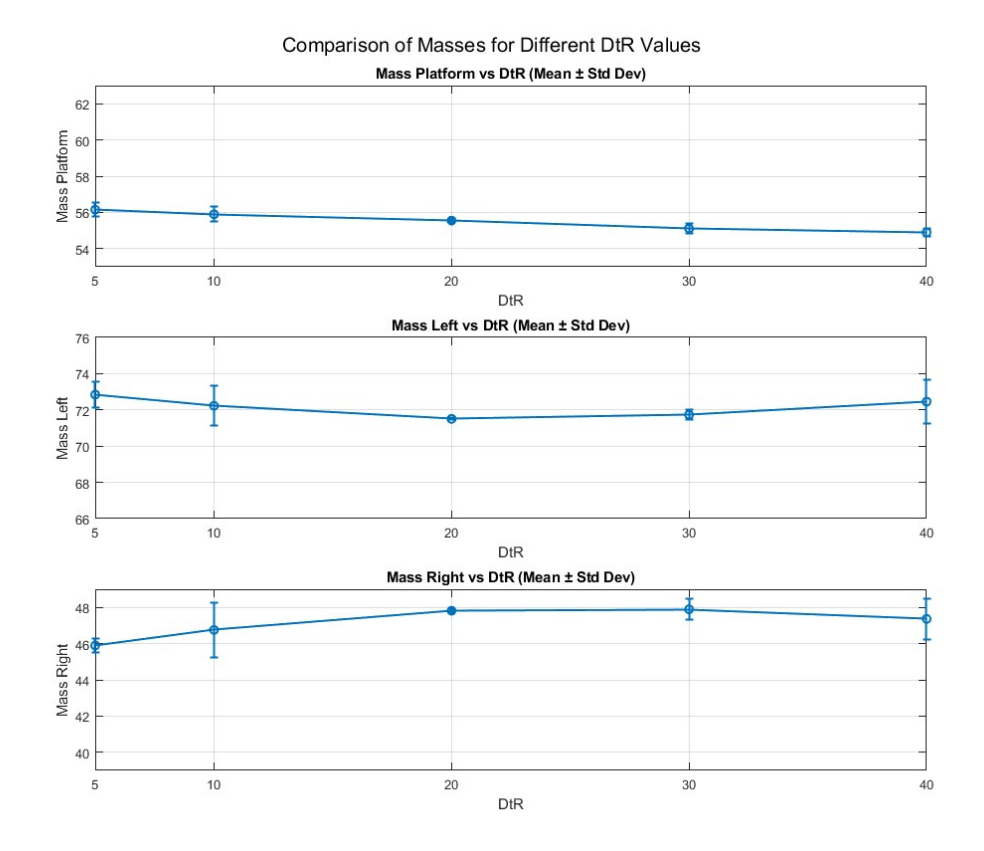


Figure 3.2: Time step analysis of pellet.

The results indicated minimal influence of the time step on the KPIs across this range. Consequently, a time step of 40% was initially chosen for subsequent simulations, as it was the least computationally expensive. The chosen values for the interaction parameters are shown in Table 3.2. These are taken based on literature where pellets are used [19, 8, 46].

Parameter	Value
C_{pp}	0.5
μ_{s-pp}	0.455
μ_{r-pp}	0.145
C_{pq}	0.41
μ_{s-pg}	0.405
μ_{r-pg}	0.2

Table 3.2: Values for the interaction parameters of pellet for the time step analysis.

However, during the sensitivity analysis, which involved a broader range of interaction parameters, simulations with a 40% time step were instable as can be seen in Figure 3.3. Therefore, the simulations were repeated using a more conservative time step of 10%, which was stable across the parameter space. 10% was also used for the simulations of sinter.



Figure 3.3: Instable simulation with a DtR of 40%.

The lack of an initially observed correlation between the KPIs and the Rayleigh time step contradicts the results of previous studies [35, 36, 9], where such a relationship was typically reported. It is likely that this discrepancy resulted from the initial narrow parameter selection, which obscured potential dependencies. The revised approach, which uses a more conservative time step, ensures stability across a range of interaction conditions.

3.3.2. Amount of Runs

The KPIs exhibit some variation, which is why it is important to have multiple runs, this ensures that observed differences in output are due to input changes rather than random chance. That is why the simulation is repeated seven times and the results are analysed to determine when the KPIs converge. In Table 3.3 the parameter values used for this analysis are presented.

Parameter	Value
C_{pp}	0.45
μ_{s-pp}	0.45
μ_{r-pp}	0.45
C_{pq}	0.45
μ_{s-pq}	0.45
μ_{r-pg}	0.45

Table 3.3: Values for the interaction parameters of pellet for the amount of runs analysis.

The convergence of the KPI values is shown in Figure 3.4. As can be seen in this graph, all KPIs converge at 4 runs.

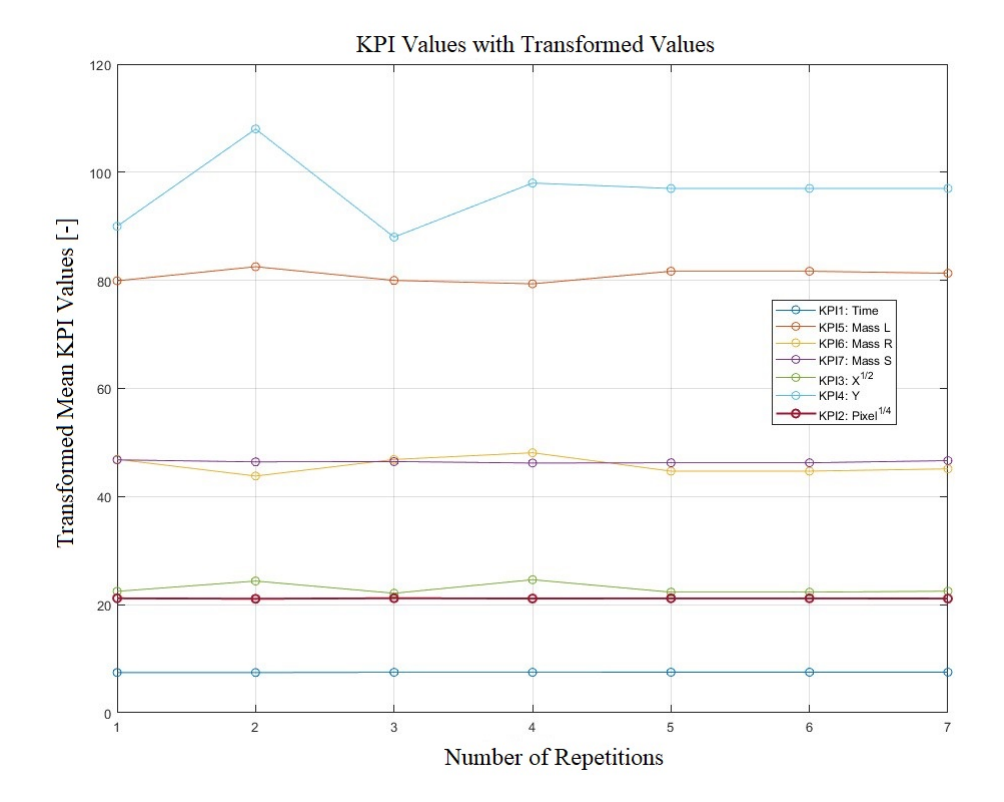


Figure 3.4: Convergence of the KPI values, pixel count of the heap and value of the x-coordinate of the highest point of the heap are transformed to compress their magnitudes while maintaining their relative differences.

Due to time constraints, these tests were not repeated for sinter but assumed to have similar results. Once the amount of necessary runs and the percentage of DtR have been determined, it is possible to look at the remaining configuration of the DEM model, starting with the particle shape.

3.3.3. Sinter Particle Shape

As mentioned in Section 2.4, the pellet particle shape is represented as a sphere in EDEM. For sinter particle shape, it is decided for this study, to choose *one* particle shape to represent all sinter particles, instead of multiple particle shapes, to reduce complexity and computational cost. Therefore, if feasible, we would like a "typical" particle shape for this DEM model. This approach should adequately capture the effects of particle shape within the scope of this study. However, if not, it could prevent us from achieving an optimal parameter set. To get a typical particle shape, the particle shapes need to be put in order.

There are several characteristics of the particle shape which have an influence on the segregation of the mixture. We categorize the particle shape in two ways. One is on the basis of the elongation, flatness and compactness of the particle shape as can be seen in Figure 3.5a and the other is based on the complexity of the particle shape as can be seen in Figure 3.5b.

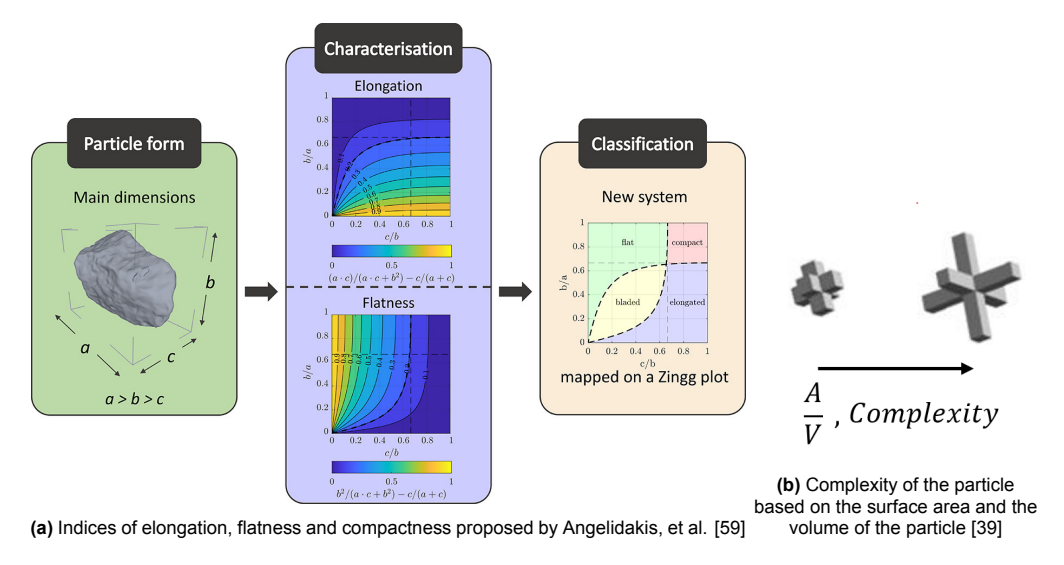


Figure 3.5: Comparison of particle properties: elongation, flatness, compactness, and complexity.

285 STL files of sinter particles were available. Each STL file describes the surface geometry of a three-dimensional sinter particle. The 285 measured sinter particles were categorized based on elongation, flatness, compactness, and complexity using the dimensions of the STL file. Their distribution is visualized in Figure 3.6.

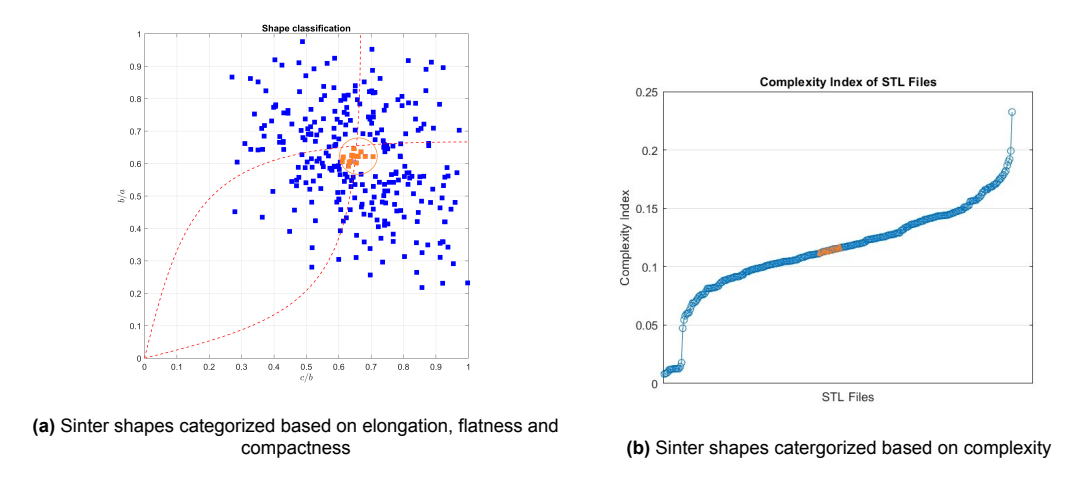


Figure 3.6: Categorization of the measured sinter particles.

To determine the sinter particle shape, we analyzed the distribution of 285 measured sinter particles based on their shape characteristics. Specifically, we categorized them using elongation, flatness, compactness (as shown in Figure 3.6a), and complexity indices (as shown in Figure 3.6b).

From these datasets, shown in Figure 3.6, we computed the average characteristics of the distributions. The 15 particles which are closest to these average characteristics are colored orange in the graphs.

Among these 15, we looked for a single particle shape that appeared consistently across both ranking criteria. STL file number 158 emerged. This particle shape, shown in Figure 3.7, was selected for use in the DEM simulation.



Figure 3.7: STL file 158, chosen as the sinter particle shape

In EDEM, an STL file can be imported and used as a template to generate a particle, with its properties automatically computed by the software. Users can adjust two key parameters for the generated multisphere: the smoothing value and the minimum radius. A higher smoothing value (greater than 1) reduces the fidelity of the particle, leading to fewer used spheres. The minimum radius ensures that excessively small spheres are not included in the multi-sphere representation. Smaller spheres require a smaller simulation time step, increasing computational cost [33]. To assess the impact of these two parameters on the KPIs, a small study was conducted using different values for both.

For the smoothing value, three levels were selected: 5, 7 and 10. For the minimum radius 0.15 or 0.3 was set. The different multi-spheres are shown in Figure 3.8, where the first multi-sphere represents the original template. These values were chosen to have an acceptable multi-sphere for the sinter simulations, meaning that the sphere count does not exceed 40 spheres. A multi-sphere with more than 40 spheres (a very low smoothing value) and a minimum radius of less than 0.15 would result in very costly simulations, an example of how a multi-sphere would look without constraints is the second multi-sphere shown in Figure 3.8. Different combinations of these values are tested, resulting in six simulations. The results of these simulations can be found in Appendix B.

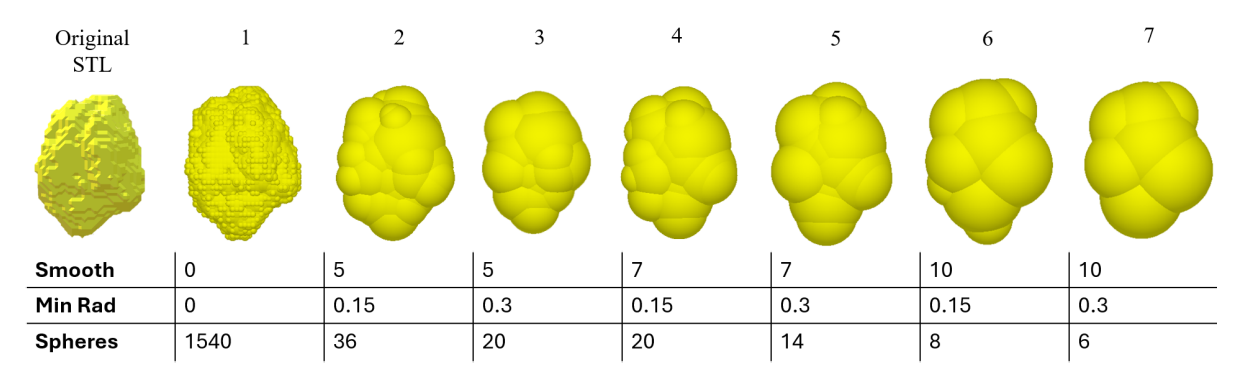


Figure 3.8: Different multi-spheres of the sinter particle.

The effects of these two parameters on the KPIs are described in Figure 3.9, the numerical results can also be found in Appendix B, Table B.1. As can be seen in the figure, and is further confirmed by the ANOVA analysis in Appendix B, Table B.2, these two parameters have almost no effect on the KPIs of the system. This could be because the 6 shapes are still very similar in the performed study. Consequently the smallest smoothing factor was selected, as it matches the original shape as closely as possible. The largest minimum radius was chosen as it significantly influences the computational cost as also demonstrated in Appendix B, Table B.3. Based on these findings, a smoothing value of 5 with minimum radius of 0.3 were used, sphere number three in the figure.

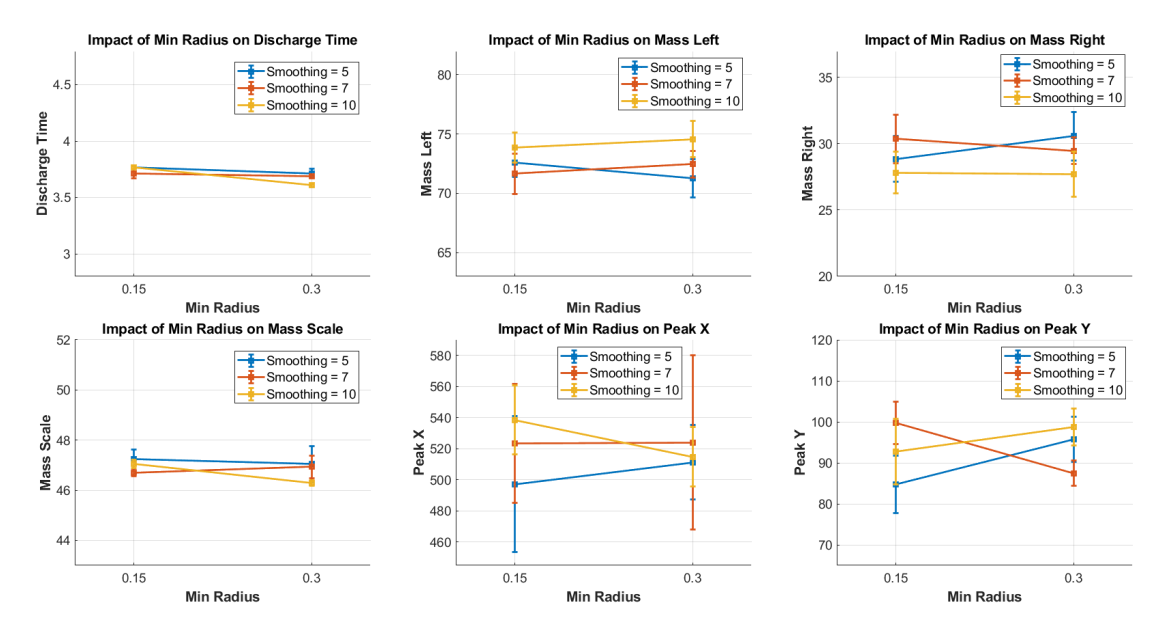


Figure 3.9: Main effect plots of the smoothing value and the minimum radius on the KPIs

3.4. Dominant DEM Parameters using Plackett-Burman

For the sensitivity analysis of the interaction parameters, Plackett-Burman (PB) will be used, as mentioned in Section 2.4. There are two levels possible for PB and they selected values for the parameters and levels are shown in Table 3.4 for pellet. The values for the 8 simulations and the resulting KPIs can be found in Appendix C, in Section C.1.

Parameter	Low Level (-1)	High Level (+1)
C_{pp}	0.0001	0.9
μ_{s-pp}	0	0.9
μ_{r-pp}	0	0.9
C_{pq}	0.0001	0.9
μ_{s-pg}	0	0.9
μ_{r-pg}	0	0.9

Table 3.4: Parameters with corresponding levels for the Plakett-Burman (PB) Design of Experiments (DoE).

3.4.1. Results Plackett-Burman

Table 3.5 displays the effect of DEM interaction parameters on the KPIs. It is a summary of the Pareto plots of each KPI which can be found in Appendix C, Section C.2. The parameters which are significant, influence the KPI for up to 90%. One of the key observations that arise from Table 3.5 is that μ_{r-pg} is not a significant parameter for any of the measured KPIs. Another observation is that C_{pp} has an affect on almost every KPI. Here it should be noted that the pixel count of the heap is taken into account instead of the height at different points of the heap because this was changed during the study.

Parameter	Discharge Time	Pixel Count Heap	Highest Point X	Highest Point Y	Mass Left	Mass Right	Mass Heap
C_{pp}	Х	(-)	(-)	(+)	(-)	(-)	(-)
μ_{s-pp}	(+)	(+)	X	(-)	X	X	(+)
μ_{r-pp}	(+)	(+)	X	(-)	X	(-)	(+)
C_{pg}	X	X	(-)	X	(-)	(-)	X
μ_{s-pg}	X	(+)	(-)	X	X	(-)	(+)
μ_{r-pg}	X	X	X	X	X	X	X

Table 3.5: The effect of DEM interaction parameters on the KPIs, with the effect of each significant parameter on the KPIs in parentheses (e.g., "(+)" denotes that with an increase in the parameter value, KPI increases.). "x" means insignificant effect.

A visual representation of the results can be seen in Figure 3.10, where the dotted line represents 90% of the contribution to the KPI.

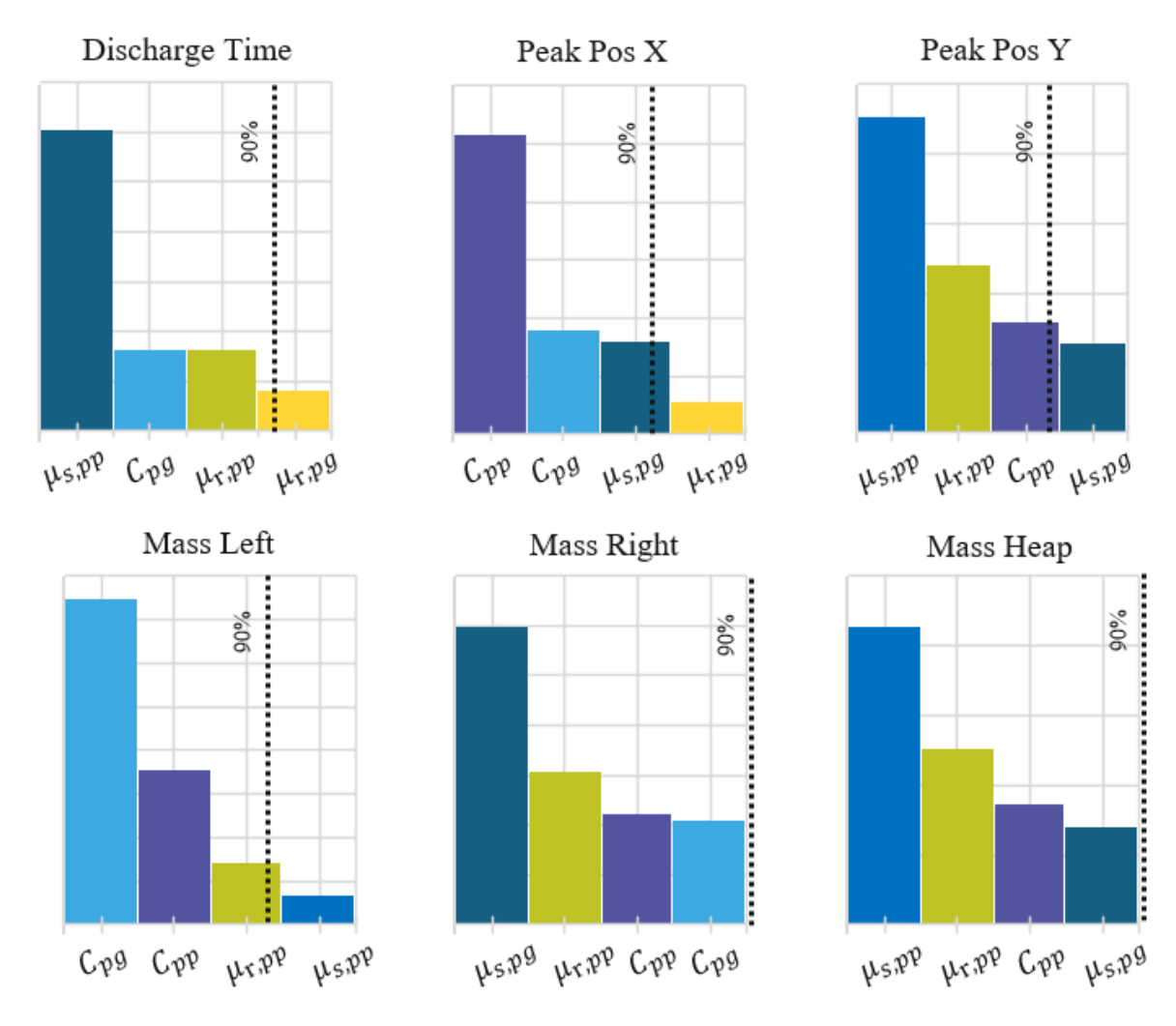


Figure 3.10: Overview of the Pareto plots of each KPI. The line with 90% is placed where the parameters have 90% effect on the KPI. For a more detailed graph, see Appendix 3.

One potential explanation for the insignificance of μ_{r-pg} may be that the particle shape itself governs the rolling behavior more than the rolling friction coefficient does. Another potential explanation is that PB is not well-suited for capturing interaction effects between parameters [60]. This limitation could result in some interaction effects being overshadowed by main effects, thereby masking the true significance. However, further research is necessary to confirm this hypothesis.

3.5. Concluding Remarks

To summarize, decisions were made on the DEM model inputs, such as the particle shapes: a sphere for pellet and a clumped sphere for sinter, the Rayleigh time step: 10% of the DtR is used for the simulations, and the amount of necessary runs: 4 runs are performed of each simulation.

The sensitivity analysis using the Plackett-Burman DoE has revealed that most interaction parameters significantly influence the simulation KPIs. The coefficient of restitution between pellet particles (C_{pp}) was found to be one of the most dominant parameters, affecting nearly all KPIs. In contrast, the rolling friction between pellet and and the geometry had no significant effect on any of the measured KPIs, answering subquestion two of the research questions. As a result, this parameter will not be included in the calibration process, as adjusting it would not improve the simulation accuracy. These findings are used to define which parameters are used into the response surface modeling and optimization in the next chapter.

Calibration of Sinter and Pellet

The calibration procedure is one of the final steps in establishing an accurate DEM simulation. This chapter outlines the steps used to calibrate the parameters to ensure consistency between experimental and simulated results, under which different optimization techniques are compared.

The same methods used for measuring the KPIs of pellet are also used for sinter. The calibration of sinter and pellet is performed at a hopper height of 4.665 m. The steps in the flowchart which are discussed in this chapter are highlighted by an orange box, in Figure 4.1.

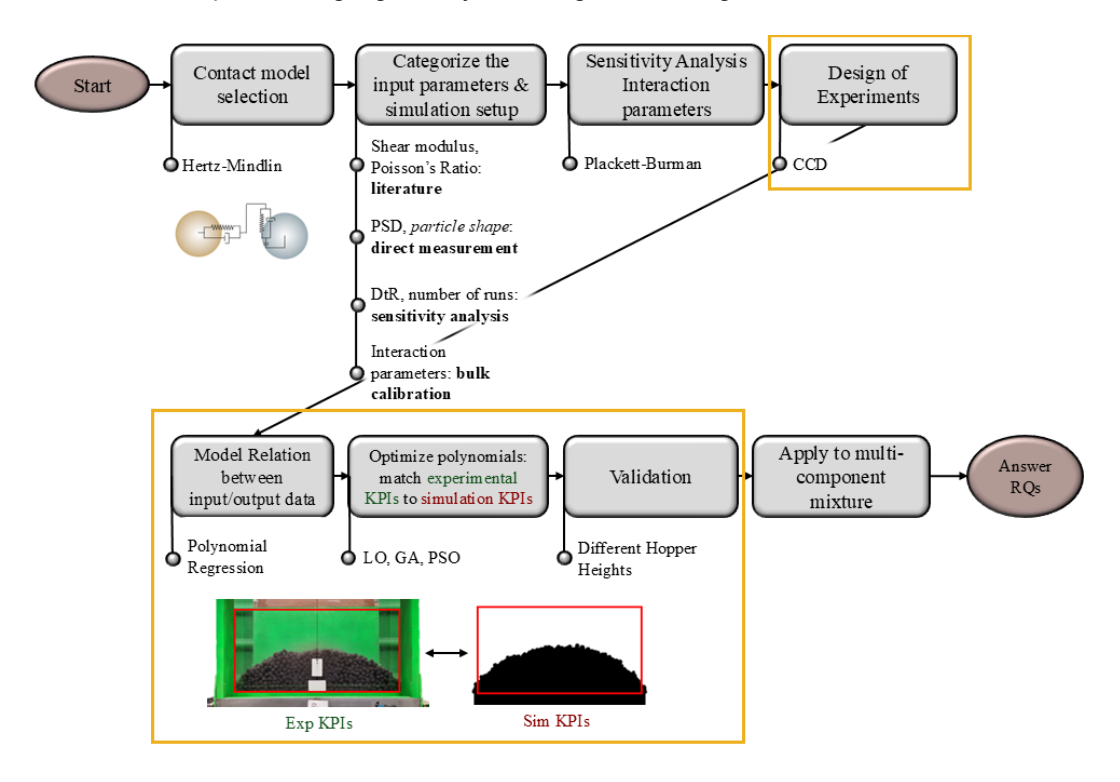


Figure 4.1: Steps described in this chapter

4.1. Polynomial Regression using CCD

As mentioned in Chapter 2, Section 2.7 this study uses CCD and polynomial regression to create a RSM for pellet and sinter. The result of the CCD can be found in Appendix E. The resulting polynomial model can also be found in that appendix, in Section E.2, Table E.4 displays the polynomial model for pellet and Table E.5 shows the polynomial model for sinter. In Table 4.1 the R^2 of the models which measures how well a model explains the variance in the data are shown per KPI, with values closer to one indicating a better fit.

	Time	M heap	M left	M right	PeakX	PeakY	0.25Y	0.5Y	0.75Y
Pellet	0.98776	0.96546	0.81121	0.70841	0.86276	0.96751	0.96942	0.97609	0.90973
Sinter	0.77077	0.98438	0.98438	0.70017	0.87183	0.98468	0.97609	0.98889	0.93775

Table 4.1: Comparison of R-squared values for pellet and sinter models.

As can be seen in this table most \mathbb{R}^2 values are above the 0.95. Notably, the discharge time for sinter, the mass on the right side of the container are lower values (=< 0.7). This could have an affect on the quality of the predicted values.

What was interesting to see was that during the CCD simulations, sometimes one of the sinter particles remains "stuck" in the hopper as can be seen in Figure 4.2. This means that the maximum y-coordinate of all particles remains above that of the hopper gate, meaning the discharge time cannot be measured using the maximum y-coordinate. When this happens, the measurement is excluded from the analysis, so instead of 4 runs, 3 runs are used for the discharge time because it would take too long to rerun those runs specifically, and it is found that it does not vary significantly over runs as can be seen in Appendix F, where the instances are written as 'NaN'. This probably occurs because of the specific particle shape which can 'interlock' with the sides of the hopper, there seems to be no clear correlation with the input parameters of why this might occur, and it does not happen with pellet simulations, leaving only the particle shape as possible reason.

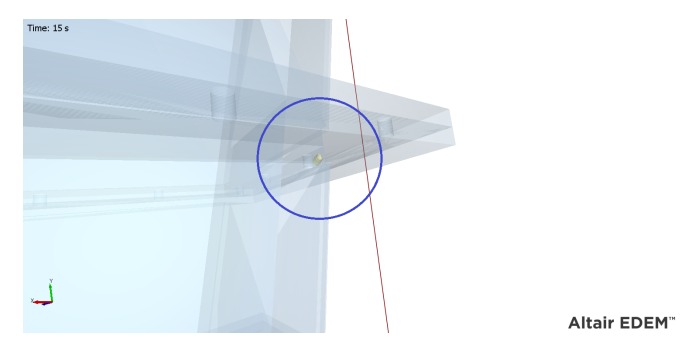


Figure 4.2: Screenshot of DEM simulation where one of the particles is "stuck" in the hopper.

This did not significantly affect the overall calibration results, but it does highlight a potential limitation in capturing irregular particle interactions.

4.2. Optimization Setup and Results

This section describes the different optimization techniques used to calculate the parameter values that give the closest match between the results from the laboratory tests and those from the simulations.

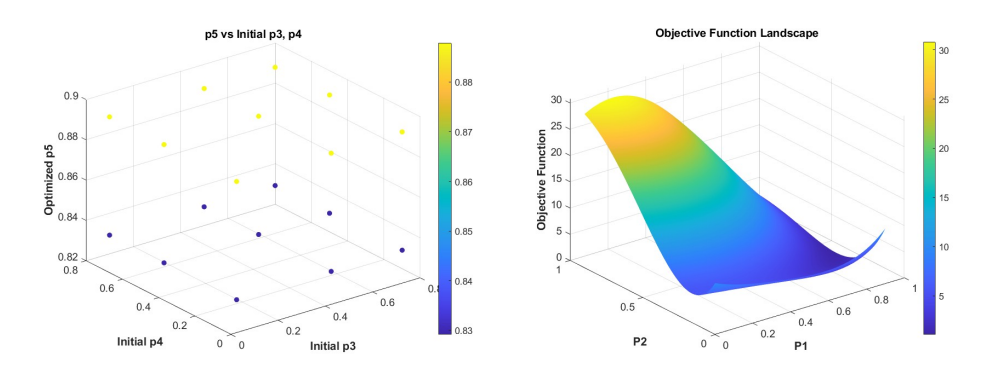
4.3. Local Optimization

This gradient-based optimization, used in this study, performs polynomial regression on CCD data and optimizes parameters to match the target KPIs values using the function 'fmincon' provided in the MatLab optimization toolbox (version R2024b). At each computational step, a set of parameter values is determined, whilst the optimization solver monitors the objective function value, searching for the optimal solution.

4.3.1. Effect of Initial Guess

Besides the bounds and the objective function, the initial guess has to be determined from where the optimization can be taken. The parameter values are very dependent on the initial guess of the parameters as can be seen in Figure 4.3a, where different combinations of initial guesses are taken from [0.1, 0.1, 0.1, 0.1, 0.1], [0.5, 0.5, 0.5, 0.5, 0.5] and [0.8, 0.8, 0.8, 0.8, 0.8]. In the figure only the initial guesses of C_{pp} and μ_{r-pp} are shown; however, the optimization process has a five-dimensional parameter space to determine the optimal solution.

Figure 4.3a shows the difference in the optimal parameter value found with different initial guesses. P1, P2, P3, P4, and P5 stand for C_{pp} , μ_{r-pp} , μ_{s-pp} , C_{pg} , and μ_{s-pg} respectively. In Figure 4.3b the effect of the different initial guesses on the objective function value of pellet is shown.

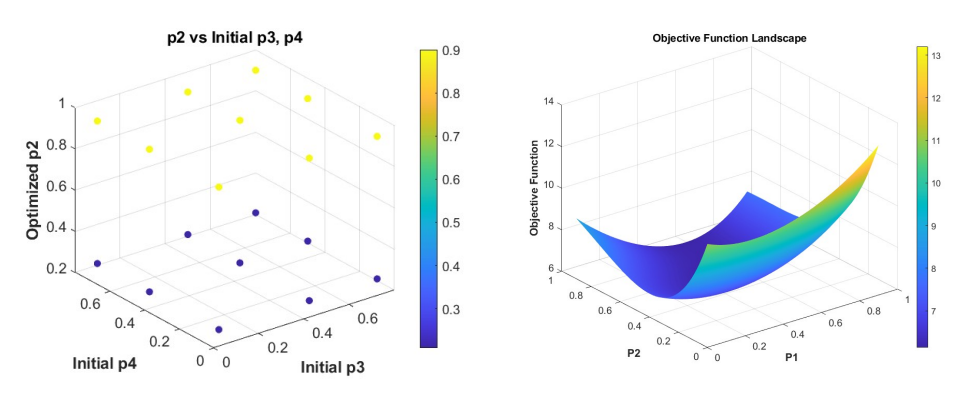


(a) Parameter value dependency on the initial guess of the optimization (b) Objective value dependency on the initial guess of the optimization

In Appendix G, the graphs with different combinations of parameters can be found. From these initial guesses, the combination which gives the smallest optimal solution was used as the final initial guess for pellet.

Initial Guess: [0.10, 0.10, 0.80, 0.80, 0.80]

As can be seen in Figure 4.4a, the optimization of sinter is more dependent on the initial guess than for pellet. The parameter values change drastically depending on the initial guess. Figure 4.4a shows the different results for μ_{s-pg} with different initial guesses for μ_{s-pp} and C_{pg} . The same results are found for the remaining four input parameters, these graphs can be found in Appendix G. Note that in these graphs only the values of initial guess for two parameters are shown but that during the analysis, all five parameters were adjusted.



(a) Parameter value dependency on the initial guess of the the optimization (b) Objective value dependency on the initial guess of the optimization

From the 243 different combinations of initial guesses, the following initial guess gives the smallest error (object function value) for the sinter simulations:

Initial Guess: [0.80, 0.10, 0.80, 0.80, 0.10]

4.3.2. Results Local Optimization

Once the algorithm is fine-tuned and the best initial guess from the tested combinations is selected, it converges to an objective function value of "for pellet and "for sinter.

With the best initial guess found for pellet, the optimization has been run 10 times and each time the same optimal values are found, meaning there is little variability in the results. The optimization gives an objective function value of '0.0242' when compared to the target KPIs.

Parameter	C_{pp}	μ_{r-pp}	μ_{s-pp}	C_{pg}	μ_{s-pg}	Error
Value	0.151	0.453	0.04	0.359	0.83	0.1465

Table 4.2: Optimal parameter set found for pellet with local optimization.

When taking the best initial guess for sinter the optimization gives the following optimal parameter set, which gives an objective function value of '3.1753' when compared to the target KPIs.

Parameter	C_{pp}	μ_{r-pp}	μ_{s-pp}	C_{pg}	μ_{s-pg}	Error
Value	0.258	0.9	0.350	0.9	0.532	3.1753

Table 4.3: Optimal parameter set found for sinter with local optimization.

4.4. Global Optimization Methods

Local optimization methods, such as 'fmincon', are designed to converge to the nearest local minimum based on the initial guess. The objective function has many local minima, meaning the result will depend heavily on the starting point, as was found. A global optimization method explores the parameter space more comprehensively and increases the likelihood of finding the global minimum rather than getting stuck in a local one. In this case genetic algorithm (GA) and particle swarm optimization (PSO) are applied using the convenient MatLab Global Optimization Toolbox [50].

For both GA and PSO there are several inputs which can be tuned to look at the effect it has on the objective function value.

4.4.1. Effect of Swarm and Population Size

As mentioned in Section 2.9.3, GA and PSO have several user-defined inputs. In this section the population size of GA and the swarm size of PSO are compared. Both sizes represent the number of candidate solutions considered per iteration. Comparing them provides insight into how efficiently each algorithm uses its agents to converge toward solutions.

Although GA and PSO both have several user-defined parameters, this section focuses specifically on comparing population size in GA and swarm size in PSO. These parameters are directly comparable, as they represent the number of candidate solutions evaluated per iteration. They have a similar impact on the convergence behavior and computational effort of the optimization process.

Other parameters, such as mutation rate and crossover probability in GA, or inertia weight and acceleration coefficients in PSO, influence the algorithm in more algorithm-specific ways. For example, the mutation rate controls genetic variation in GA, while the cognitive and social coefficients in PSO determine how particles are influenced by their own best position and that of the swarm. Since these parameters do not have a direct counterpart in the other algorithm, comparing them would not provide a fair or consistent basis for evaluation.

Therefore, all algorithm-specific parameters were kept constant to isolate the effect of population and swarm size on the optimization results.

In Figure 4.5 the effect of the particle swarm and the population size on the objective function value of the pellet simulation are shown.

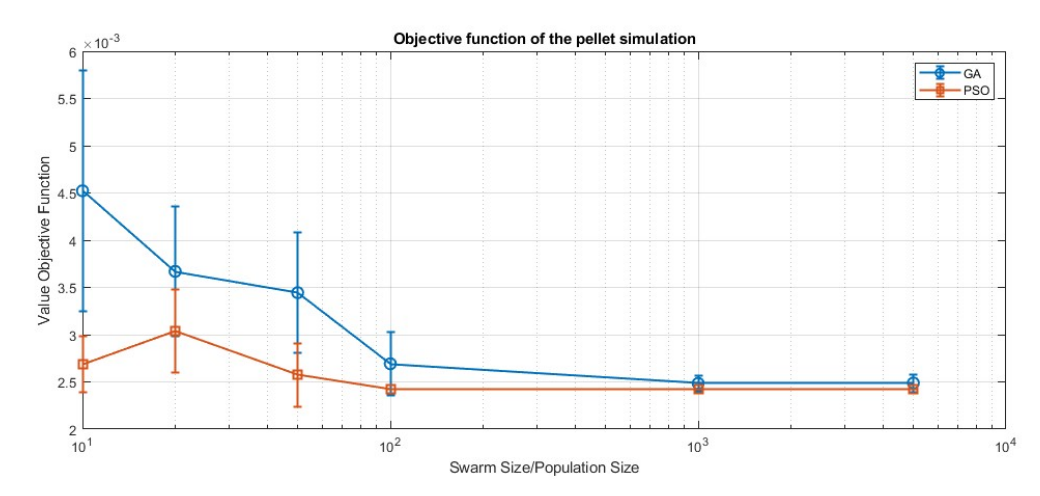


Figure 4.5: Pellet optimizer objective function value for different population and swarm sizes of GA and PSO with error bars.

As can be concluded from this figure, the population size of GA needs to be significantly bigger than the particle swarm of PSO in order to converge to an objective function value. Additionally, The error bars indicate that GA results showed more variability across runs, possibly due to stochastic effects in crossover and mutation, whereas PSO showed less variable outcomes. The following figure, Figure 4.6, shows the same but then for sinter simulations.

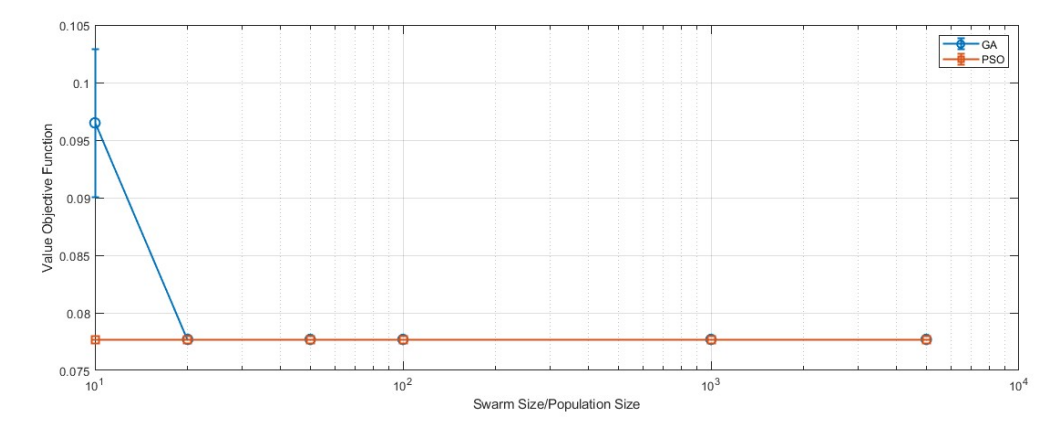


Figure 4.6: Sinter optimizer objective function value for different population and swarm sizes of GA and PSO with error bars.

This figure looks different than the one for pellet. Although GA still needs a larger population, the difference is smaller compared to pellet, and GA converges almost as quickly as PSO. Therefore, based on the observed convergence behavior and stability, the following swarm and population sizes were selected for the pellet and sinter optimizations, as shown in Table 4.4.

Material	Swarm size	Population size
Pellet	100	1000
Sinter	20	20

Table 4.4: Swarm and population size for the optimization of pellet and sinter.

The corresponding optimal input parameters found, are described in the following section.

4.4.2. Results Global Optimization

Once the algorithm has been fine tuned, they converge to an objective function value of '0.0024213' for pellet and '0.077' for sinter. This is a much smaller objective function value compared to the one found using the local optimization.

In Appendix G, Table G.1 shows the results of the five best cases and their corresponding optimal parameters for GA and PSO for each material. These cases were obtained after fine-tuning the population and swarm sizes, followed by 15 optimization runs per algorithm. The number of runs was chosen to assess variability across multiple trials while keeping the total computational effort manageable. From these, the five runs with the lowest objective function values were selected to reduce the impact of outliers of GA and present the results more clearly. The outcomes are visualized in Figure 4.7 and Figure 4.8.

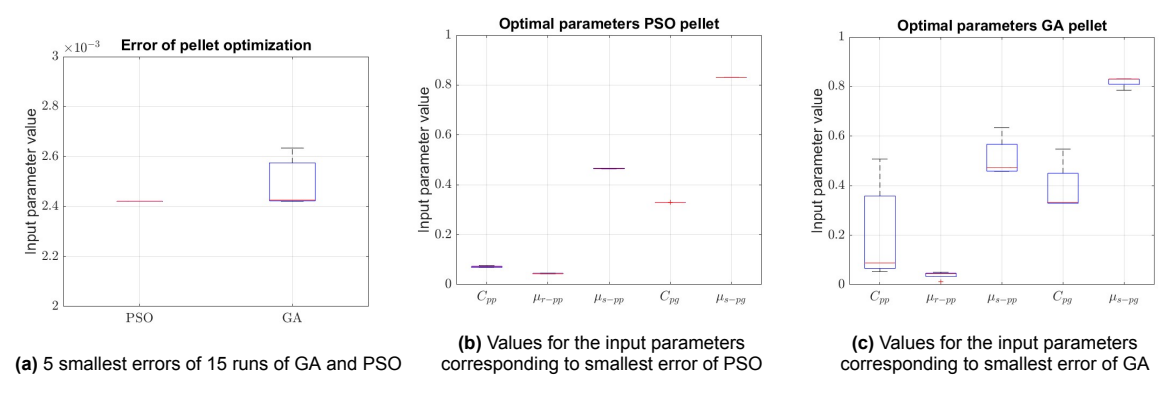


Figure 4.7: Optimization results for pellet

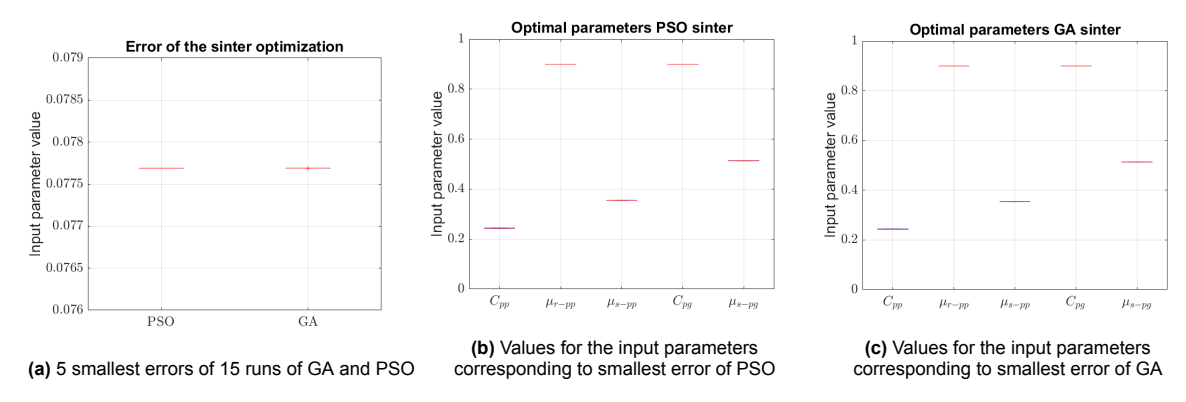


Figure 4.8: Optimization results for sinter

Based on these findings, Table 4.5 shows the optimal parameter sets found for each material. PSO and GA find the same optimal parameter set, once they are fine-tuned.

Material							
Pellet	0.071	0.045	0.465	0.329	0.5	0.83	0.0024213
Sinter	0.243	0.9	0.355	0.9	0.5	0.514	0.077

Table 4.5: Optimal parameter set found for each material.

4.5. Comparison Performance of the Optimization Techniques

Based on these findings, the following overview has be created in Figure 4.9. In the case of pellet, GA also has a higher variability in the objective function value than PSO, which can also be seen in the resulting optimal parameters found for pellet using GA. For the sinter optimization, this difference is not observed.

Algorithm	Optimization Efficiency	Minimum Error Found	C_{pp}	μ_{r-pp}	μ_{s-pp}	C_{pg}	μ_{s-pg}
LO	Affected by initialization variables (initial guess)	Pellet: 0.1465	0.151	0.04	0.453	0.359	0.83
LO	Only locates local minima of error surface	Sinter: 3.1753	0.258	0.9	0.35	0.9	0.532
PSO	Able to identify global minima Requires fewer processing steps than GA	Pellet: 0.0024213	0.071	0.045	0.465	0.329	0.83
P30		Sinter: 0.077	0.243	0.9	0.355	0.9	0.514
CA	Able to identify global minima	Pellet: 0.0024213	0.071	0.045	0.465	0.329	0.83
GA	Requires more processing steps than PSO	Sinter: 0.077	0.243	0.9	0.355	0.9	0.514

Figure 4.9: Comparison of the performance of the three algorithms

Looking back on the evaluation metrics mentioned in section 2.9.5, these optimization techniques can be compared. The differences between the global and local optimization is clear, the objective function

value is much larger of the local optimization and the global optimization. However, it is interesting to see that the parameter inputs which are found for the local optimization are very similar to those found using global optimization. Only C_{pp} has a slightly larger difference for both materials. This is in line with what was found in the sensitivity analysis, that C_{pp} has an affect on all KPIs, and a slight difference in its value could cause a larger deviation in the objective function values. Local optimization does have the smallest variability and a significantly shorter run time than the global optimization methods. However, it is still not recommended due to its significant sensitivity to the user inputs.

The performance of PSO and GA are very similar, both are able to reach a small objective function and are not as sensitive to user inputs as local optimization. **PSO** is recommended because of its lower variability in the objective function value and PSO needs less iterations to converge to the minimum error. However, it should be highlighted that GA is also able to reach that minimum error.

That the performance of local optimization would be the least was anticipated. In literature it is documented that is very dependent on the initial guess [48] and these findings align with the results found in this study.

That PSO finds the optimal solution quicker than GA is also in line with research. PSO tends to converge faster in problems with smooth or continuous search spaces, often requiring fewer iterations or population evaluations. GA's operators (crossover, mutation) introduce more diversity, which can delay convergence but potentially avoids local minima better [61]. The fact that PSO performs better in this study means our fitting model is smooth and continuous, which could be expected because second-order polynomials are continuous and differentiable.

Another observation which was made, in these results, is the difference between the optimization results of pellet and sinter. LO, GA and PSO behave differently for both materials. This may be due to the smoother nature of the response surface for sinter compared to pellet, or due to differences in sensitivity of certain KPIs to parameter variation. It is also observed that the optimal input parameters for sinter are 0.9 for μ_{r-pp} and C_{pg} (the upper bound of the parameter range), which could mean that the optimal value lies outside this range. Further exploration would be needed to confirm this.

According to the polynomial model these parameter sets corresponding to the minimum objective function, should give KPIs closest to the experimental values. Using these input parameters the results of the polynomial model and the optimization are validated. The KPIs are discussed in the next section.

4.6. Simulation Results Pellet

Figure 4.10 compares the experimental KPIs and the simulation KPIs. The deviation between the mean of the two values are shown as percentages on the bars. The exact values can be found in Appendix H, where the values for sinter can also be found.

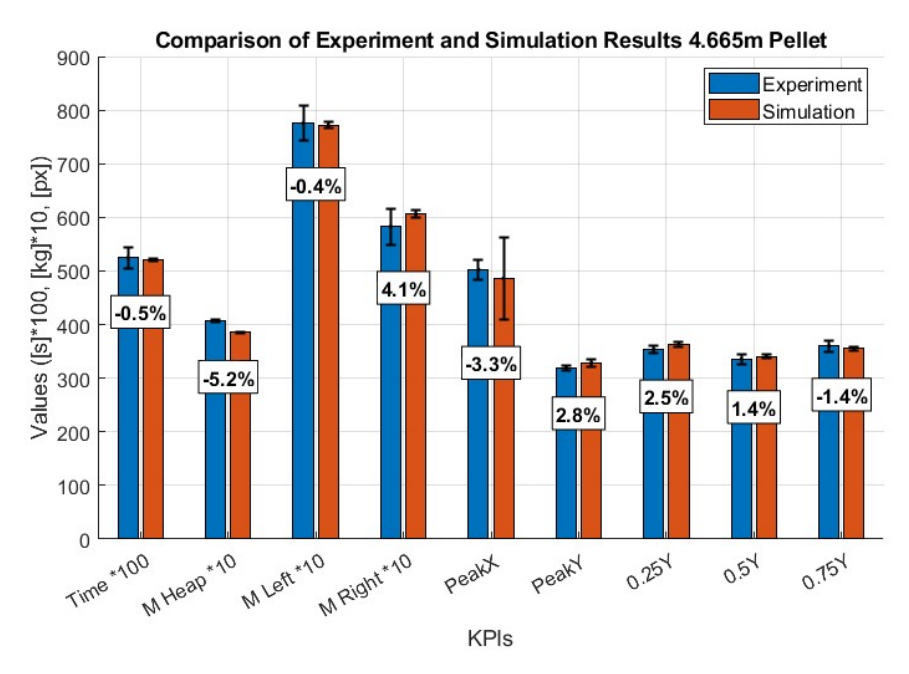


Figure 4.10: Comparison of the experimental and simulation KPIs of pellet. The percentages display the deviation of the mean compared to the experimental values. Note that some KPIs have been scaled for a better visualization.

In addition to numerical KPIs, visual comparison of heap shapes offers insight into simulation accuracy. Figure 4.11 overlays the contours of the experimental and simulated heaps, showing a visual analysis of how well the model replicates observed behavior. The standard deviation of the edges of the heaps are shown in the light red and blue color, the average edge is shown as a dark line and the highest points are shown as dots.

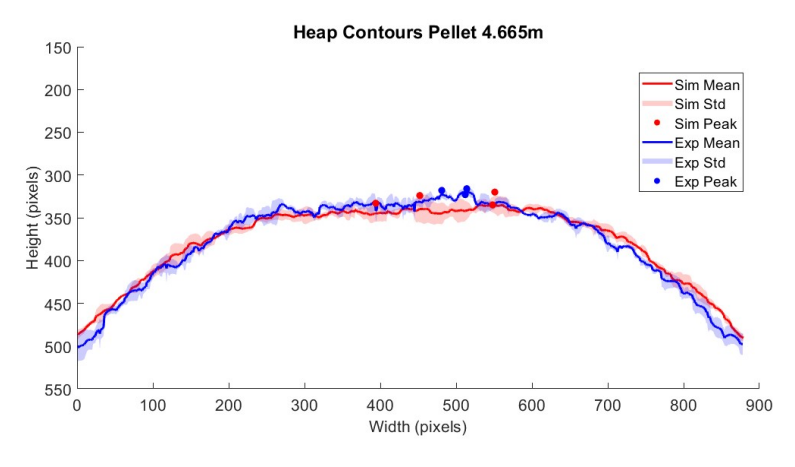


Figure 4.11: Edges of the heap of the optimal solution of pellet compared to the experimental heap edges.

Discharge time and the mass distribution all show very low deviations between simulation and experimental values, ranging from 0.4% to 5.2%, and the means lie well within each other's 95% confidence intervals. This suggests the simulation is able to capture the discharge time and mass distributions of

pellet.

For the heap shape KPIs (PeakX, PeakY, 0.25Y, 0.5Y, 0.75Y), the deviations are also very small, all under 3.5%, and again, the confidence intervals largely overlap. This indicates the simulated material closely resemble the experimental values.

The confidence intervals for the simulation values are generally narrower, indicating less variability, while the experimental data exhibit broader CIs, which is expected due to greater variability inherent in physical measurements.

As mentioned in Section 2.10, it is necessary to validate the results to ensure no overfitting has occurred.

4.7. Validation Pellet Simulations

Using the same optimal parameter set the height of the hopper is adjusted as shown in Section 2.5, Figure 2.4. The hopper height is decreased from 4.665 m to 3 m and 1m. The resulting KPIs of these simulations are again compared to their experimental counterparts, the results for 3m are shown in Subfigure 4.12a, and the resulting KPIs for 1m are shown in Subfigure 4.12b. Figure 4.13 shows the contours of the heaps and the highest points of the heaps. Like the simulations at 4.665m, these validation experiments are also run 4 times.

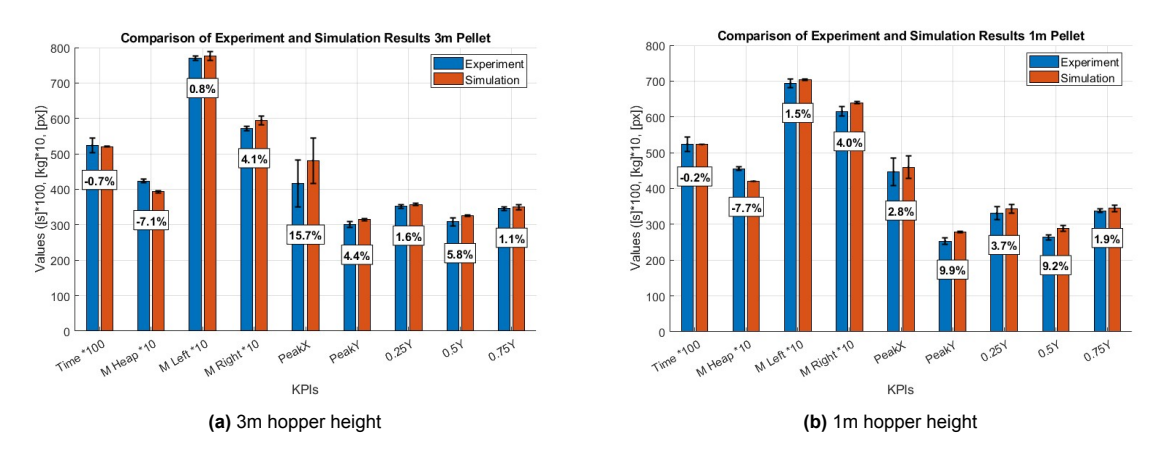


Figure 4.12: KPIs of the pellet simulation at different hopper heights. The percentages display the deviation of the mean compared to the experimental values. Note that some KPIs have been scaled for a better visualization.

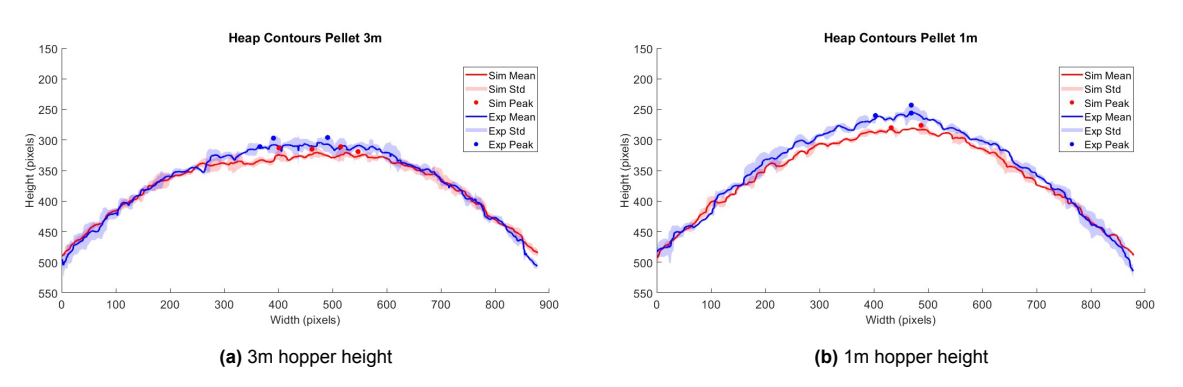


Figure 4.13: Edges of the pellet simulation at different hopper heights.

Generally it can be observed that the deviations increase when the hopper height decreases. When taking into account the confidence intervals they generally overlap for all KPIs, with the exception of the height halfway (0.5Y) and the y-coordinate of the peak (PeakY) at a hopper height of 1m. These are underpredicted when compared to the experimental results. Note that the graph may be misleading

because the simulation results of the heap shape are shown as higher values than the contour images, this is because pixels in the vertical direction are counted the other way around than a traditional coordinate system (so a high pixel count means a lower position of the heap). An equivalent analysis was conducted for the sinter simulations.

4.8. Simulation Results Sinter

Figure 4.14 compares the sinter experimental KPIs and the simulation KPIs. Figure 4.15 shows the edges of the heap of the sinter simulation compared to the experimental contours of the heap. These are presented the same way as the results of pellet.

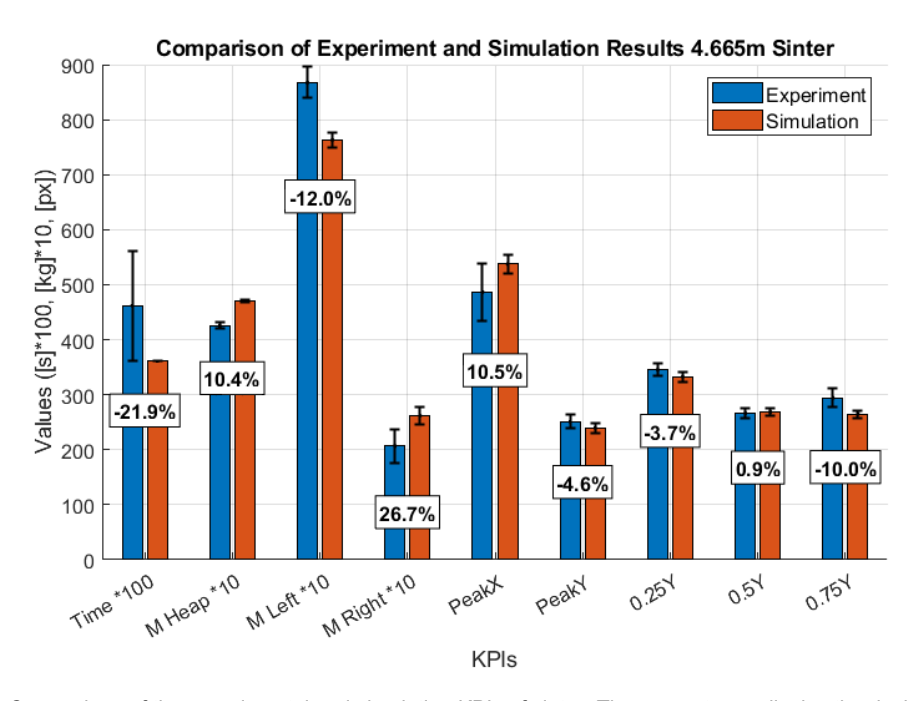


Figure 4.14: Comparison of the experimental and simulation KPIs of sinter. The percentages display the deviation of the mean compared to the experimental values. Note that some KPIs have been scaled for a better visualization.

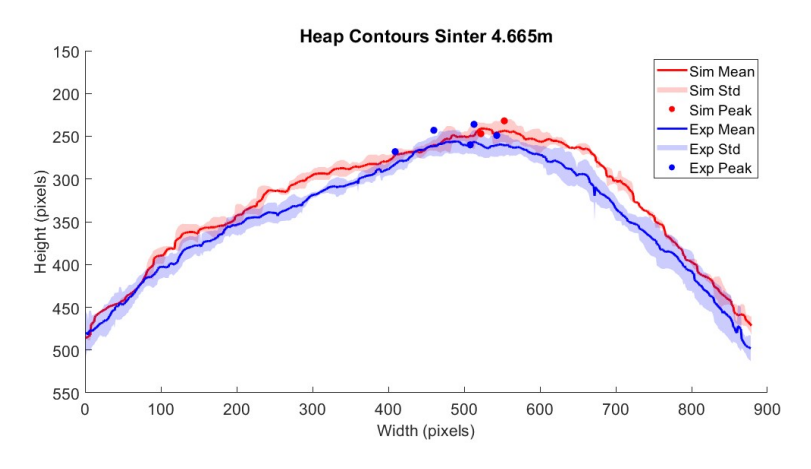


Figure 4.15: Edges of the heap of the optimal solution of sinter compared to the experimental heap edges.

Note that the deviations between the means of the KPIs are quite large, where most are around to 10% and the discharge time and the mass on the right even above 20%. However, some deviations look large numerically, but the confidence intervals do overlap in many cases, indicating that the variation

in the experimental data might account for the observed differences.

For the discharge time, the experimental value is 4.6191 ± 0.72 , giving a 95% confidence interval (CI) of [3.8991, 5.3391], while the simulation reports a value of 3.61 with no variation (found in Appendix H). Although the simulation mean falls just below the experimental CI, it is close to the lower bound, making this a borderline case for overlap. In the case of the mass on the right side, the experimental value is 20.68 ± 3.82 , yielding a CI of [16.86, 24.5], and the simulation gives 26.2 ± 2.46 , corresponding to a CI of [23.74, 28.66]. Here, the CIs slightly overlap because the experimental upper bound (24.5) overlaps with the simulation's lower bound (23.74). Despite the noticeable difference in means, the overlapping confidence intervals suggest the values are not drastically inconsistent, and the difference may be explained by the variability in the experimental data.

4.9. Validation Sinter Simulations

Like pellet, the experiments of sinter are performed at different hopper heights if which the results are shown in Figure 4.16 and the contours of the edges are shown in Figure 4.17.

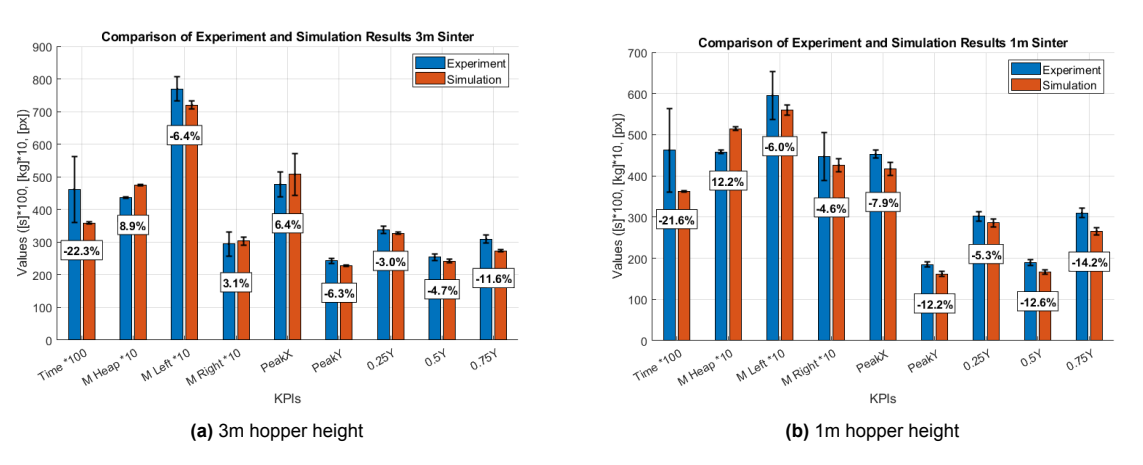


Figure 4.16: KPIs of the sinter simulation at different hopper heights. The percentages display the deviation of the mean compared to the experimental values. Note that some KPIs have been scaled for a better visualization.

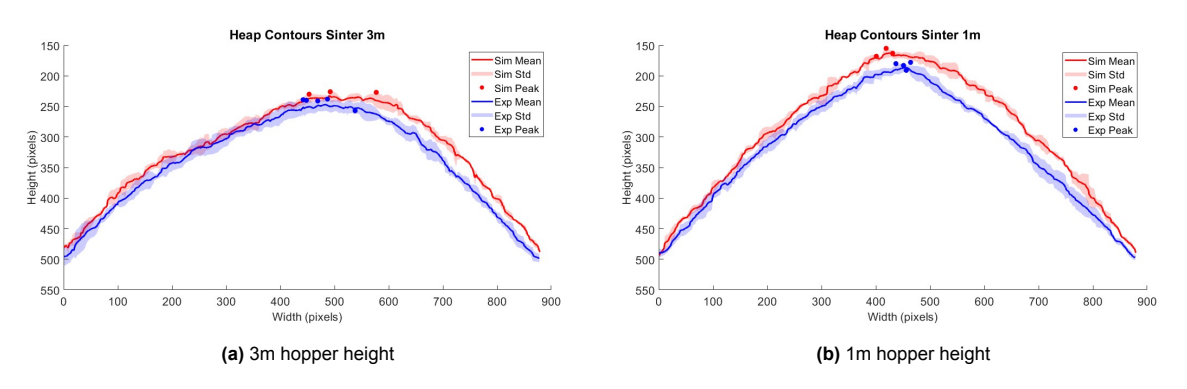


Figure 4.17: Edges of the sinter simulation at different hopper heights.

As can be seen in these figures, the deviation becomes larger when the hopper height decreases, especially the deviation for the heap height halfway, where the deviation increases from 0.9% to 4.7% to 12.6%. This can be seen clearly in the figures of the contours. Also when taking into account the variability of the results, there is no overlap for the KPI results of the heap height halfway and at three quarters at a hopper height of 1m. Notably, the mass distribution shows less deviation when compared to the hopper height of 4.665m. The deviation of the discharge time remains large and the other KPIs keep a similar deviation.

4.10. Discussion Results

4.10. Discussion Results

The deviation between the simulation and experimental results could be attributed to several factors. A notable observation is the higher degree of deviation exhibited by sinter in comparison to pellet. Furthermore, the validation results demonstrated greater deviation than the results obtained from the highest hopper height. These observations will be discussed in the following section.

4.10.1. Sensitivity Analysis

During the sensitivity analysis, the original KPI, pixel count of the heap, was used to assess parameter influence. However, in later stages of the study, this KPI was refined to pixel height at different fixed locations, providing a more detailed representation of heap shape. This change may have influenced the sensitivity analysis results, as the selected dominant parameters were based on the initial metric rather than the final one. This would need to be investigated further to check if it affects the results of the sensitivity analysis.

4.10.2. Objective Function Value

As can be seen in the Figures 4.10 and 4.14, the experimental results of sinter have a higher variability than pellet because the error bars of sinter are mostly wider than those of pellet.

As can be seen in Table 4.6, the experimental KPIs of sinter like the x-coordinate of the peak has a high variability. However, the average of the experimental values is taken into with the same weights as, say the masses at different location even though their variability is much lower.

KPI	Time	M heap	M left	M right	Peak X	Peak Y	0.25Y	0.5Y	0.75Y
Pellet	0.246906	0.169967	2.65623	2.694851	15.36952	2.94392	5.557777	7.133645	8.041559
Sinter	0.950216	0.56356	2.554486	2.752562	47.04296	11.51347	10.22546	8.158431	15.71751

Table 4.6: Standard deviation of the experimental results of sinter and pellet.

What could therefore improve the results, is adding weights to the objective function based on the standard deviation as shown the following equation.

$$\mathsf{Error} = \sum_{k=1}^{n} w_k \left(\frac{\mathsf{Target} \; \mathsf{KPI}_k - \mathsf{Predicted} \; \mathsf{KPI}_k}{\mathsf{Target} \; \mathsf{KPI}_k} \right)^2 \tag{4.1}$$

where w_k is a weighting factor applied to each KPI. For the sinter calibration, these weights were chosen based on the inverse of the squared relative standard deviation (RSD) of the experimental values:

$$w_k = \frac{1}{\mathsf{RSD}_k^2} \tag{4.2}$$

This weighting approach could ensure that KPIs with high experimental variability contribute less to the total error, allowing the optimization to focus more strongly on reliable measurements. Further investigation would be needed to confirm this.

4.10.3. Fitting Model

There was a low \mathbb{R}^2 value for several KPIs as could be seen in Table 4.1, especially for the discharge time, which is in line with the results. The \mathbb{R}^2 value was the lowest value for the discharge time and the discharge time also showed the highest deviation in the results. This means more simulations with different input parameters need to be performed in order to increase the \mathbb{R}^2 value. Another option would be to try a different fitting model instead of polynomial regression. Different fitting models are better at capturing different relationships and will therefore likely give different results [48], it would need to be tested to see if these results improve.

4.11. Conclusion 45

4.11. Conclusion

It can be concluded that particle swarm optimization and genetic algorithm are both capable of finding the minimum error, and have a better performance than local optimization. While the global optimization methods require more computational time than local optimization, the improved accuracy and reduced sensitivity to initial guesses makes them more suitable for this calibration task.

Both GA and PSO converge to the same optimal objective function, however, PSO needs less runs to achieve this. Meaning PSO is the recommended optimizer in this situation. The optimal parameter set found using PSO, gives excellent simulation results for pellet, including the validation results. However, the KPIs of the sinter validation results come close but still has some significant deviations from the experimental values.

This work provides a strong foundation for multi-objective optimization of DEM models of sinter and pellet. One of the most important takeaways from this study is the value of evaluating the calibration using multiple KPIs. If the comparison had only been based on one KPI, the calibration might have looked much better than it actually was. By using a range of KPIs that describe discharge time, mass distribution and heap shape, a more complete picture of the material behavior was captured. This made it possible to identify where the model performed well and where it did not, and helped avoid drawing conclusions based on limited information. It also made sure that there were no multiple parameter sets possible as the optimal result.

It also became clear how important the validation step is. While the calibration results initially showed good agreement between the simulation and experimental KPIs at the original hopper height, this changed when the hopper height was adjusted. As the validation results showed, the deviations increased, especially for sinter, which highlights that a good agreement under one condition does not necessarily mean the model will perform well under different conditions. Without this validation step, it would have been easy to assume the calibration was accurate, while in reality the model was overfitted to a single setup.

Case Study: Mixture Simulation

Once pellet and sinter have been calibrated the mixture model can be made and tested. The mixture consists of 50% of pellet and 50% of sinter.

5.1. Results Mixture Simulation

In a study performed by Chakrabarty *et al* [8], the interaction parameter values are found by taking the average between the interaction parameter values of sinter and pellet. These lead to good results and is therefore tested in this thesis. The averages of sinter and pellet interaction parameters lead to the following interaction parameters for the mixture as seen in Table 5.1.

DEM input parameter	Pellet-Sinter
C_{es}	0.157
μ_{r-es}	0.473
μ_{s-es}	0.41

Table 5.1: DEM parameters chosen for pellet-sinter interactions.

With these input parameters the following KPIs, see Figure 5.1, were found. The exact results can also be found in Appendix H.

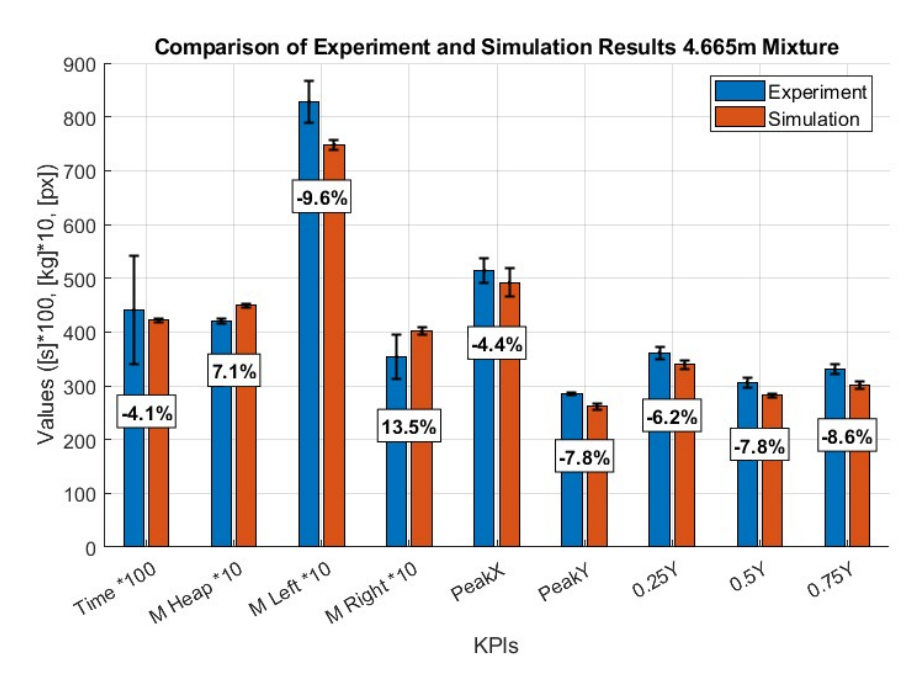


Figure 5.1: Resulting KPIs of the simulations compared to the experimental values.

The edges of the heaps from the experimental and simulation heaps can be observed in Figure 5.2.

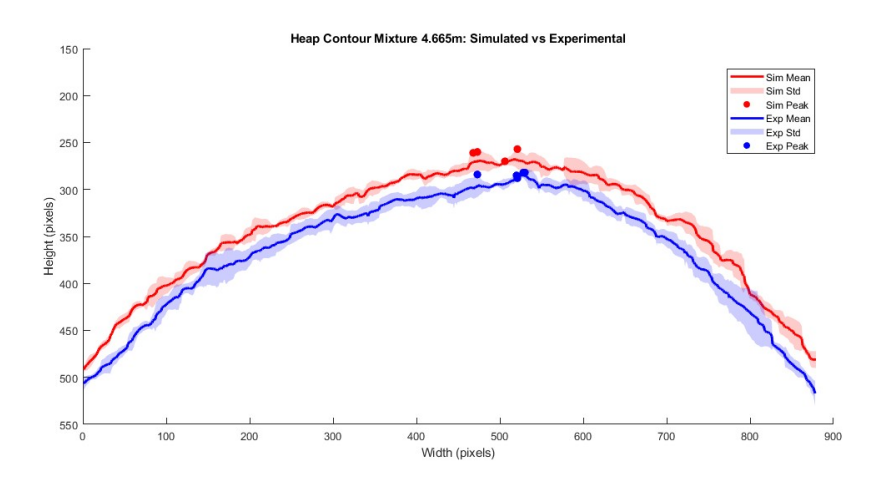


Figure 5.2: Edges of the experimental and the simulation heap of the mixture. Note that some KPIs have been scaled for a better visualization.

As can be observed from the table, the deviation of most KPIs are under the 10%. Only the mass at the right side is slightly higher, which can also be observed in the figure. This was also the case for sinter simulations.

What is interesting to see is that the simulation heap height is slightly higher than the experimental heap height. Interestingly, this is a different outcome than for the pellet and sinter components, where the experimental heap was slightly higher than the simulation heap. Further investigation is necessary to come up with reasons for this difference.

5.2. Segregation 48

5.2. Segregation

One of the key factors influencing the efficiency of the blast furnace, as outlined in Chapter 1, is the segregation of the sinter-pellet mixture. Therefore, one of the main goals for researchers, is to eventually develop a model that can predict segregation behavior inside the blast furnace. For that reason, segregation in the mixture is an important KPI to consider and evaluate here.

To quantify segregation, the Relative Standard Deviation (RSD) is used. This index gives a measure of how well mixed or segregated the material is across the heap. The calculation is based on image analysis of the colored heap.

Figure 5.3 is used to calculate the RSD of the mixture. In the experiments, pellets were dyed blue to allow easier distinction between pellet and sinter particles in the images. These images were imported into MATLAB, and the pixel count of pellets and sinter was used to determine the RSD.

The MatLab script used for this analysis is adapted from code provided by Ahmed Hadi, PhD researcher at Dingena Schott's Lab, with some modifications including the color mask and the exclusion of tiles with zero pixels, as shown in Appendix D, Section D.3. The heap image is divided into tiles and the pixel fraction (R_{ij}) is calculated for each tile as follows:

$$R_{ij} = \frac{\sum E_{ij}}{\sum E_{ij} + \sum S_{ij}} \tag{5.1}$$

Here, $\sum E_{ij}$ and $\sum S_{ij}$ represent the number of white pixels (i.e., detected particles) for pellet and sinter, respectively, in tile (i,j). The RSD is calculated using the average (\bar{R}) and standard deviation (σ_i) of R_{ij} over all tiles as follows:

$$RSD = \frac{\sigma_i}{\bar{R}} \tag{5.2}$$

This process is visualized in Figure 5.3, showing how the image is processed from raw data to tiled analysis. In this image the top row show the experimental and the simulation heap, the following rows only show the simulation results, however the same technique has been applied to the experimental results.

5.2. Segregation 49

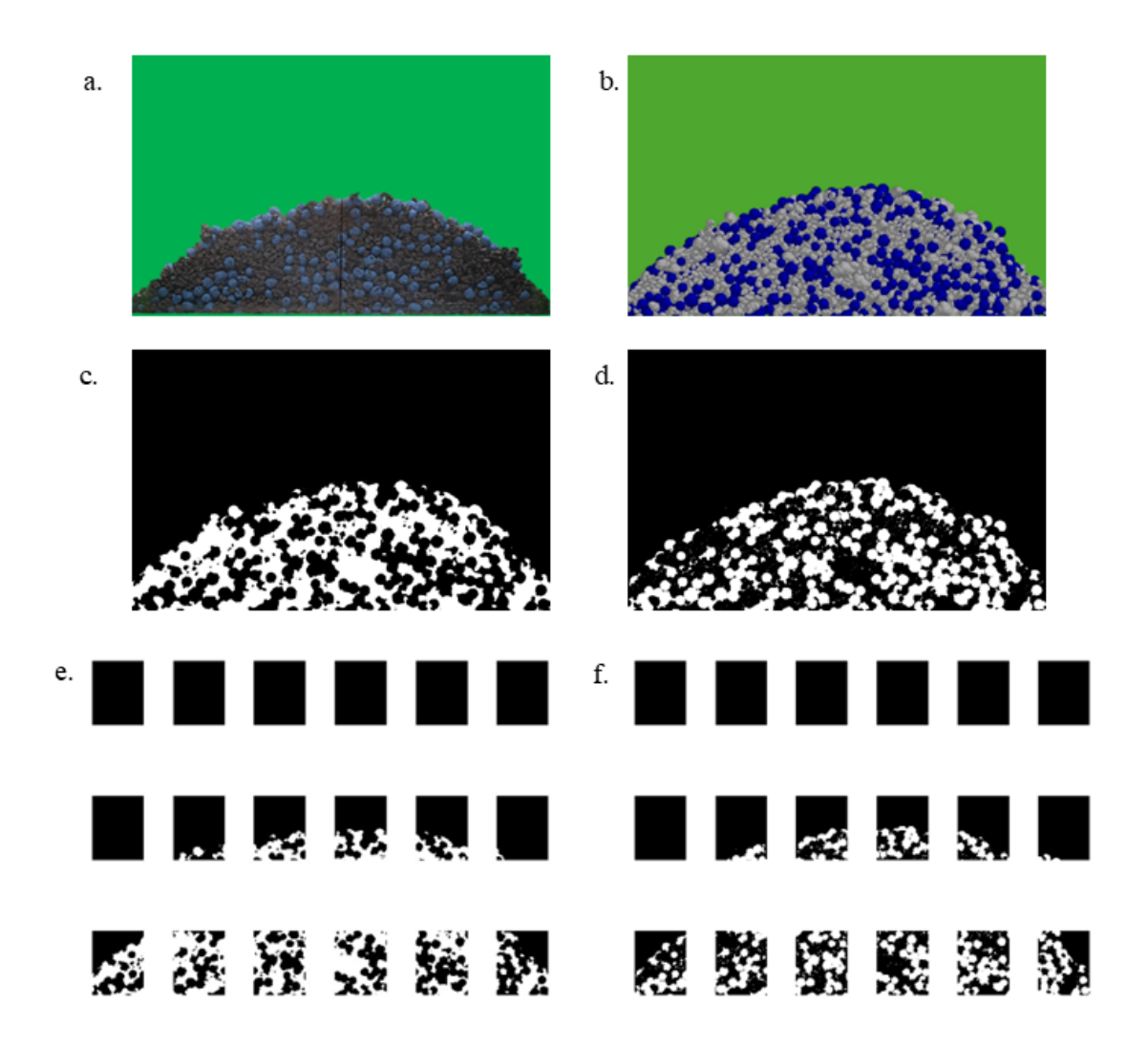


Figure 5.3: Segregated heap of the multi-component mixture, analyzed by dividing the image into tiles for RSD (relative standard deviation) calculation. From top left to bottom right: (a) edited experimental heap image, (b) edited simulation heap showing colored components, (c) highlighted simulation pellet particles, (d) highlighted simulation sinter particles, (e) tiled image of simulation pellet particles, and (f) tiled image of simulation sinter particles.

The results of the experimental and simulation values are found in Table 5.2. The values are close, with overlapping confidence intervals.

Exp RSD (95% CI, n=5)	0.311 ± 0.075
Sim RSD (95% CI, n=4)	0.313 ± 0.191

Table 5.2: RSD values for the mixture of sinter and pellet.

See Appendix I for all the simulation results and the experimental results. The simulation slightly over-predicts the segregation, but the difference falls within the range of experimental variation. A possible explanation is the difficulty in detecting all pellet particles in the experimental images. In some cases, the blue color was not picked up cleanly, which may have led to a slightly lower RSD value.

5.3. Conclusion 50

5.3. Conclusion

The calibration process for the mixture, composed of 50% pellet and 50% sinter, was performed using averaged interaction parameter values from the individually calibrated materials. This method, following the approach by Chakrabarty *et al.* [8], led to relatively accurate results when compared with experimental data. Most KPIs showed deviations below 10%. With the exception being the mass on the right, with a deviation of 13.5%. A notable discrepancy was observed in the heap shape over the whole profile. This difference is likely caused by the relatively high rolling friction values assigned to sinter in the model, which may restrict material from flowing to the sides and result in a taller heap shape.

Segregation of the mixture was also evaluated, since this is a key performance indicator for blast furnace applications where segregation of components can affect process efficiency. The RSD was used as a measure of segregation, and was calculated from both simulation and experimental images using the same image analysis method. The simulated RSD was 0.313, while the experimental RSD was 0.311. These values are very close, and the confidence intervals overlap. While the simulation slightly overpredicts segregation, the results show that the model captures the degree of separation between pellet and sinter well. Minor differences may also be due to limitations in image detection and processing.

Although the RSD shows strong agreement, the simulation is less accurate in predicting the other KPIs. This suggests that the model is more successful in reproducing the distribution of different materials in the heap than in fully capturing the behavior responsible for heap formation, mass distribution and discharge time. The geometric KPIs, such as heap height, are more sensitive to contact parameters like rolling friction and restitution, which remain a source of uncertainty, particularly for sinter, which already showed deviations during its individual validation.

In summary, the mixture model was successful in reproducing the segregation, and showed moderate accuracy in heap geometry. These results indicate that the current model is capable of capturing some behavior of the sinter–pellet mixture. However, some differences remain, particularly in heap shape and mass distribution, which could potentially be improved by refining frictional parameters and further validating the individual components, however, further investigation would need to be performed.



Conclusion and Recommendations

6.1. Conclusion

This study aimed to compare different optimization techniques for pellet and sinter DEM simulations. These could be compared by looking at the efficiency of the optimizer and the accuracy of the KPIs found with the optimal parameter set. The results show that both PSO and GA were able to identify highly accurate parameter sets that produced DEM simulation results closely matching experimental KPIs. However, PSO consistently required fewer iterations to converge, making it the most computationally efficient method. Local Optimization, while fast, showed high sensitivity to initial guesses and was therefore not recommended. These findings show that global optimization methods, particularly PSO, are more suitable for DEM calibration when multiple KPIs are considered.

The determination of DEM input parameters follows a structured approach that includes three key steps: defining known material and morphological properties, identifying influential parameters, and calibrating those parameters against experimental outcomes. Parameters such as particle size, density, and shape can often be sourced from literature or measured directly. Parameters that influence the interaction between particles, like friction and restitution coefficients, are more complex and require calibration. A sensitivity analysis helps to prioritize which of these have the most impact on the simulation results. Finally, optimization techniques are applied to adjust these dominant parameters so that the simulation outputs closely match experimental data.

The sensitivity analysis revealed that the coefficient of restitution and the static friction coefficients had the most significant effect on the KPIs. In contrast, the rolling friction between geometry and pellet had minimal influence and was therefore excluded from the calibration. These findings helped narrow the focus to the parameters with the highest impact on simulation accuracy.

PSO consistently outperformed GA in computational efficiency, requiring fewer iterations while achieving high accuracy. LO proved sensitive to initial parameter guesses, making it less suitable for complex parameter spaces. To validate the calibrated parameter values, simulation results were compared against experimental data at multiple hopper heights. The optimized DEM models generally replicated experimental KPIs successfully, especially the pellet simulations, validating the framework's effectiveness. The validation of the sinter simulation lead to less accurate KPIs, meaning further investigation is necessary. Both GA and PSO converged to the same optimal objective function, however PSO did so in less runs, leading to a preference of the latter.

Lastly a case study was performed where the sinter and pellet were combined to create a DEM simulation of the mixture. The average of the interaction parameters of the individual components was taken as the interaction coefficients of the pellet and sinter. In the mixture, a new KPI was measurable, the segregation index, which plays an important part in the blast furnace efficiency. The simulation in this study was able to capture the segregation well because it was found that the indices of the simulation and the experiments are very close. However, the values of the other KPIs had a larger deviation, meaning a more in-depth investigation needs to be performed.

6.2. Recommendations 52

6.2. Recommendations

Many studies about the calibration of DEM simulations have been performed, it is a large field with a lot of potential for further investigation. This thesis lays a groundwork for multi-objective optimization. There are several recommendations for future work to further expand this study.

One of the main challenges of this study was the computational expense of simulations, largely due to the complex shape of sinter particles but also the general complexity of DEM simulations. This led to assumptions about the dominant parameters in sinter simulation. Therefore, to improve this study, one of the first areas to look at in further depth, is the sensitivity analysis of sinter.

The current study used a Plackett-Burman design to identify the most influential parameters, but this method has limitations in terms of the number of levels it considers and its ability to capture interaction effects between parameters. For this study it was sufficient for pellet but might not be for sinter. Plackett-Burman has limitations in the number of levels it considers and its ability to capture interaction effects between parameters.

Beyond the sensitivity analysis, there is a much broader range of techniques which can be used for the steps of calibrating a material. Instead of using CCD there are many other options such as Latin Hypercube Sampling, Full Factorial Design, and Box Behnken. Since the choice of sampling method directly influences the response surface model's ability to capture parameter-KPI relationships, comparing and identifying the most effective technique could improve the calibration process.

The same goes for the fitting method used to model the relationship between input parameters and KPIs. Alternative techniques, such as Gaussian Process Regression, Neural Networks, or Support Vector Regression, to name a few, could offer advantages. Furthermore, these could also have an effect on the performance of the optimization algorithms, leading to a different variability, different amount of necessary iterations or a smaller objective function.

Additionally, the interaction parameters of the sinter-pellet mixture could also be calibrated. Using the same techniques as the calibration of sinter and pellet instead of taking the average of the individual materials for the interaction parameters could lead to different results.

Lastly, looking at different KPIs which were not measured in the experiments could be useful as they might be affected by the input parameters. Examples could include the shape of the heap on the side of the container or flow properties of the materials when it flows of the scale. Further investigation would be necessary to see if these are affected by the parameters.

The investigation of these aspects could lead to an improved calibration strategy.

6.3. Broader Impact

This study has implications for the scientific community, industry, and society as a whole, as it develops a more reliable DEM calibration framework using multi-objective optimization.

From a scientific perspective, this research highlights the importance of using multiple KPIs during the calibration process. Many prior studies have often relied on single KPIs (often the angle of repose) which leads to underdetermined systems and a blind-spot for the accuracy of the parameter sets. By using a broader range of KPIs, this study demonstrates how to reduce ambiguity in the calibration process. This approach sets a start for future DEM studies, encouraging multi-objective calibration strategies that better reflect the complexity of granular material behavior.

From a societal and industry level, more accurate and efficient DEM simulations have a direct implication for the steel industry, one of most energy-intensive and polluting sectors worldwide [62]. Improved calibration can help engineers better predict material flow in blast furnaces, ensuring smarter design, minimizing waste, and reducing the energy consumption. In turn, this contributes to the broader goals of sustainability, decarbonization in manufacturing, and a stronger competitive position. Contributing to better health, a stronger economy, and a more sustainable planet.

Moreover, the benefits of accurate DEM models extend beyond steelmaking to industries such as agriculture, pharmaceuticals, and mining. In these fields, improved calibration can support more efficient, data-driven, and environmentally conscious industrial processes.

- [1] Ahmed Hadi et al. "DEM Modelling of Segregation in Granular Materials: A Review". In: KONA Powder and Particle Journal 41 (2024), pp. 78–107.
- [2] Dixon Valve & Coupling Company. 6 Steps of the Steel Manufacturing Process. Copyright © Dixon Valve & Coupling Company, LLC 2021-2025. 1 Dixon Square, Chestertown, MD 21620, US, Nov. 2023. URL: https://dixonvalve.com/en/news-and-events/news/6-steps-steel-manufacturing-process.
- [3] C.K. Ho et al. "Experimental and numerical investigations of gouge formation related to blast furnace burden distribution". In: *Minerals Engineering* 22.11 (2009). Cited by: 56, pp. 986–994. DOI: 10.1016/j.mineng.2009.03.004. URL: https://www.scopus.com/inward/record.uri? eid=2-s2.0-67650711457&doi=10.1016%2fj.mineng.2009.03.004&partnerID=40&md5=8e0cfc6f398d930ea95131a449d62936.
- [4] Chin Eng Loo, Leanne Tracy Matthews, and Damien Paul O'Dea. "Lump ore and sinter behaviour during softening and melting". In: *ISIJ International* 51.6 (2011). Cited by: 76; All Open Access, Gold Open Access, Green Open Access, pp. 930–938. DOI: 10.2355/isijinternational.51. 930. URL: https://www.scopus.com/inward/record.uri?eid=2-s2.0-80054074576&doi=10. 2355%2fisijinternational.51.930&partnerID=40&md5=e8c0cb55052ffcd490a05e128a4e910 b.
- [5] Yongliang Yang et al. "Development of blast furnace burden distribution process modeling and control". In: ISIJ International 57.8 (2017). Cited by: 36; All Open Access, Gold Open Access, Green Open Access, pp. 1350–1363. DOI: 10.2355/isijinternational.ISIJINT-2017-002. URL: https://www.scopus.com/inward/record.uri?eid=2-s2.0-85027858902&doi=10.2355%2fisijinternational.ISIJINT-2017-002&partnerID=40&md5=c1a8a3911f0089ee9316f a3dbe3134af.
- [6] B.D. Pandey and U.S. Yadav. "Blast furnace performance as influenced by burden distribution". In: *Ironmaking and Steelmaking* 26.3 (1999). Cited by: 28, pp. 187–192. DOI: 10.1179/030192 399677059. URL: https://www.scopus.com/inward/record.uri?eid=2-s2.0-0032660894&doi=10.1179%2f030192399677059&partnerID=40&md5=ac4e827450b26cedaed3552c2b09ae0b.
- [7] Haifeng Li et al. "Model-based analysis of factors affecting the burden layer structure in the blast furnace shaft". In: *Metals* 9.9 (2019), p. 1003.
- [8] Arijit Chakrabarty et al. "Characterisation of binary mixtures of pellets and sinter for DEM simulations". In: Advanced Powder Technology 33.1 (2022), p. 103358. ISSN: 0921-8831. DOI: https://doi.org/10.1016/j.apt.2021.11.010. URL: https://www.sciencedirect.com/science/article/pii/S0921883121005380.
- [9] Raïsa Roeplal, Yusong Pang, and Dingena Schott. "Effects of pellet-sinter interaction parameters on component segregation and bed porosity considering flow velocity and mixture composition: A DEM study". In: Advanced Powder Technology 35 (2024). This is an open access article under the CC BY-NC-ND license (http://creativecommons.org/licenses/by-nc-nd/4.0/), p. 104322. DOI: 10.1016/j.apt.2023.104322. URL: https://www.sciencedirect.com/science/article/pii/S0921883123003221.
- [10] P. A. Cundall and O. D. L. Strack. "A discrete numerical model for granular assemblies". In: *Géotechnique* 29.1 (1979), pp. 47–65. DOI: 10.1680/geot.1979.29.1.47. eprint: https://doi.org/10.1680/geot.1979.29.1.47. URL: https://doi.org/10.1680/geot.1979.29.1.47.
- [11] Christian Richter et al. "Development of a standard calibration procedure for the DEM parameters of cohesionless bulk materials Part II: Efficient optimization-based calibration". In: *Powder Technology* 360 (2020), pp. 967–976. ISSN: 0032-5910. DOI: https://doi.org/10.1016/j.powtec.2019.10.052. URL: https://www.sciencedirect.com/science/article/pii/S0032591019308757.

[12] M. Marigo and E. Stitt. "Discrete Element Method (DEM) for Industrial Applications: Comments on Calibration and Validation for the Modelling of Cylindrical Pellets". In: *KONA Powder and Particle Journal* 32 (Feb. 2015), pp. 236–252. DOI: 10.14356/kona.2015016.

- [13] X.Liu, Q. Wang, and Y. Wang. "Review of calibration strategies for discrete element model in quasi-static elastic deformation". In: *Sci Rep* 13 (2023), p. 13264. DOI: https://doi.org/10.1038/s41598-023-39446-2.
- [14] Dingena Schott et al. "Granular Flow to a Blast Iron Ore Furnace: Influence of Particle Size Distribution on Segregation of a Mixture". In: *Traffic and Granular Flow'15*. Springer. 2016, pp. 621–628.
- [15] Shiyu Wei et al. "Numerical analysis of the relationship between friction coefficient and repose angle of blast furnace raw materials by discrete element method". In: *Materials* 15.3 (2022), p. 903.
- [16] Deside Kudzai Chibwe et al. "Charge material distribution behaviour in blast furnace charging system". In: *Powder Technology* 366 (2020). Cited by: 21, pp. 22–35. DOI: 10.1016/j.powtec.2020.02.048. URL: https://www.scopus.com/inward/record.uri?eid=2-s2.0-85080079511&doi=10.1016%2fj.powtec.2020.02.048&partnerID=40&md5=768009c62bc2fd0f2aa2bece263f09d3.
- [17] Chengzhi Li et al. "The angle of repose and size segregation of iron ore granules: DEM analysis and experimental investigation". In: *Powder Technology* 320 (2017), pp. 257–272.
- [18] Sida Liu et al. "Numerical investigation of burden distribution in a blast furnace". In: *steel research international* 86.6 (2015), pp. 651–661.
- [19] Ahmed Hadi et al. "Identification of dominant DEM parameters for multi-component segregation during heap formation, hopper discharge and chute flow". In: *Powder Technology* 444 (June 2024), p. 119985. DOI: 10.1016/j.powtec.2024.119985.
- [20] C. J. Coetzee. "Calibration of the Discrete Element Method and the Effect of Particle Shape". In: *Powder Technology* 297 (2016), pp. 50–64. URL: https://www.sciencedirect.com/science/article/pii/S0032591016301620.
- [21] Raïsa Roeplal, Yusong Pang, and Dingena Schott. "Towards Realistic DEM Modeling of Blast Furnace Mixture Charging: Calibration and Verification of Model Parameters under High-Velocity Flow Conditions". In: *Powder Technology* (2025). Under review.
- [22] C. J. Coetzee and O. C. Scheffler. "Calibration of DEM Parameters for Bulk Modeling of Cohesive Materials". In: *Processes* 11.1 (2022), p. 5. URL: https://www.mdpi.com/2227-9717/11/1/5/pdf.
- [23] J. Quist and M. Evertsson. "Framework for DEM Model Calibration and Validation". In: 14th European Symposium on Comminution and Classification (2015). URL: https://www.researchgate.net/profile/Johannes-Quist/publication/308990814_Framework_for_DEM_Model_Calibration_and_Validation/links/57fcdfe408aeb857afa09542/Framework-for-DEM-Model-Calibration-and-Validation.pdf.
- [24] A. P. Grima and P. W. Wypych. "Development and Validation of Calibration Methods for Discrete Element Modelling". In: *Granular Matter* 13.3 (2011), pp. 205–214. URL: https://link.springer.com/article/10.1007/s10035-010-0197-4.
- [25] V. A. Payor A. V. Boikov R. V. Savelev. "DEM Calibration Approach: Design of Experiment". In: *Journal of Physics: Conference Series* 1015 (2018), p. 032017. URL: https://iopscience.iop.org/article/10.1088/1742-6596/1015/3/032017/meta.
- [26] L. Benvenuti, C. Kloss, and S. Pirker. "Identification of DEM Simulation Parameters by Artificial Neural Networks and Bulk Experiments". In: *Powder Technology* 301 (2016), pp. 174–183. URL: https://www.sciencedirect.com/science/article/pii/S003259101630002X.

[27] F. Ye et al. "Calibration and Verification of DEM Parameters Using Backpropagation Neural Networks". In: Advanced Powder Technology (2019). URL: https://www.researchgate.net/profile/Fangping-Ye/publication/329173098_Calibration_and_verification_of_DEM_parameters_for_dynamic_particle_flow_conditions_using_a_backpropagation_neural_network/links/5c8f5f4e45851564fae49f63/Calibration-and-verification-of-DEM-parameters-for-dynamic-particle-flow-conditions-using-a-backpropagation-neural-network.pdf.

- [28] M. J. Chegeni M. Asghari M. Noaparast. "Implementation of DEM to calibrate contact parameters, as a novel simulation of the elastoplastic behavior of green iron pellet classified by roller screen". In: *Advanced Powder Technology* (2024). DOI: 10.1016/j.apt.2023.12.015. URL: https://www.sciencedirect.com/science/article/pii/S092188312400133X.
- [29] G. Degrassi et al. "Discrete element simulation of the charge in the hopper of a blast furnace, calibrating the parameters through an optimization algorithm". In: SN Applied Sciences (2021). DOI: 10.1007/s42452-021-04254-8. URL: https://link.springer.com/content/pdf/10. 1007/s42452-021-04254-8.pdf.
- [30] H. Wei et al. "Measurement and simulation validation of DEM parameters of pellet, sinter, and coke particles". In: *Powder Technology* (2020). URL: https://research.abo.fi/files/272807 95/Measurement_and_simulation_validation_of_DEM_parameters_of_pellet_sinter_and_coke_particles.pdf.
- [31] Heinrich Hertz. In: Journal für die reine und angewandte Mathematik 1882.92 (1882), pp. 156–171. DOI: doi:10.1515/crll.1882.92.156. URL: https://doi.org/10.1515/crll.1882.92.156.
- [32] Luigi C. Capozzi, Antonello A. Barresi, and Roberto Pisano. "Supporting data and methods for the multi-scale modelling of freeze-drying of microparticles in packed-beds". In: *Data in Brief* 22 (2019), pp. 722–755. ISSN: 2352-3409. DOI: https://doi.org/10.1016/j.dib.2018.12.061. URL: https://www.sciencedirect.com/science/article/pii/S2352340918316019.
- [33] Altair EDEM. *EDEM Simulator Settings*. https://help.altair.com/EDEM/Simulator.htm. [Online; accessed 2024-07-05]. 2024.
- [34] D. L. Schott A. Hadi Y. Pang. "Calibration of DEM parameters for multi-component segregation". In: *ICBMH2023: 14th International Conference on Bulk Materials Storage, Handling, and Transportation.* 2023. URL: https://search.informit.org/doi/pdf/10.3316/informit.446099244110008.
- [35] Marco Lupo et al. "Calibration of Dem Simulation of Cohesive Particles". In: Chemical Engineering Transactions 74 (May 2019), pp. 379–384. DOI: 10.3303/CET1974064. URL: https://www.cetjournal.it/index.php/cet/article/view/CET1974064.
- [36] Michael Rackl and Kevin J Hanley. "A methodical calibration procedure for discrete element models". In: *Powder technology* 307 (2017), pp. 73–83.
- [37] Edouard Izard, Maxime Moreau, and Pascal Ravier. "Discrete element method simulation of segregation pattern in a sinter cooler charging chute system". In: *Particuology* 59 (2021). Towards Modelling Solids and Multiphase Flow for Large Scale Industrial Systems and Applications, pp. 34–42. ISSN: 1674-2001. DOI: https://doi.org/10.1016/j.partic.2020.08.004. URL: https://www.sciencedirect.com/science/article/pii/S1674200120300900.
- [38] D. Hernández-Delfin et al. "Shape matters: Competing mechanisms of particle shape segregation". In: *Phys. Rev. E* 106 (5 Nov. 2022), p. 054614. DOI: 10.1103/PhysRevE.106.054614. URL: https://link.aps.org/doi/10.1103/PhysRevE.106.054614.
- [39] Stephen J. Roskilly et al. "Investigating the effect of shape on particle segregation using a Monte Carlo simulation". In: *Powder Technology* 203.2 (2010), pp. 211–222. ISSN: 0032-5910. DOI: https://doi.org/10.1016/j.powtec.2010.05.011. URL: https://www.sciencedirect.com/science/article/pii/S0032591010002494.
- [40] Atsuko Shimoska et al. "Effect of Particle Shape on Size Segregation of Particles". In: *Chemical Engineering Transactions* 32 (2013). Ed. by Sauro Pierucci and Jiří J. Klemeš, p. 2143. ISSN: 1974-9791. URL: http://www.aidic.it/cet.

[41] Shunying Ji, Siqiang Wang, and Zongyan Zhou. "Influence of particle shape on mixing rate in rotating drums based on super-quadric DEM simulations". In: *Advanced Powder Technology* 31.8 (2020), pp. 3540–3550. ISSN: 0921-8831. DOI: https://doi.org/10.1016/j.apt.2020.06.040. URL: https://www.sciencedirect.com/science/article/pii/S0921883120303307.

- [42] R. Roeplal, Y. Pang, and D. Schott. "The effect of particle properties on binary mixture segregation during blast furnace charging". In: *Particles2023*. 2024. URL: https://www.scipedia.com/public/Roeplal_D._2024a.
- [43] Muhammad Kashif Saeed and Muhammad Shafiq Siraj. "Mixing study of non-spherical particles using DEM". In: *Powder Technology* 344 (2019), pp. 617–627. ISSN: 0032-5910. DOI: https://doi.org/10.1016/j.powtec.2018.12.057. URL: https://www.sciencedirect.com/science/article/pii/S0032591018310945.
- [44] Ya Zhao and Jia Wei Chew. "Effect of lognormal particle size distributions of non-spherical particles on hopper discharge characteristics". In: Chemical Engineering Research and Design 163 (2020), pp. 230–240. ISSN: 0263-8762. DOI: https://doi.org/10.1016/j.cherd.2020.09.001. URL: https://www.sciencedirect.com/science/article/pii/S0263876220304548.
- [45] C.M. Wensrich and A. Katterfeld. "Rolling friction as a technique for modelling particle shape in DEM". In: *Powder Technology* 217 (2012), pp. 409–417. ISSN: 0032-5910. DOI: https://doi.org/10.1016/j.powtec.2011.10.057. URL: https://www.sciencedirect.com/science/article/pii/S0032591011006000.
- [46] Mohammadreza Alizadeh et al. "The effect of particle shape on predicted segregation in binary powder mixtures". In: *Powder Technology* 319 (2017), pp. 313–322. ISSN: 0032-5910. DOI: ht tps://doi.org/10.1016/j.powtec.2017.06.059. URL: https://www.sciencedirect.com/science/article/pii/S0032591017305181.
- [47] Jeoungseok Yoon. "Application of experimental design and optimization to PFC model calibration in uniaxial compression simulation". In: *International Journal of Rock Mechanics and Mining Sciences* 44.6 (2007), pp. 871–889. ISSN: 1365-1609. DOI: https://doi.org/10.1016/j.ijrmms.2007.01.004. URL: https://www.sciencedirect.com/science/article/pii/S1365160907000135.
- [48] A. Hadi, M. Moradi, Y. Pang, et al. "Adaptive Al-based surrogate modelling via transfer learning for DEM simulation of multi-component segregation". In: *Scientific Reports* 14 (2024), p. 27003. DOI: 10.1038/s41598-024-78455-7. URL: https://doi.org/10.1038/s41598-024-78455-7.
- [49] Neda Hesam Mahmoudi Nezhad et al. "Comparison of Different Optimization Techniques in Electron Lens Design". In: 2023 9th International Conference on Optimization and Applications (ICOA). Oct. 2023, pp. 1–5. DOI: 10.1109/ICOA58279.2023.10308847.
- [50] Inc. MathWorks. *Global Optimization Toolbox User's Guide*. R2024a. The MathWorks, Inc. Natick, Massachusetts, 2024. URL: https://www.mathworks.com.
- [51] Huy Q. Do, Alejandro M. Aragón, and Dingena L. Schott. "A calibration framework for discrete element model parameters using genetic algorithms". In: *Advanced Powder Technology* 29.6 (2018), pp. 1393–1403. ISSN: 0921-8831. DOI: https://doi.org/10.1016/j.apt.2018.03.001. URL: https://www.sciencedirect.com/science/article/pii/S0921883118300773.
- [52] D. Wang, D. Tan, and L. Liu. "Particle swarm optimization algorithm: an overview". In: *Soft Computing* 22.2 (2018), pp. 387–408. DOI: 10.1007/s00500-016-2474-6. URL: https://doi.org/10.1007/s00500-016-2474-6.
- [53] James Kennedy and Russell Eberhart. "Particle swarm optimization". In: *Proceedings of ICNN'95-international conference on neural networks*. Vol. 4. ieee. 1995, pp. 1942–1948.
- [54] H.P. Zhu et al. "Discrete particle simulation of particulate systems: Theoretical developments". In: Chemical Engineering Science 62.13 (2007). Frontier of Chemical Engineering Multi-scale Bridge between Reductionism and Holism, pp. 3378–3396. ISSN: 0009-2509. DOI: https://doi.org/10.1016/j.ces.2006.12.089. URL: https://www.sciencedirect.com/science/article/pii/S000925090700262X.

[55] Jun Ai et al. "Assessment of rolling resistance models in discrete element simulations". In: *Powder Technology* 206.3 (2011), pp. 269–282. ISSN: 0032-5910. DOI: https://doi.org/10.1016/j.powtec.2010.09.030. URL: https://www.sciencedirect.com/science/article/pii/S0032591010005164.

- [56] Delft High Performance Computing Centre (DHPC). *DelftBlue Supercomputer (Phase 2)*. https://www.tudelft.nl/dhpc/ark:/44463/DelftBluePhase2. 2024.
- [57] Aman Tripathi et al. "Quantitative DEM simulation of pellet and sinter particles using rolling friction estimated from image analysis". In: *Powder Technology* 380 (2021), pp. 288–302. ISSN: 0032-5910. DOI: https://doi.org/10.1016/j.powtec.2020.11.024. URL: https://www.sciencedirect.com/science/article/pii/S0032591020310779.
- [58] Han Wei et al. "Measurement and simulation validation of DEM parameters of pellet, sinter and coke particles". In: *Powder Technology* 364 (2020), pp. 593–603. ISSN: 0032-5910. DOI: https://doi.org/10.1016/j.powtec.2020.01.044. URL: https://www.sciencedirect.com/science/article/pii/S0032591020300565.
- [59] Vasileios Angelidakis, Sadegh Nadimi, and Stefano Utili. "Elongation, flatness and compactness indices to characterise particle form". In: *Powder Technology* 396 (2022), pp. 689–695. ISSN: 0032-5910. DOI: https://doi.org/10.1016/j.powtec.2021.11.027. URL: https://www.sciencedirect.com/science/article/pii/S0032591021009785.
- [60] Altair EDEM. *Plackett-Burman Design*. https://2017.help.altair.com/2017/hst/hst.htm? plackett-burman.htm. Accessed: 2025-03-14.
- [61] Rasoul Rahmani and Rubiyah Yusof. "A new simple, fast and efficient algorithm for global optimization over continuous search-space problems: Radial Movement Optimization". In: Applied Mathematics and Computation 248 (2014), pp. 287–300. ISSN: 0096-3003. DOI: https://doi.org/10.1016/j.amc.2014.09.102. URL: https://www.sciencedirect.com/science/article/pii/S0096300314013368.
- [62] International Energy Agency. *Iron and Steel Technology Roadmap*. https://www.iea.org/reports/iron-and-steel-technology-roadmap. Accessed: 2025-04-04. 2020.



Scientific Paper

(This page is left intentionally blank)

Comparison of Calibration Strategies for Mixture-Components: A DEM study of pellet and sinter

Department of Multi-Machine Engineering, Delft University of Technology

Sabine van Epen Dingena Schott Raïsa Roeplal

Abstract—To improve the accuracy of Discrete Element Method (DEM) simulations for blast furnace materials, we present a structured calibration methodology for pellet and sinter particles based on nine key performance indicators (KPIs). For each material, the following process is followed: a Plackett-Burman sensitivity analysis to identify influential parameters, a Central Composite Design to develop polynomial regression models, and a comparison of multi-objective optimization techniques, including local optimization, genetic algorithms, and particle swarm optimization (PSO). This approach enables parameter input estimation of the DEM model. Experimental data is used to find input parameter values for the calibrated models, showing that PSO achieves faster convergence than GA and delivers accurate predictions at the original hopper height. However, discrepancies in the validation model suggest the need for refined parameter estimation to ensure robustness under varied conditions.

Keywords-Discrete element method, sensitivity analysis, particle swarm, genetic algorithm, multi-objective optimization, calibration

I. INTRODUCTION

The blast furnace, shown in context in Figure 1 is used for steel production, the most widely used engineering and construction material worldwide. It is a vertical shaft furnace containing a mixture of ferrous materials such as pellet, sinter, along with coke, which serves as fuel. The arrangement of these materials, known as the bed configuration, affects gas flow through the furnace. This permeability plays a key role in the efficiency of the iron extraction process. Since bed configuration influences permeability, understanding their configuration is crucial. However, placing sensors inside the furnace to monitor this distribution, and thus assess permeability, is challenging due to harsh conditions.

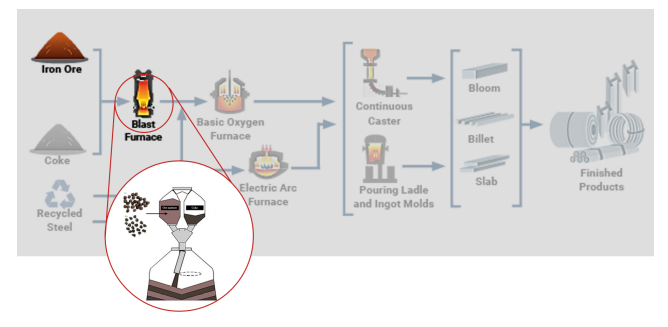


Fig. 1: The blast furnace is context of the steel making process. Modified from [1, 2, 3].

To overcome these challenges and gain deeper insights into granular material mixtures, the discrete element method (DEM), developed by Cundall and Strack [4], can be used. DEM provides particle-level insights that are difficult and expensive to obtain experimentally, making it a valuable tool for designing production processes and optimizing bulk material handling. As a computational approach, DEM simulates granular material behavior by calculating forces acting on each particle and predicting their motion over time using numerical integration. These interactions are governed by contact models, each with multiple parameters that must be quantified. These parameters influence both the bulk and particle-level behavior of the simulated material.

Determining these parameters remains a major obstacle to the adoption of DEM [5]. Many parameters cannot be directly measured due to the stochastic nature of granular materials, necessitating calibration to align simulations with real-world behavior. Calibration is inherently an optimization problem, yet common approaches such as trial-and-error remain inefficient, requiring expert knowledge and often failing to yield optimal parameter sets [6].

Additionally, usually only one KPI is used to determine multiple input parameters, often the angle of repose [7, 8, 9, 10, 11]. This leads to an underdetermined system because there are more unknowns than outputs.

The remainder of this paper is structured as follows. Section II introduces the calibration procedure, simulation setup, and optimization methods: genetic algorithm (GA), particle swarm optimization (PSO), and local optimization. Section III begins with an analysis of the appropriate time step and particle shape, followed by the calibration results, a comparison of different optimization techniques, and an evaluation of the sinter and pellet simulations.

The main contribution of this work is that, for the first time, to the best of the author's knowledge, this study is the first to systematically compare multiple optimization techniques (GA, PSO, and local optimization) within the context of DEM calibration using multi-objective optimization.

II. METHODS

A. DEM Simulation

The Discrete Element Method is used to model flows of particles by tracking the motion of particle by using Newton's second law. Hertz-Mindlin (no-slip) [12] contact model is used and rolling friction model C, an elastic-

plastic spring-dashpot model, according to Ai et al. [13]. We used commercial software EDEM version 2024.1 to develop the DEM model and we conducted all simulations on the DelftBlue high performance cluster [14]. When using the Hertz-Mindlin contact model with rolling friction type C, all the parameters necessary to define a DEM model for the mixture of pellet and sinter as well as the approach for determining them are listed in Table I. Each category with its corresponding DEM Parameters are shown. In Table I, bulk calibration refers to the calibration of parameters by replicating the Key Performance Indicators (KPIs) found in experiments in the laboratory.

B. Laboratory and DEM setup

The experimental setup used by Roeplal *et al.* [15] consists of a hopper, a hopper gate and a container. The hopper height can be adjusted, with calibration experiments conducted at 4.665 m and validation experiments for sinter and pellet at 3 m and 1 m.

In the physical experiments shown in Figure 2a, the material (sinter, pellet, or a combination) was placed into the hopper, and upon opening the gate, the material flowed onto a scale positioned below. A camera recorded the discharge process at the hopper gate to determine the discharge time. The mass was measured at three locations: directly on the scale and on both sides of the scale, separated by a partition for clear distinction. Additionally, images of the heap formed on the scale were captured with a green background for enhanced contrast, for the heap shape analysis. This raw data was provided by Roeplal [15]. To ensure comparability with simulations, the experimental images were cropped and scaled to match the DEM-generated images.

The DEM simulation was designed to replicate the laboratory setup as closely as possible, as illustrated in Figure 2b. The same KPIs can be extracted from the simulations: the discharge time, heap mass distribution, and heap shape. The discharge time was determined by tracking the maximum y-coordinate of particles over time. Masses at different locations were obtained using MATLAB post-processing of particle positions, and heap shape parameters were extracted from simulation images.

From these experiments the discharge time is extracted (Time), the masses at heap, the left side, right side of the container (M heap, M left, and M right) are measured, and using an image of the heap the x-, y-coordinates of the peak, and the pixel height at three different locations are measured as shown in Figure 3 (PeakX, PeakY, 0.25Y, 0.5Y, and 0.75Y), resulting in a total of nine KPIs.

C. Set Parameters

The model parameters are taken from provided data [15] and are shown in Table II. The particle shape of sinter is one particle which has average characteristics with regards to elongation, flatness, compactness and complexity as described by [16, 17], from the available STL files for sinter. Most of the interaction coefficients are used for the sensitivity analysis and their corresponding ranges used in the Design of Experiments are shown in Table II as well.



(a) Experimental setup in the laboratory (b) Geometries in DEM and the exwith the image of the heap.

Fig. 2: Experimental setups in the laboratory and setup in DEM, made to match the laboratory setup.

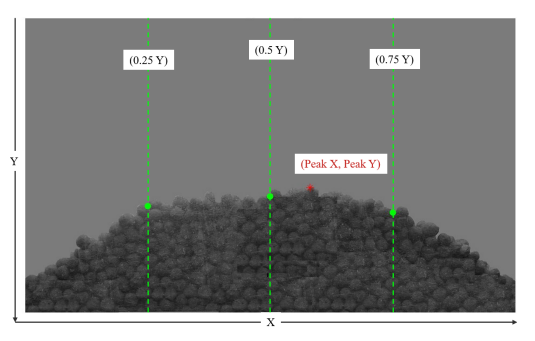


Fig. 3: KPIs: PeakX, PeakY, 0.25Y, 0.5Y, and 0.75Y extracted from the image of the heap.

D. Sensitivity Analysis

To reduce the complexity of the calibration task, it first needs to be tested which interaction parameters are useful to calibrate. Therefore, a sensitivity analysis is applied, to find out which interaction parameters have a dominant effect on the KPIs. Plackett-Burman (PB) is employed to efficiently explore the relationship between certain input variables and one or more outputs (or KPIs). PB is chosen because it is computationally the least expensive DoE, it is sufficient for the sensitivity analysis, and it is available in Altair Hyperstudy. It consists of two levels for the input parameters and 8 runs with different combinations of these levels. The dominant parameters found, will be used in the calibration approach.

E. Calibration Approach

The calibration process follows a structured approach using polynomial regression as the Response Surface Methodology (RSM) and Central Composite Design (CCD) to effi-

Category	DEM Parameter	Pellet	Sinter	Sinter-Pellet
Morphological Parameters	Particle shape	Sphere	Clumped Sphere	N/A
Morphological Farameters	Size distribution	Direct Measurement	Direct Measurement	N/A
	Density	Direct Measurement	Direct Measurement	N/A
Material Parameters	Shear modulus	Literature	Literature	N/A
	Poisson's ratio	Literature	Literature	N/A
	Coefficient of restitution	Bulk Calibration	Bulk Calibration	Average
Particle-Particle Interaction	Coefficient of rolling friction	Bulk Calibration	Bulk Calibration	Average
	Coefficient of static friction	Bulk Calibration	Bulk Calibration	Average
	Coefficient of restitution	Bulk Calibration	Bulk Calibration	N/A
Particle-Geometry Interaction	Coefficient of rolling friction	N/A	N/A	N/A
	Coefficient of static friction	Bulk Calibration	Bulk Calibration	N/A

TABLE I: Overview of DEM parameters and corresponding approach for determination of the numerical value.

ciently explore the relationship between DEM input parameters and the experimental KPIs. The Face-Centered Central Composite Design (CCI) variation is selected due to strict parameter constraints, such as the limitation that restitution coefficients cannot exceed 1 or be negative. CCD ensures that linear, interaction, and quadratic terms, are accounted for, allowing for an accurate DEM response surface.

Once the CCD-generated simulations are completed, polynomial regression is applied to fit response surfaces for each KPI. These polynomial models incorporate linear, interaction, and quadratic terms. With the response surfaces established, the next step is to determine the optimal parameter values that minimize the difference between simulation results and experimental KPIs. To achieve this, three optimization methods are compared: local optimization (LO), genetic algorithm (GA), and particle swarm optimization

(PSO).

Local optimization, implemented using MATLAB's fmin function, serves as a baseline approach due to its simplicity and computational efficiency. However, it is susceptible to local minima and may not always yield globally optimal solutions. To address this limitation, global optimization is used. GA and PSO are widely used global optimization techniques in DEM calibration. GA is employed as a population-based heuristic that evolves solutions iteratively through selection, crossover, and mutation [20]. Similarly, PSO is applied as another population-based optimization technique, inspired by collective behaviors in nature, where particles iteratively adjust their positions based on both their individual best-known solutions and the global best solution found by the swarm [21]. The effectiveness of these methods is assessed based on their ability to minimize the error

Parameter (symbol)		Pellet	Sinter	Steel (Geometry)
Particle shapes				_
Density (ρ)		3602 kg/m ³ [18, 2]	3449 kg/m ³ [18, 2]	7800 kg/m ³ [19]
Poisson's ratio (ν)		0.25 [18, 2]	0.25 [18, 2]	0.3 [19]
Shear modulus (G)		2.5e+8 Pa [18, 2]	2.5e+8 Pa [18, 2]	2e+11 Pa [19]
Restitution coefficient (C)	P-P	[0.0001 - 0.9]	[0.0001 - 0.9]	-
	P-W	[0.0001 - 0.9]	[0.0001 - 0.9]	-
Static friction coefficient (μ_s)	P-P	[0-0.9]	[0-0.9]	-
	P-W	[0-0.9]	[0-0.9]	-
Rolling friction coefficient (μ_r)	P-P	[0-0.9]	[0-0.9]	-
	P-W	0.5	0.5	-
Numerical time step (Dt)		10%	10%	-

TABLE II: Model parameters or parameter ranges for this study. Abbreviations: P-P = particle-particle, P-W = particle-wall.

between simulated and experimental KPIs, computational efficiency, and variability in parameter estimates.

The objective is to make the absolute value of the difference between all KPI values, one from the laboratory test and the other from the simulation, close to zero. To prevent larger KPI values from disproportionately influencing the optimization process, the objective function is normalized. The error is also squared to give a balanced outcome between the parameter values. The objective function combines the errors of all KPIs and can be written as follows:

$$Error = \sum_{k=1}^{n} \left(\frac{\text{Target KPI}_{k} - \text{Predicted KPI}_{k}}{\text{Target KPI}_{k}} \right)^{2} \quad (1)$$

where k refers to each individual KPI. Both GA and PSO were configured to prioritize convergence by using stopping criteria based on minimal changes in the objective function. Using this objective function and the chosen optimization methods, a parameter set is identified that closely predicts the experimental KPIs at the calibrated hopper height. These results are tested in DEM and then validated by testing the calibrated parameters at different hopper heights, as illustrated in Figure 2.

III. RESULTS AND DISCUSSION

A. Sensitivity Analysis

The sensitivity analysis results, shown in Appendix I, summarized in Table III, highlight the effect of DEM interaction parameters on various KPIs. This table condenses the findings from the Pareto plots. A key observation from these results is that the rolling friction coefficient between particles and geometry, μ_{r-pg} , does not have a significant effect on any KPI, and is set to 0.5 in this study. In contrast, the coefficient of restitution for particle-particle interactions, C_{pp} , has a noticeable influence across almost all KPIs. Additionally, the heap's shape is assessed using the total pixel count rather than height at specific locations, as the methodology evolved during the study.

B. RSM

Using CCD and polynomial regression the RSM is created for pellet and sinter. The results of the CCD can be found in Appendix II. The resulting polynomial model can also be found in that appendix, in Section III, Table X displays the polynomial model for pellet and Table XI shows the polynomial model for sinter. In Table IV the R^2 of the models which measures how well a model explains the variance in the data are shown per KPI, with values closer to one indicating a better fit.

As can be seen in this table most R^2 values are above the 0.95. Notably, the discharge time for sinter, the mass on the right side of the container are lower values (\leq 0.7). This could have an affect on the quality of the predicted values.

C. Local optimization

Using the polynomials, local optimization is used to minimize the error. As can be seen in Figure 4, the results of local optimization is highly dependent on the initial guess.

In this figure different combinations of initial guesses are taken from [0.1, 0.1, 0.1, 0.1, 0.1], [0.5, 0.5, 0.5, 0.5, 0.5] and [0.8, 0.8, 0.8, 0.8, 0.8].

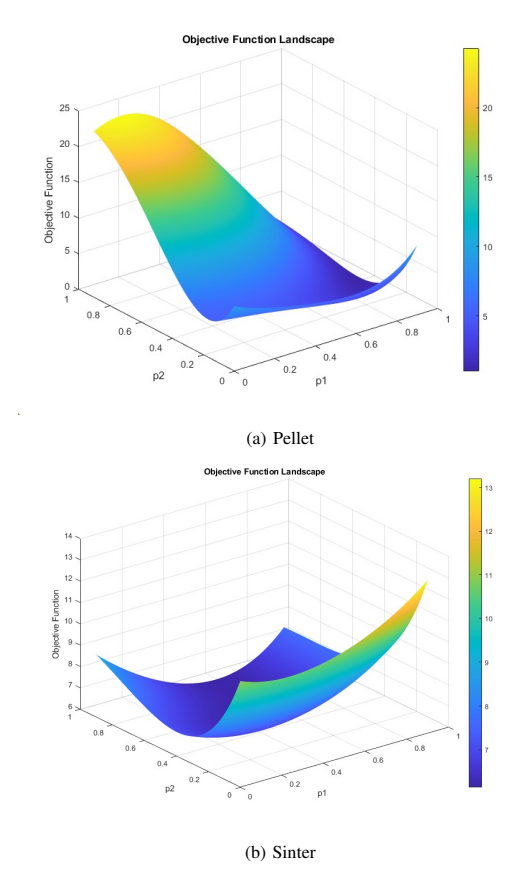


Fig. 4: Objective function value dependency on initial guess for both materials.

From the different combinations the following initial guesses give the best results (the smallest error) for pellet and sinter respectively: [0.10, 0.10, 0.80, 0.80, 0.80], [0.80, 0.10, 0.80, 0.80, 0.10]. These initial guesses are used to arrive at the results presented in Table V.

D. Global optimization: PSO & GA

The optimization is also performed using PSO and GA, and different population and swarm sizes are compared. These sizes represent the number of candidate solutions considered per iteration. Comparing them provides insight into how efficiently each algorithm uses its agents to converge toward solutions. As can be concluded from Figure 5, the population size of GA needs to be significantly bigger than the particle swarm of PSO in order to converge to an objective function value. The same results are found for sinter but then with a much faster convergence.

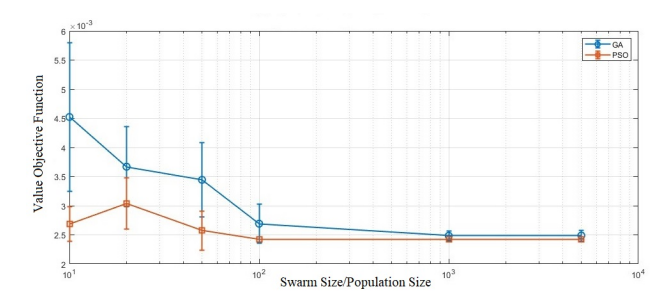
From these experiments, the following swarm and population sizes were selected based on where the error values converged. For pellet, a swarm size of 100 was used along with a population size of 1000. For sinter, both the swarm size and the population size were set to 20. The optimal parameters sets found are presented in Table V. These results

Parameter	Time	Pixel Count Heap	PeakX	PeakY	M Left	M Right	М Неар
C_{pp}	X	(-)	(-)	(+)	(-)	(-)	(-)
μ_{s-pp}	(+)	(+)	X	(-)	X	X	(+)
μ_{r-pp}	(+)	(+)	X	(-)	X	(-)	(+)
C_{pg}	X	X	(-)	X	(-)	(-)	X
μ_{s-pg}	X	(+)	(-)	X	X	(-)	(+)
μ_{r-pg}	X	X	X	X	X	X	X

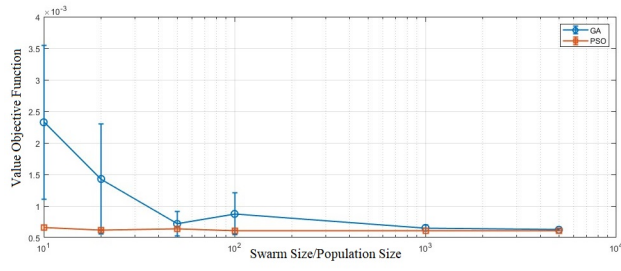
TABLE III: The effect of DEM interaction parameters on the KPIs, with the effect of each significant parameter on the KPIs in parentheses (e.g., "(+)" denotes that with an increase in the parameter value, KPI increases.). "x" means insignificant effect.

	Time	M heap	M left	M right	PeakX	PeakY	0.25Y	0.5Y	0.75Y
Pellet	0.98776	0.96546	0.81121	0.70841	0.86276	0.96751	0.96942	0.97609	0.90973
Sinter	0.77077	0.98438	0.98438	0.70017	0.87183	0.98468	0.97609	0.98889	0.93775

TABLE IV: Comparison of R-squared values for pellet and sinter models.







(b) Sinter optimization results.

Fig. 5: Pellet and sinter optimizer objective function value for different population and swarm sizes of GA and PSO with error bars.

are found after the fine-tuning of the optimizers.

As can be seen in the table, GA and PSO find the smallest error for both materials, but since PSO converges faster it is preferred. Consequently, the parameter set found using PSO will be used in DEM simulations.

E. Simulation Results at Calibrated Height

In Figure 6a, the simulation and experimental KPIs of pellet are compared. The DEM simulations created with the optimal parameter sets taken from Table V. The same results are shown for sinter in Figure 6c. Figure 6b and 6d show the edges of the heap of the experimental results and of the simulation results. Note that some KPIs have been scaled for a better visualization.

The simulation results for pellet show a strong agreement with the experimental data. Deviations in discharge time and

Pellet	C_{pp}	μ_{r-pp}	μ_{s-pp}	C_{pg}	μ_{s-pg}	Error
LO	0.151	0.04	0.453	0.359	0.83	0.1465
GA	0.071	0.045	0.465	0.329	0.83	0.0024213
PSO	0.071	0.045	0.465	0.329	0.83	0.0024213
Sinter	C_{pp}	μ_{r-pp}	μ_{s-pp}	C_{pg}	μ_{s-pg}	Error
Sinter	C_{pp} 0.258	$\frac{\mu_{r-pp}}{0.9}$	$\frac{\mu_{s-pp}}{0.35}$	C_{pg} 0.9	$\mu_{s-pg} = 0.532$	Error 3.1753
				- 10	. 10	

TABLE V: Best results from the three optimization techniques. These are the parameter input values which give the smallest error for each optimizer.

mass distribution are minimal, ranging from 0.4% to 5.2%, with overlapping 95% confidence intervals, indicating the model captures these behaviors well. The heap shape KPIs (PeakX, PeakY, 0.25Y, 0.5Y, 0.75Y) also show deviations below 3.5%, with confidence intervals that largely overlap, further supporting the accuracy of the simulation.

For sinter, the differences between simulated and experimental KPIs are more pronounced. Most deviations are around 10%, with some exceeding 20%, notably the discharge time and M right. While these differences appear significant, overlapping confidence intervals in many cases suggest that experimental variability may account for the discrepancies. For example, the experimental discharge time (mean = 4.62, CI = [3.90, 5.34]) and the simulated value (3.61) show minimal overlap at the lower bound. Similarly, the mass on the right side has CIs of [16.86, 24.50] for the experiment and [23.74, 28.66] for the simulation, with slight overlap at the bounds.

F. Validation Results

The validation of these optimal parameter sets is found by testing the simulation results when the hopper is positioned at different heights. A comparison of experimental and simulated results is shown in Figure 7. The pellet validation shows that deviations between simulated and experimental values tend to increase as hopper height decreases. For most KPIs, the 95% confidence intervals overlap, indicating good agreement. However, at a hopper height of 1 meter, the

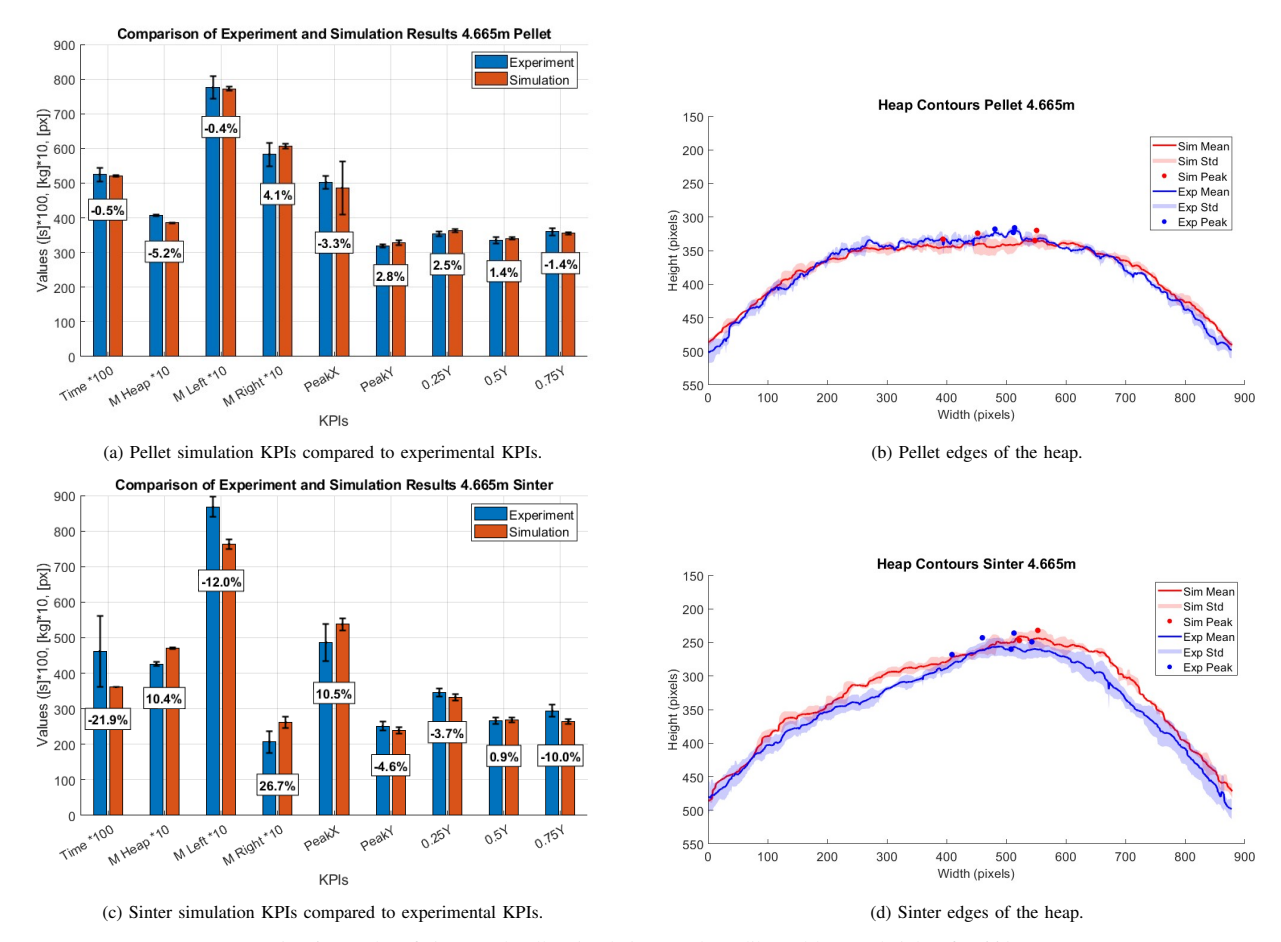


Fig. 6: Results of sinter and pellet simulations at the calibrated hopper height of 4.665m.

y-coordinate of the peak (PeakY) and the midpoint height (0.5Y) are underpredicted, and their confidence intervals do not overlap.

In the sinter simulations, deviations also increase with decreasing hopper height. The deviation in midpoint height rises from 0.9% at 4.665 meters to 12.6% at 1 meter, with the largest differences observed at the lowest height. At this height, the confidence intervals for both midpoint and three-quarters width (0.75Y) no longer overlap, indicating notable disagreement. In contrast, the mass distribution aligns better than at the highest height. The discharge time continues to deviate across all cases, and other KPIs show consistent deviation.

The differences between simulation and experimental results can be attributed to several factors.

Sinter showed greater deviation than pellet, which may relate to its higher experimental variability and broader particle shape distribution. Additionally, the initial sensitivity analysis used a different metric than the final KPIs, potentially affecting which parameters were identified as most influential. The unweighted objective function may also have contributed to deviations, particularly for KPIs with high variability. Incorporating weights based on the relative standard deviation of experimental values could improve accuracy by reducing the influence of uncertain measurements. Finally, low prediction accuracy for some KPIs, especially discharge time, suggests that more simulations may be needed or that alternative fitting models should be explored to better capture the relationships.

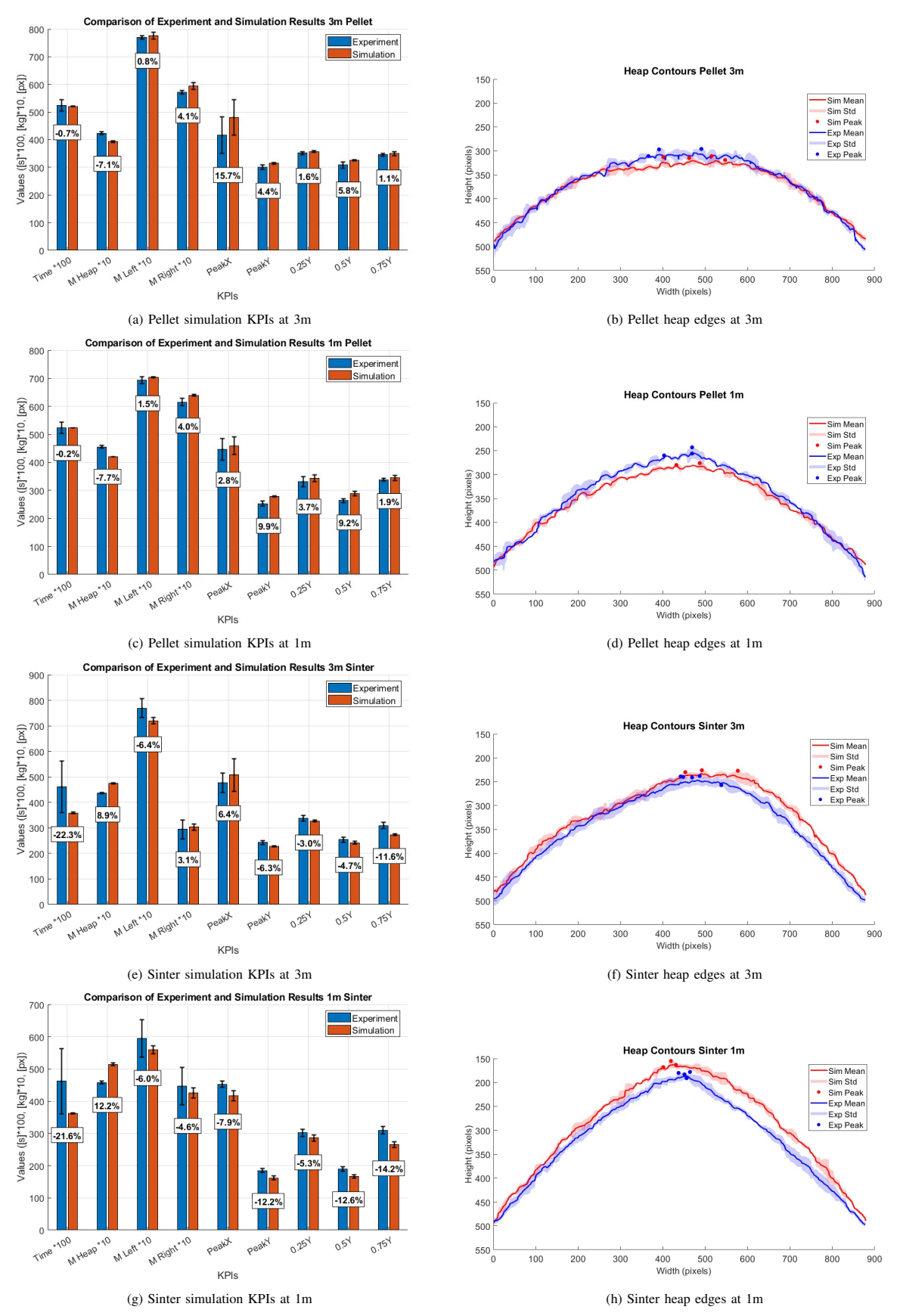


Fig. 7: Validation results at 3m and 1m hopper heights for pellet and sinter.

IV. CONCLUSIONS

This study evaluated different calibration strategies for DEM simulations, focusing on sinter and pellet materials used in blast furnaces. The calibration process combined sensitivity analysis, structured sampling of the parameter space, and optimization techniques to determine the most accurate interaction parameters.

A key finding is that PSO consistently outperformed the GA in terms of computational efficiency, requiring fewer iterations to converge while maintaining high accuracy. Local optimization proved less reliable due to its strong dependence on initial parameter estimates. This research makes three main contributions to the advancement of calibrating DEM simulations.

ACKNOWLEDGMENT

The author thanks Ahmed Hadi from the Machines and Materials Interactions research group for the guidance on DEM calibration.

First, it demonstrates the value of using multiple KPIs in the calibration process. Relying on a single KPI can create blind spots, whereas multiple KPIs offer a more complete and reliable calibration of the simulation model. Second, the study highlights the necessity of thorough validation. Although good agreement was found at the original hopper height, increased deviations at lower heights suggest that overfitting may have occurred. Third, the results show that PSO is an effective optimization method within the proposed calibration framework.

Further research is needed to understand the reasons for the higher deviations observed during validation and to explore whether the suggestions outlined in the discussion could improve the accuracy of the calibration approach.

APPENDIX I RESULTS PLACKETT-BURMANN

Sim #	Срр	Spp	Rpp	Cpg	Spg	Rpg	Time	Pixel	x	y	M-left	M-right	M-scale
Sim1	0.9	0.9	0.9	0.0001	0	0.9	6.21	247157	1012.3	415.0	71.25	61.65	42.72
Sim2	0.0001	0.9	0.9	0.9	0.9	0	9.54	341332	1055.8	272.3	63.04	50.93	55.81
Sim3	0.0001	0.9	0	0.9	0	0.9	5.10	149617	1292.8	566.8	67.25	81.29	25.39
Sim4	0.9	0	0	0.9	0.9	0.9	8.96	43414	841.0	718.8	56.15	55.44	6.72
Sim5	0.0001	0	0.9	0.0001	0.9	0.9	7.79	148799	1264.0	589.5	77.32	71.01	27.74
Sim6	0.9	0.9	0	0.0001	0.9	0	7.15	180789	1002.8	542.8	75.10	69.91	30.20
Sim7	0.9	0	0.9	0.9	0	0	5.31	22104	963.0	746.3	56.00	75.14	3.81
Sim8	0.0001	0	0	0.0001	0	0	4.56	97332	1258.3	660.3	80.27	76.60	18.49

TABLE VI: Simulation parameters with corresponding KPIs.

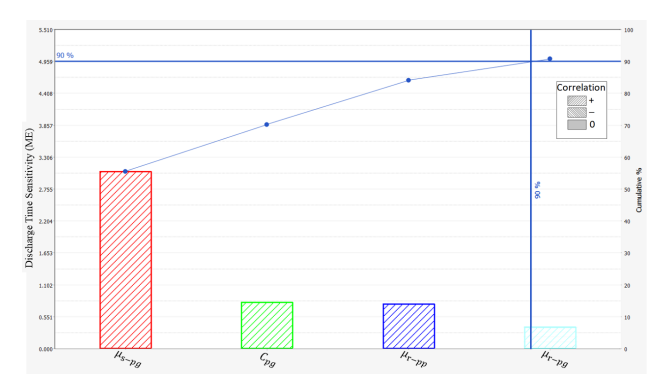


Fig. 8: Pareto plot of the discharge time.

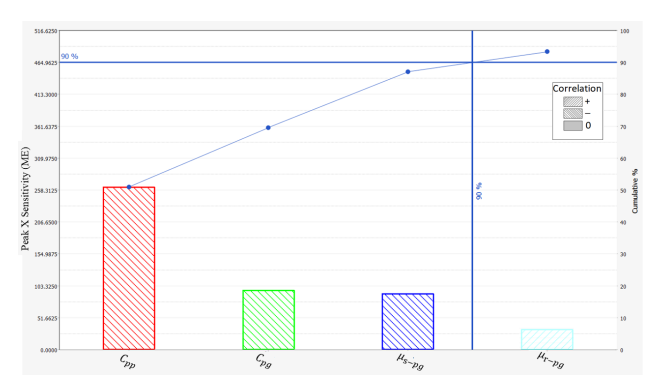


Fig. 9: Pareto plot of the x-coordinate of the highest point of the heap, PeakX.

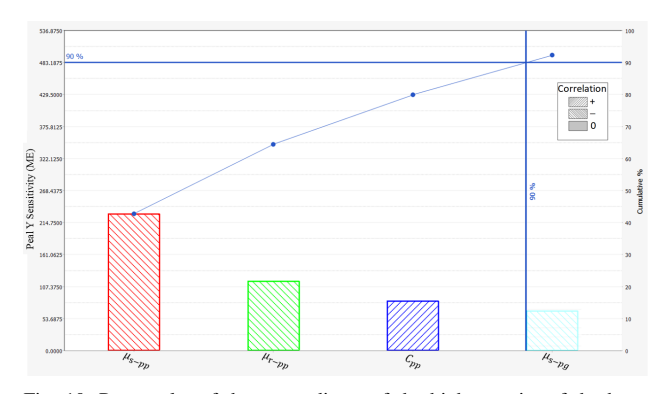


Fig. 10: Pareto plot of the y-coordinate of the highest point of the heap, PeakY.

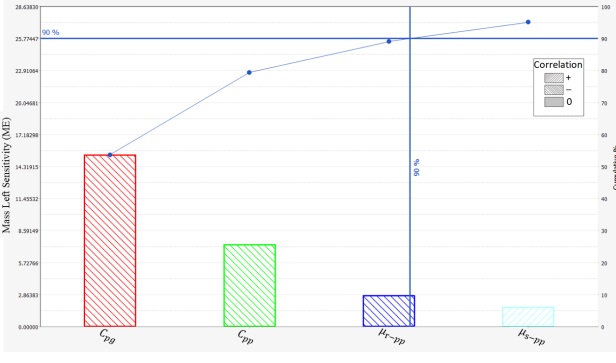


Fig. 11: Pareto plot for the mass on the left side of the container, M left.

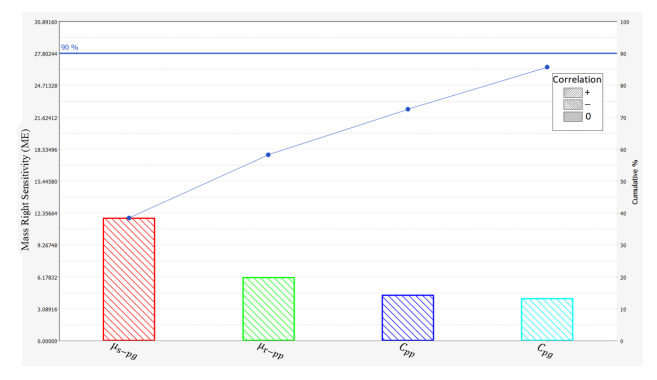


Fig. 12: Pareto plot for the mass on the right side of the container, M right.

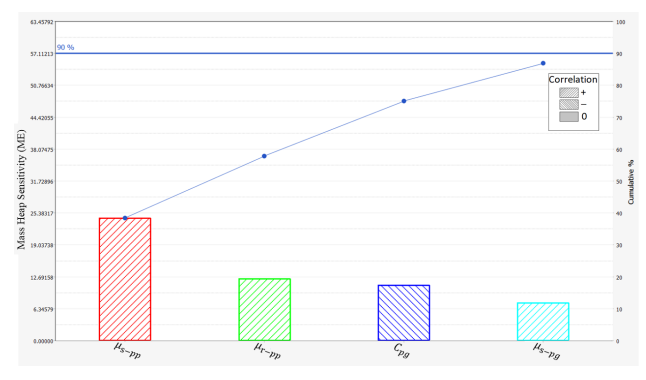


Fig. 13: Pareto plot for the mass on the scale, M heap.

APPENDIX II RESULTS CCD

Run	C_{pp}	μ_{r-pp}	μ_{s-pp}	C_{pg}	μ_{s-pg}
1	0.2608693	0.260798	0.260798	0.260869	0.260798
2	0.2608693	0.260798	0.260798	0.260869	0.639202
3	0.2608693	0.260798	0.260798	0.639231	0.260798
4	0.2608693	0.260798	0.260798	0.639231	0.639202
5	0.2608693	0.260798	0.639202	0.260869	0.260798
6	0.2608693	0.260798	0.639202	0.260869	0.639202
7	0.2608693	0.260798	0.639202	0.639231	0.260798
8	0.2608693	0.260798	0.639202	0.639231	0.639202
9	0.2608693	0.639202	0.260798	0.260869	0.260798
10	0.2608693	0.639202	0.260798	0.260869	0.639202
11	0.2608693	0.639202	0.260798	0.639231	0.260798
12	0.2608693	0.639202	0.260798	0.639231	0.639202
13	0.2608693	0.639202	0.639202	0.260869	0.260798
14	0.2608693	0.639202	0.639202	0.260869	0.639202
15	0.2608693	0.639202	0.639202	0.639231	0.260798
16	0.2608693	0.639202	0.639202	0.639231	0.639202
17	0.6392307	0.260798	0.260798	0.260869	0.260798
18	0.6392307	0.260798	0.260798	0.260869	0.639202
19	0.6392307	0.260798	0.260798	0.639231	0.260798
20	0.6392307	0.260798	0.260798	0.639231	0.639202
21	0.6392307	0.260798	0.639202	0.260869	0.260798
22	0.6392307	0.260798	0.639202	0.260869	0.639202
23	0.6392307	0.260798	0.639202	0.639231	0.260798
24	0.6392307	0.260798	0.639202	0.639231	0.639202
25	0.6392307	0.639202	0.260798	0.260869	0.260798
26	0.6392307	0.639202	0.260798	0.260869	0.639202
27	0.6392307	0.639202	0.260798	0.639231	0.260798
28	0.6392307	0.639202	0.260798	0.639231	0.639202
29	0.6392307	0.639202	0.639202	0.260869	0.260798
30	0.6392307	0.639202	0.639202	0.260869	0.639202
31	0.6392307	0.639202	0.639202	0.639231	0.260798
32	0.6392307	0.639202	0.639202	0.639231	0.639202
33	0.0001	0.45	0.45	0.45005	0.45
34	0.9	0.45	0.45	0.45005	0.45
35	0.45005	0	0.45	0.45005	0.45
36	0.45005	0.9	0.45	0.45005	0.45
37	0.45005	0.45	0	0.45005	0.45
38	0.45005	0.45	0.9	0.45005	0.45
39	0.45005	0.45	0.45	0.0001	0.45
40	0.45005	0.45	0.45	0.9	0.45
41	0.45005	0.45	0.45	0.45005	0
42	0.45005	0.45	0.45	0.45005	0.9
43	0.45005	0.45	0.45	0.45005	0.45
44	0.45005	0.45	0.45	0.45005	0.45
45	0.45005	0.45	0.45	0.45005	0.45
46	0.45005	0.45	0.45	0.45005	0.45
47	0.45005	0.45	0.45	0.45005	0.45
-	1				

TABLE VII: Input parameter values for CCD

Run	Time +3	M_h	MJ	$M_{-}r$	HighX	HighY	0.25Y	0.5Y	0.75Y
1	6.45	36.68015	94.01253	45.6913	626	321	399.25	371	335.75
2	7.58	40.56808	86.43811	49.35311	587.5	300.5	359	327.25	317.5
3	6.45	37.13583	93.38976	45.66619	614.5	320.5	398.75	363	334.75
4	7.58	40.69089	85.30302	49.24754	608.5	305.75	357.25	321.75	327.25
5	6.89	40.92542	88.58243	46.87409	546.5	286.25	358	308	313
6	8.09	44.66442	81.70815	49.98505	482.75	253.5	324.25	266	305.25
7	6.90	41.01399	89.05329	46.1574	576.25	286.25	363	309	316.75
8	8.07	44.78455	82.06709	48.56278	476.5	257.75	333	262.75	302.25
9	6.59	40.80903	93.2345	42.34343	632.75	290.5	368.5	327	314.25
10	7.68	44.45355	87.04547	44.86426	522.5	271.25	334.5	288.75	304
11	6.62	40.96381	94.32931	40.87765	594.75	296.5	376.25	336.5	311
12	7.70	44.49632	85.77401	45.15074	524.75	277	328	289.25	298.5
13	7.43	49.84414	83.3522	43.18652	501.5	201.25	296.75	210.75	247.75
14	8.55	53.27353	75.72827	47.37756	476.75	164.25	246.5	173.25	244
15	7.47	50.24528	83.7251	42.24707	489.5	200.5	292.75	211.5	255.75
16	8.55	53.16328	75.07804	47.2197	472.25	169.5	263.75	177.75	241.25
17	6.43	35.76399	90.31018	50.28574	633	327	402.75	377.5	337.75
18	7.58	39.11967	82.33834	54.8536	525.25	316.75	370.5	341.75	343
19	6.45	35.71481	88.65436	51.58316	645.5	339.25	404.75	380.25	346.25
20	7.57	39.18475	80.61357	54.60616	529.25	322.75	365	336.75	347.75
21	6.86	40.56241	85.74752	50.05134	568.25	288.5	359.5	319.5	314.25
22	7.99	43.98508	78.96905	53.3807	443.5	264.25	328.5	276.5	314.75
23	6.85	40.68909	85.00901	50.3328	510.25	300.5	361.5	317.25	325.25
24	7.94	44.5189	77.34351	53.05047	532.5	272.75	323.75	280.25	308
25	6.59	39.10674	89.21604	48.04464	596.25	312.5	379.25	344.5	327.75
26	7.70	42.00348	80.62535	53.70718	509.25	299.75	344	305.75	325.75
27	6.59	39.10798	89.23658	47.59931	596	316.5	385.25	347.25	329.5
28	7.66	42.07947	80.14214	52.49904	529.5	299.25	351.25	313.75	324.5
29	7.28	48.894	78.50738	48.96004	464	214.75	300.5	223	269.25
30	8.43	51.9976	72.8187	51.50185	501.25	186.5	277.75	199.5	254
31	7.27	49.01394	78.52692	48.40921	500.75	227.75	304.5	235.5	276.75
32	8.29	51.59355	72.57155	50.73755	482	191.25	277.75	203.75	269
33	7.50	47.5254	86.87821	41.97218	523	237.5	309	249.75	274.75
34	7.28	37.57443	77.09311	61.19166	500.25	333.75	385.25	351.25	358.25
35	6.84	32.85769	85.74917	57.7025	635	370.5	408.25	409	379.25
36	7.76	53.17426	77.81742	45.33966	497	189.25	270	200	246
37	6.28	23.70403	80.31799	71.4959	703.25	460.5	493	500.25	469.5
38	7.82	48.0105	81.19631	47.13049	490	220.75	310	231.5	269
39	7.45	46.3087	83.61504	46.45573	502	238.5	310.25	259	291.75
40	7.47	46.56074	84.04358	44.35102	553	251.5	324.5	257.75	289
41	5.60	41.21905	75.669	59.13641	502	298.25	358.25	308.75	331.25
42	8.99	49.68634	71.34851	55.07318	466.5	218.5	285.5	225.5	282
43	7.46	46.1905	86.18969	43.95401	534.25	250.75	322.5	262	282
44 45	7.48	46.30918	85.85627	44.1812	508 521.5	249.25	324	264.25	285.75
45 46	7.49	46.63257	83.9534	45.7633	521.5	244.75	327	254	280.75
46 47	7.49	46.68384	84.06608	45.59198	537.75	246.25	323.75	253.75	281
47	7.46	46.53896	84.61121	45.20596	525.5	241	326	261.75	285

TABLE VIII: Results CCD of pellet. The input parameters are displayed in the previous table.

Run	Time +3	PeakX	PeakY	M-heap	M-left	M-right	0.25Y	0.5Y	0.75Y
1	5.723333	610.5	325	37.86236	75.60987	36.52563	395.75	387.25	334
2	6.315	579.75	297.75	40.84144	82.04778	27.10528	387	343.5	318.5
3	5.715	593.75	318.5	38.42059	77.96515	33.58133	410	369.25	328
4	6.32	575.25	299.75	41.09753	81.43499	27.18243	383.75	337.25	318
5	6.175	568	279.25	41.84885	75.33801	32.81353	355.25	307.25	304.25
6	6.98	510.75	252.75	45.18698	74.58308	30.22053	338.75	261.25	297.25
7	6.19	550.5	289	41.37694	73.8439	34.72725	357.25	310.75	313.25
8	6.995	522.25	255.25	45.17105	73.51231	31.00657	335.25	271.25	297.5
9	5.845	619.5	306.25	39.68603	78.05972	32.25304	387.5	354.75	313.25
10	6.48	567.25	276.75	42.73814	83.09411	24.15421	373.5	308.5	304.5
11	5.83	635.75	307.5	39.41071	78.6637	31.8902	383.75	358	318.25
12	6.485	580.5	281.75	42.65491	81.34524	25.73893	365.75	313.25	302
13	6.383333	515	228	46.50189	73.79153	29.70144	318.6667	253	265.6667
14	7.206667	507.3333	206.3333	48.96552	71.14055	29.87743	301.3333	217	265
15	6.3775	477	229.25	46.50213	72.80169	30.65563	311.6667	238.5	277
16	7.23	478	204.25	49.37879	71.76559	28.5404	305	216.5	265.5
17	5.72	637.75	319.25	38.07514	77.46079	34.43902	409.25	376.75	328.5
18	6.385	581.75	308.5	40.89826	80.98641	28.082	381	339.5	319
19	5.72	644.5	322	37.88226	78.65275	33.40428	402.75	390.5	328.75
20	6.34	587	306	41.03083	79.07933	29.52863	382.25	341.5	329.25
21	6.186667	530.25	286.25	42.24012	71.49637	36.22754	357.75	313.75	312.5
22	6.98	477	249.75	45.80338	74.60394	29.52386	339.75	264	303.25
23	6.16	558	283	42.43465	74.9372	32.55311	344.75	312.75	307.75
24	6.9725	517.25	257.5	45.49859	72.83626	31.32476	330.25	268.75	300.5
25	5.84	602	308.75	39.01468	79.15118	31.81379	386.25	362.5	317
26	6.466667	568.75	287	42.12993	80.98399	26.85712	377	316.25	307.25
27	5.8625	623	308.75	39.60846	79.41717	30.89963	388.25	351.25	319.5
28	9.303333	564.5	287	42.19508	80.11359	27.36886	372.25	320.25	309.5
29	6.3275	500	232	46.8388	70.91749	32.2088	335.75	239	284.5
30	7.19	483.75	215.5	49.4481	68.83597	31.65264	304.25	221.25	265.75
31	6.3375	510.5	233	46.24977	70.74005	32.92569	337	254.25	279.75
32	7.175	491.25	208.75	49.67364	71.56681	28.37448	308.5	224.25	263.75
33	6.45	540.6667	243.6667	46.20383	73.09346	30.68875	342.6667	266	277
34	6.425	530	268.5	45.03356	71.66356	32.95549	342.25	289.75	293.5
35	6.19	565	311.75	39.98262	80.19888	29.80303	396.5	350	328.75
36	6.63	514.5	217	48.90558	72.07197	29.01189	312.75	239.75	259
37	5.566667	641.25	424.75	28.45555	72.52367	48.90715	472	480.5	426.75
38	6.846667	507.6667	245.6667	44.98039	72.00209	32.95565	332	266.3333	288.3333
39	6.43	540	259.5	45.50506	74.64499	29.84353	328.5	290	290.5
40	6.4475	562	252	45.77776	75.13847	28.57529	340.5	275	285.25
41	5.1525	507	306	41.32419	56.55238	52.09474	359	319.25	332.5
42	7.255	506.5	236.5	47.93706	64.93363	36.97124	316.75	248	282.5
43	6.42	542.5	255.75	45.68792	75.03282	29.26132	349.25	285.25	288
44	6.466667	568.5	264.25	45.37045	76.33119	28.2719	348.25	280	283
45	6.455	557.5	259.25	45.39721	77.58587	27.00266	347.75	281.25	283.25
46	6.455	512.25	252.25	46.07919	75.34051	28.56153	343.25	272.25	282.25
47	6.449	545.2	257.88	45.63	76.08	28.24	347.13	279.69	283.2

TABLE IX: Results CCD of sinter. The input parameters are the same as pellet.

APPENDIX III POLYNOMIALS

Pellet	Time	M heap	M left	M right	X peak	Y peak	0.25Y	0.5Y	0.75Y
Constant	43.118	14.373	87.827	71.835	93.68	47.743	54.577	63.233	48.576
P1	7.5632	12.663	-5.8712	-4.3645	-11.116	-14.337	-5.1764	-17.213	-10.073
P2	8.1241	21.6	15.838	-37.22	-36.188	-12.093	-12.053	-26.655	-13.936
P3	27.416	49.403	7.462	-55.09	-73.115	-37.819	-39.55	-56.634	-34.748
P4	2.4892	0.9383	-3.4368	7.664	-6.8941	2.7301	3.4109	-2.2578	0.26415
P5	41.381	16.175	25.734	-38.181	-17.755	-5.8483	-12.052	-17.001	-10.488
P1^2	-2.4413	-18.676	-5.5434	22.829	-5.539	17.513	9.9502	19.689	13.712
P2^2	-7.0086	-16.37	-6.5415	22.523	21.314	14.669	8.5899	21.66	11.302
P3^2	-19.169	-51.722	-11.609	61.003	36.438	44.669	38.899	51.969	39.45
P4^2	0.89253	0.5125	3.5631	-7.6893	2.3023	-2.5536	-3.0157	-1.1176	-1.044
P5^2	-7.3171	-4.3371	-47.403	50.097	-19.056	4.0519	-0.54587	3.2036	7.413
P1P2	-4.0597	-5.699	-4.412	10.115	9.3855	6.8172	8.2214	5.0347	7.0646
P1P3	-8.25	6.161	7.499	-13.245	12.223	-2.0008	-4.2635	1.1932	-5.2457
P1P4	-2.6195	-0.70387	-4.412	2.2518	10.172	3.107	-3.9147	2.4158	2.001
P1P5	-1.3532	-2.486	0.65584	0.30838	-1.6588	2.6701	0.058205	3.8124	3.6596
P2P3	22.915	33.801	-40.781	6.4996	0.26189	-40.557	-28.866	-38.251	-23.825
P2P4	-0.61121	-1.032	4.8267	-3.472	-9.3855	-0.96765	0.81486	5.1366	0.44381
P2P5	-3.623	-3.4524	-0.31973	4.3584	14.404	-2.3643	1.4695	4.1757	-0.16732
P3P4	-1.746	0.005922	3.264	-2.3457	2.8811	0.69118	1.3387	1.3824	-0.9531
P3P5	0.56754	-0.45501	6.8823	-5.7555	26.233	-10.134	4.5249	2.3425	-3.5719
P4P5	-2.7065	-0.74434	-5.0115	-1.2092	11.786	-0.66208	1.4697	-1.0622	1.055

TABLE X: Polynomial model for the pellet KPIs. P1, P2, P3, P4, and P5 stand for C_{pp} , μ_{r-pp} , μ_{s-pp} , C_{pg} , and μ_{s-pg} respectively.

Sinter	Time	M heap	M left	M right	X peak	Y peak	0.25Y	0.5Y	0.75Y
Constant	53.685	22.429	56.776	70.268	69.545	44.483	-222.63	-159.85	-177.45
P1	-19.495	0.7622	8.9546	-9.0925	3.3208	0.9244	296.21	237.51	242.04
P2	-18.168	7.9645	0.4826	-8.4843	2.8821	-2.5462	285.98	226.6	236.87
P3	56.422	46.138	16.714	-62.482	-28.706	-39.11	260.56	179.65	205.51
P4	-21.592	2.0898	-4.7871	4.0941	-9.8772	1.7051	302.28	232.17	241.27
P5	1.9683	13.891	82.989	-96.025	-0.77411	-12.753	296.28	220.49	229.14
P1^2	2.9608	-1.931	-5.8737	7.0625	-1.029	-0.9699	-330.37	-265.01	-268.35
P2^2	1.6021	-7.731	12.68	-4.8633	1.1523	3.125	-324.29	-256.56	-264.03
P3^2	-8.4391	-45.885	-6.4434	52.045	18.292	38.104	-300.89	-217.77	-232.59
P4^2	3.0225	-1.8188	6.54	-5.8426	6.7093	-1.1345	-334.3	-262.73	-267.05
P5^2	-8.5831	-6.8099	-63.332	69.831	-15.144	6.52	-332.56	-262.11	-257.3
P1P2	22.823	-2.3898	-4.0631	6.4337	-5.1802	2.2409	6.7517	0.85124	1.4915
P1P3	-27.349	4.4806	-7.3924	2.8688	-9.4146	-1.0768	1.9935	-0.37105	0.88034
P1P4	23.932	-0.22404	4.5746	-4.4505	15.702	-1.237	-1.7172	4.213	-1.4043
P1P5	25.195	-0.07937	-5.7769	5.7297	-7.4938	3.0703	-3.2304	0.45836	0.47291
P2P3	-19.955	19.789	-23.73	3.8517	-19.395	-22.93	-10.417	-21.41	-13.669
P2P4	25.443	0.1698	0.2651	-0.43269	-4.8746	-1.1204	0.53839	-0.41471	0.57477
P2P5	26.502	-1.7595	-7.4	9.178	8.8025	0.77112	1.1785	5.8707	-1.5641
P3P4	-24.38	-1.3991	1.7625	-0.42089	-2.1245	0.71301	-1.1641	2.4664	-0.38561
P3P5	-10.89	1.3156	-25.427	24.004	12.251	-3.3318	-1.2222	3.9502	-0.60381
P4P5	24.671	0.76048	-8.5721	6.057	2.5901	-0.0291	-0.77121	2.6847	-0.61842

P4P5 | 24.671 0.76048 -8.5721 6.057 2.5901 -0.0291 -0.77121 2.6847 -0.61842 TABLE XI: Polynomial model for the sinter KPIs. P1, P2, P3, P4, and P5 stand for C_{pp} , μ_{r-pp} , μ_{s-pp} , C_{pg} , and μ_{s-pg} respectively.

REFERENCES

- [1] Dixon Valve & Coupling Company. 6 Steps of the Steel Manufacturing Process. Copyright © Dixon Valve & Coupling Company, LLC 2021-2025. 1 Dixon Square, Chestertown, MD 21620, US, Nov. 2023. URL: https://dixonvalve.com/en/news-and-events/news/6-steps-steel-manufacturing-process.
- [2] Arijit Chakrabarty et al. "Characterisation of binary mixtures of pellets and sinter for DEM simulations". In: Advanced Powder Technology 33.1 (2022), p. 103358. ISSN: 0921-8831. DOI: https://doi.org/10.1016/j.apt.2021.11.010. URL: https://www.sciencedirect.com/science/article/pii/S0921883121005380.
- [3] Raïsa Roeplal, Yusong Pang, and Dingena Schott. "Effects of pellet-sinter interaction parameters on component segregation and bed porosity considering flow velocity and mixture composition: A DEM study". In: Advanced Powder Technology 35 (2024). This is an open access article under the CC BY-NC-ND license (http://creativecommons.org/licenses/by-nc-nd/4.0/), p. 104322. DOI: 10.1016/j.apt.2023.104322. URL: https://www.sciencedirect.com/science/article/pii/S0921883123003221.
- [4] P. A. Cundall and O. D. L. Strack. "A discrete numerical model for granular assemblies". In: Géotechnique 29.1 (1979), pp. 47-65. DOI: 10.1680/geot.1979.29.1.47. eprint: https://doi.org/10.1680/geot.1979.29.1.47. URL: https://doi.org/10.1680/geot.1979.29.1.47.
- [5] M. Marigo and E. Stitt. "Discrete Element Method (DEM) for Industrial Applications: Comments on Calibration and Validation for the Modelling of Cylindrical Pellets". In: KONA Powder and Particle Journal 32 (Feb. 2015), pp. 236–252. DOI: 10.14356/kona. 2015016.
- [6] Christian Richter et al. "Development of a standard calibration procedure for the DEM parameters of cohesionless bulk materials Part II: Efficient optimization-based calibration". In: Powder Technology 360 (2020), pp. 967–976. ISSN: 0032-5910. DOI: https://doi.org/10.1016/j.powtec.2019.10.052. URL: https://www.sciencedirect.com/science/article/pii/S0032591019308757.
- [7] Chengzhi Li et al. "The angle of repose and size segregation of iron ore granules: DEM analysis and experimental investigation". In: *Powder Technology* 320 (2017), pp. 257–272.
- [8] Shiyu Wei et al. "Numerical analysis of the relationship between friction coefficient and repose angle of blast furnace raw materials by discrete element method". In: *Materials* 15.3 (2022), p. 903.

- [9] M. J. Chegeni M. Asghari M. Noaparast. "Implementation of DEM to calibrate contact parameters, as a novel simulation of the elastoplastic behavior of green iron pellet classified by roller screen". In: Advanced Powder Technology (2024). DOI: 10.1016/j.apt.2023.12.015. URL: https://www.sciencedirect.com/science/article/pii/S092188312400133X.
- [10] G. Degrassi et al. "Discrete element simulation of the charge in the hopper of a blast furnace, calibrating the parameters through an optimization algorithm". In: SN Applied Sciences (2021). DOI: 10.1007/s42452-021-04254-8. URL: https://link.springer.com/content/pdf/10.1007/s42452-021-04254-8.pdf.
- [11] H. Wei et al. "Measurement and simulation validation of DEM parameters of pellet, sinter, and coke particles". In: *Powder Technology* (2020). URL: https://research.abo.fi/files/27280795/Measurement_and_simulation_validation_of_DEM_parameters_of_pellet_sinter_and_coke_particles.pdf.
- [12] H.P. Zhu et al. "Discrete particle simulation of particulate systems: Theoretical developments". In: Chemical Engineering Science 62.13 (2007). Frontier of Chemical Engineering Multi-scale Bridge between Reductionism and Holism, pp. 3378–3396. ISSN: 0009-2509. DOI: https://doi.org/10.1016/j.ces.2006.12.089. URL: https://www.sciencedirect.com/science/article/pii/S000925090700262X.
- [13] Jun Ai et al. "Assessment of rolling resistance models in discrete element simulations". In: Powder Technology 206.3 (2011), pp. 269-282. ISSN: 0032-5910. DOI: https://doi.org/10.1016/j. powtec.2010.09.030. URL: https://www. sciencedirect.com/science/article/ pii/S0032591010005164.
- [14] Delft High Performance Computing Centre (DHPC). DelftBlue Supercomputer (Phase 2). https://www.tudelft.nl/dhpc/ark:/44463/DelftBluePhase2.2024.
- [15] Raïsa Roeplal, Yusong Pang, and Dingena Schott. "Towards Realistic DEM Modeling of Blast Furnace Mixture Charging: Calibration and Verification of Model Parameters under High-Velocity Flow Conditions". In: Powder Technology (2025). Under review.
- [16] Stephen J. Roskilly et al. "Investigating the effect of shape on particle segregation using a Monte Carlo simulation". In: Powder Technology 203.2 (2010), pp. 211-222. ISSN: 0032-5910. DOI: https: //doi.org/10.1016/j.powtec. 2010.05.011. URL: https://www.sciencedirect.com/science/article/ pii/S0032591010002494.
- [17] Vasileios Angelidakis, Sadegh Nadimi, and Stefano Utili. "Elongation, flatness and compactness indices

- to characterise particle form". In: Powder Technology 396 (2022), pp. 689-695. ISSN: 0032-5910. DOI: https://doi.org/10.1016/j.powtec.2021.11.027. URL: https://www.sciencedirect.com/science/article/pii/S0032591021009785.
- [18] Aman Tripathi et al. "Quantitative DEM simulation of pellet and sinter particles using rolling friction estimated from image analysis". In: Powder Technology 380 (2021), pp. 288-302. ISSN: 0032-5910. DOI: https://doi.org/10.1016/j.powtec.2020.11.024. URL: https://www.sciencedirect.com/science/article/pii/S0032591020310779.
- [19] Han Wei et al. "Measurement and simulation validation of DEM parameters of pellet, sinter and coke particles". In: Powder Technology 364 (2020), pp. 593-603. ISSN: 0032-5910. DOI: https://doi.org/10.1016/j.powtec.2020.01.044. URL: https://www.sciencedirect.com/science/article/pii/S0032591020300565.
- [20] Huy Q. Do, Alejandro M. Aragón, and Dingena L. Schott. "A calibration framework for discrete element model parameters using genetic algorithms". In: Advanced Powder Technology 29.6 (2018), pp. 1393–1403. ISSN: 0921-8831. DOI: https://doi.org/10.1016/j.apt.2018.03.001. URL: https://www.sciencedirect.com/science/article/pii/S0921883118300773.
- [21] D. Wang, D. Tan, and L. Liu. "Particle swarm optimization algorithm: an overview". In: *Soft Computing* 22.2 (2018), pp. 387–408. DOI: 10.1007/s00500-016-2474-6. URL: https://doi.org/10.1007/s00500-016-2474-6.

B

System Inputs

B.1. Sinter particle shape in EDEM

Smoothing Value	Min Radius	Time +3	M Left	M Scale	M Right	Pixels Heap	Peak X	Peak Y
10	0.15	6.765	72.5987	47.2408	28.8565	198361.75	511.25	95.75
10	0.3	6.715	71.2548	47.0456	30.5639	195065.75	497.25	84.75
7	0.15	6.7125	73.8400	46.7034	30.3710	193557.00	514.75	98.75
7	0.3	6.6875	74.5675	46.9284	29.4545	195121.75	538.50	92.75
5	0.15	6.765	71.6496	47.0496	27.8292	196347.75	524.00	87.50
5	0.3	6.6075	72.4461	46.2757	27.7051	191228.75	523.25	99.75

Table B.1: Parameters and KPI Values.

KPI	P-value (Smoothing)	P-value (Min Radius)
Left	0.35184	0.35812
Right	0.41427	0.45432
Scale	0.82859	0.48567
Χ	0.54321	0.77542
Υ	0.73277	0.86637
Time	0.80006	0.63582
Pixel	0.90712	0.63865

Table B.2: ANOVA Results for Smoothing and Minimum Radius Effects on KPIs. As can be seen in this table no value is below 0.05, meaning neither the smoothing value and the minimum radius have an significant effect on the KPIs.

Simulation	Real Time (s)
10_0.15	23594.4
10_0.3	13276.2
7_0.15	25765.99
7_0.3	12779.89
5_0.15	42145.29
5_0.3	23936.49

Table B.3: Simulation and Real Time Data



Results Plackett-Burmann

C.1. Levels of PB and resulting KPIs

Sim #	Срр	Spp	Rpp	Cpg	Spg	Rpg	Time	Pixel	X	у	M left	M	М
												right	scale
Sim1	0.9	0.9	0.9	0.0001	0	0.9	6.21	247157	1012.3	415.0	71.25	61.65	42.72
Sim2	0.0001	0.9	0.9	0.9	0.9	0	9.54	341332	1055.8	272.3	63.04	50.93	55.81
Sim3	0.0001	0.9	0	0.9	0	0.9	5.10	149617	1292.8	566.8	67.25	81.29	25.39
Sim4	0.9	0	0	0.9	0.9	0.9	8.96	43414	841.0	718.8	56.15	55.44	6.72
Sim5	0.0001	0	0.9	0.0001	0.9	0.9	7.79	148799	1264.0	589.5	77.32	71.01	27.74
Sim6	0.9	0.9	0	0.0001	0.9	0	7.15	180789	1002.8	542.8	75.10	69.91	30.20
Sim7	0.9	0	0.9	0.9	0	0	5.31	22104	963.0	746.3	56.00	75.14	3.81
Sim8	0.0001	0	0	0.0001	0	0	4.56	97332	1258.3	660.3	80.27	76.60	18.49

Table C.1: Simulation parameters with corresponding KPIs.

C.2. Pareto Plots for the KPIs

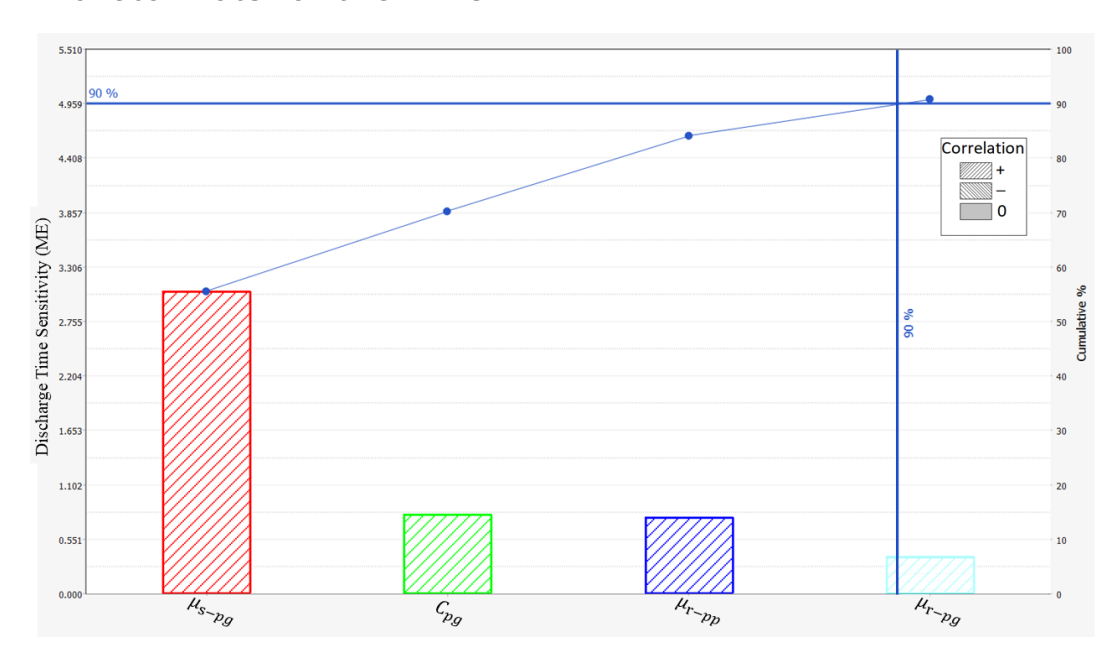


Figure C.1: Pareto plot of KPI 1, the discharge time.

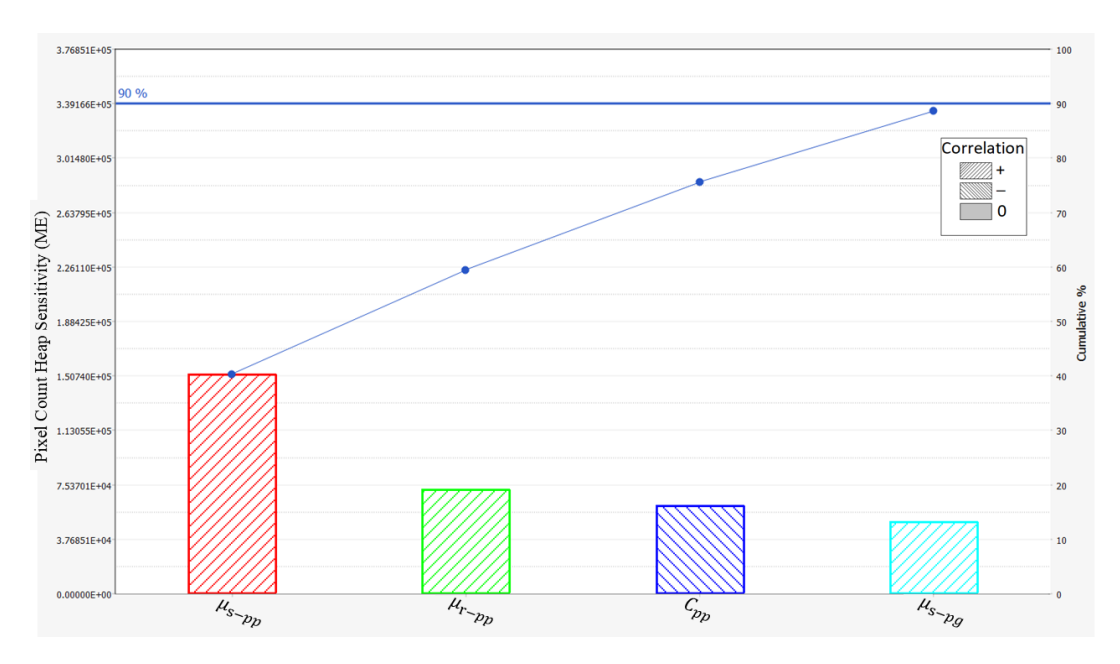


Figure C.2: Pareto plot of KPI 2, the pixel count of the heap.

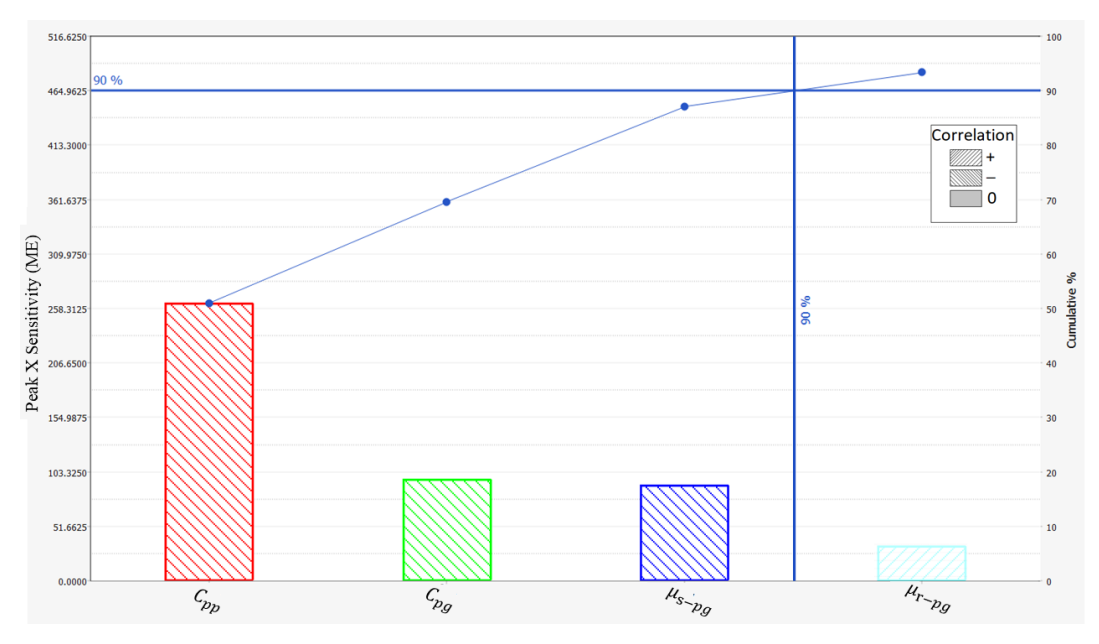


Figure C.3: Pareto plot of KPI 3, the x-coordinate of the highest point of the heap.

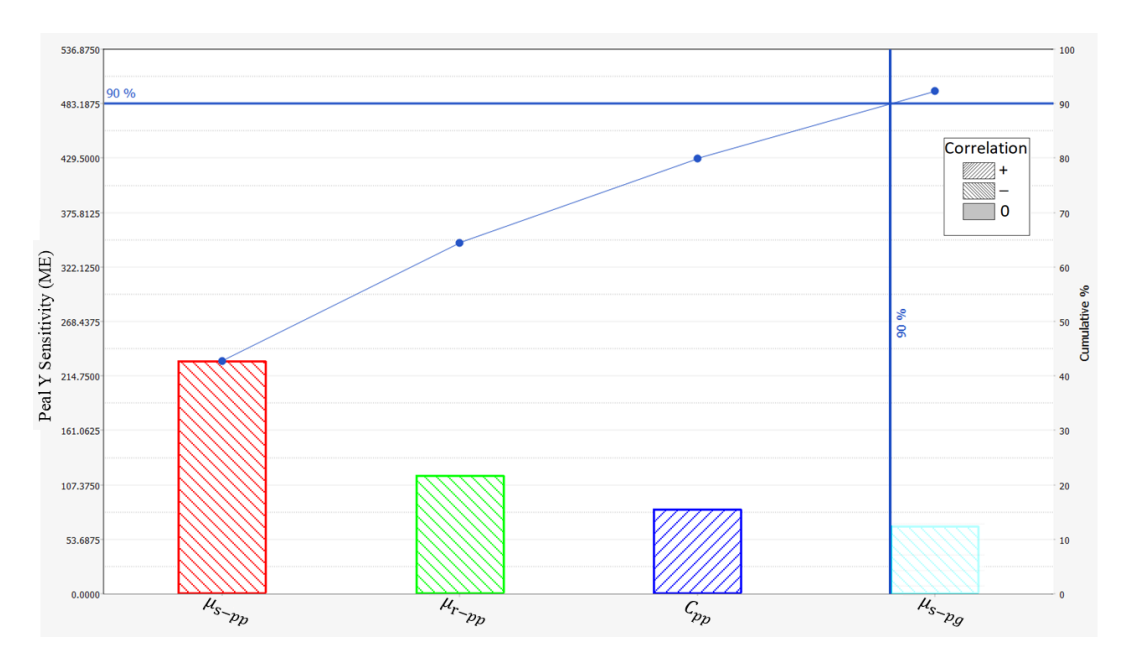


Figure C.4: Pareto plot of KPI 4, the y-coordinate of the highest point of the heap.

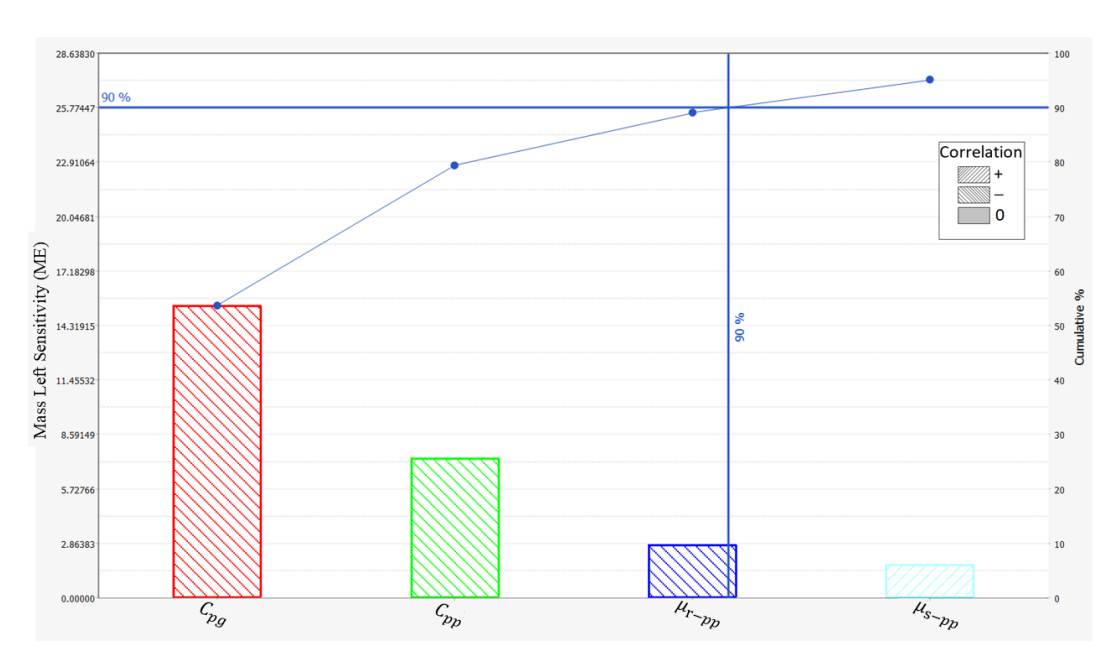


Figure C.5: Pareto plot of KPI 5, the mass of the material at the left side of the container.

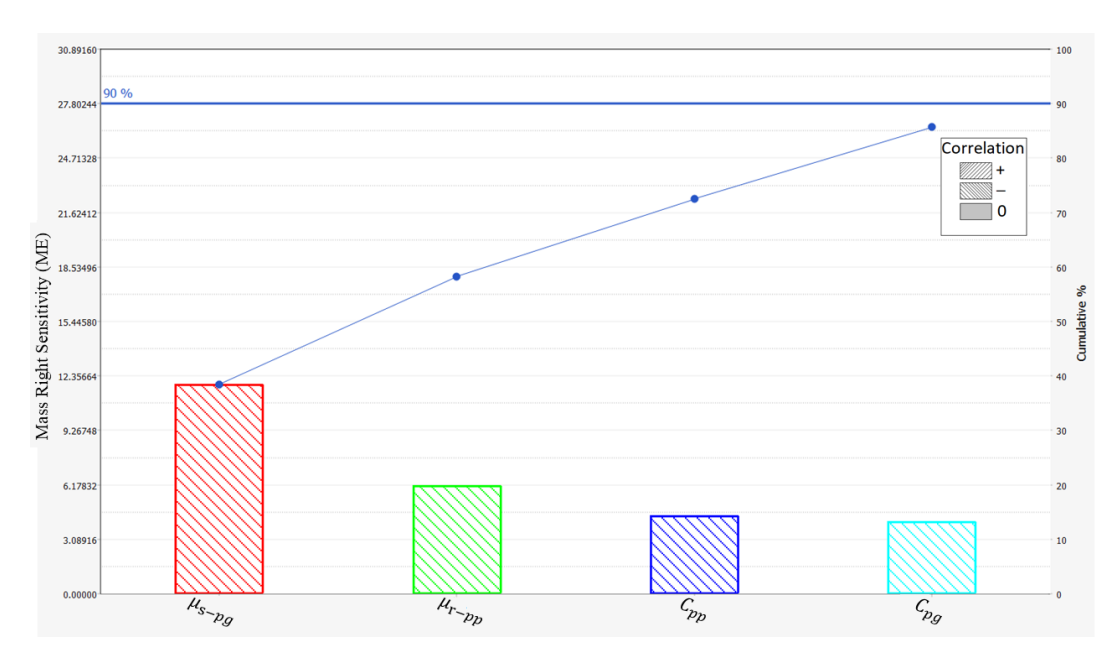


Figure C.6: Pareto plot of KPI 6, the mass of the material at the right side of the container.

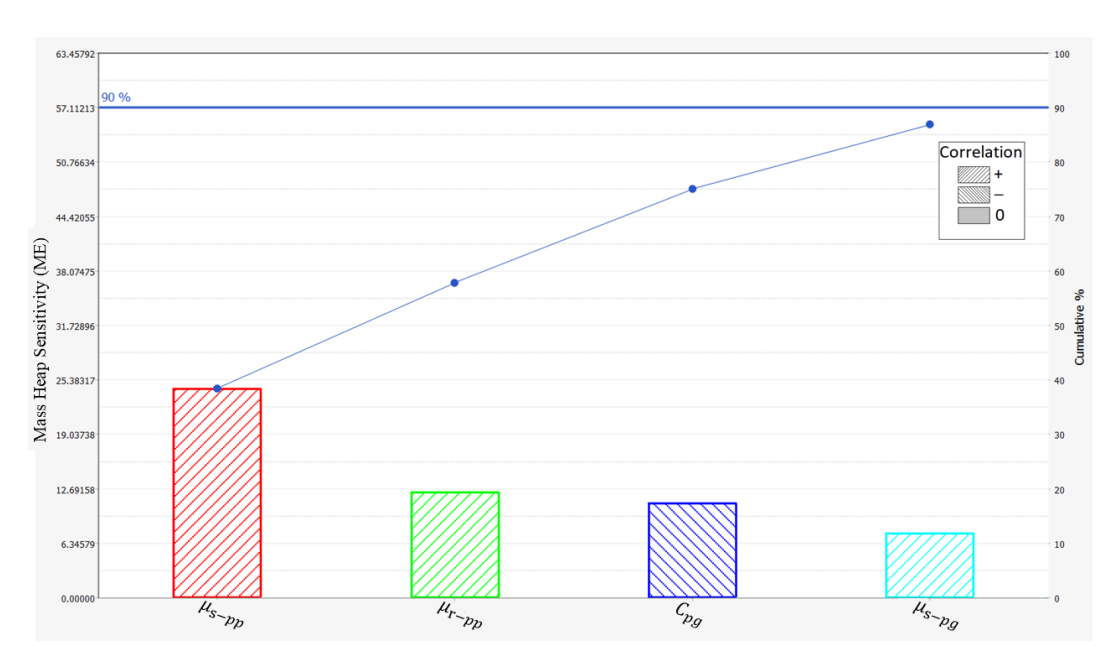


Figure C.7: Pareto plot of KPI 7, the mass of the material on the scale.



MATLAB Codes

D.1. Local Optimization and polynomial regression

```
clc; clear; close all;
4 filename = 'KPIs_pellet.xlsx';
parameters = readmatrix(filename, 'Sheet', 'CCDparameters');
responses = readmatrix(filename, 'Sheet', 'CCDkpis');
parameters(any(isnan(parameters), 2), :) = [];
responses(any(isnan(responses), 2), :) = [];
11
12 [num_samples, num_params] = size(parameters);
13 [~, num_responses] = size(responses);
14
poly_degree = 2;
16
models = cell(1, num_responses);
18 for i = 1:num_responses
      X_poly = parameters;
19
20
      if poly_degree >= 2
           X_{poly} = [X_{poly}, parameters.^2];
22
      end
23
      for j = 1:num_params
           for k = j+1:num_params
24
25
               X_poly = [X_poly, parameters(:, j) .* parameters(:, k)];
26
27
      end
28
      models{i} = fitlm(X_poly, responses(:, i));
29 end
30
31 target_kpi = [82.4, 77.53, 58.23, 52.1, 31, 34.7, 32.8, 35.3];
| 1b = [0.0001, 0, 0, 0.0001, 0];
ub = [0.9, 0.9, 0.9, 0.9, 0.9];
35
36 init_values = [0.80, 0.50, 0.80, 0.10, 0.80];
38 options = optimoptions('fmincon', 'Display', 'off', 'Algorithm', 'sqp');
40 optimal_params = fmincon(@(x) compute_kpi_error(x, models, num_params, poly_degree,
      target_kpi), ...
                             init_values, [], [], [], lb, ub, [], options);
41
42
43
44 X_poly_best = optimal_params;
45 if poly_degree >= 2
X_poly_best = [X_poly_best, optimal_params.^2];
```

D.2. PSO and GA

```
47 end
48 for j = 1:num_params
      for k = j+1:num_params
49
          X_poly_best = [X_poly_best, optimal_params(j) * optimal_params(k)];
51
52 end
53
predicted_kpis = zeros(1, length(models));
55 for i = 1:length(models)
56
      predicted_kpis(i) = predict(models{i}, X_poly_best);
57 end
58
59 fprintf('Best Optimized Parameters: p1=%.4f, p2=%.4f, p3=%.4f, p4=%.4f, p5=%.4f\n',
      optimal_params);
60 fprintf('Predicted KPIs: ');
fprintf('%.4f', predicted_kpis);
62 fprintf('\n');
63
64 %% Function to compute KPI error
function error = compute_kpi_error(x, models, num_params, poly_degree, target_kpi)
      X_poly = x;
66
      if poly_degree >= 2
67
          X_poly = [X_poly, x.^2];
      end
69
70
      for j = 1:num_params
          for k = j+1:num_params
71
72
              X_{poly} = [X_{poly}, x(j) * x(k)];
73
      end
74
75
76
      predicted_kpi = zeros(1, length(models));
      for i = 1:length(models)
77
78
          predicted_kpi(i) = predict(models{i}, X_poly);
79
80
      error = sum(((target_kpi - predicted_kpi).^2) ./ target_kpi);
81
  end
82
```

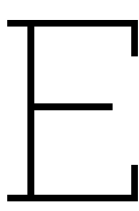
D.2. PSO and GA

```
num_runs = 15;
results_ga = zeros(num_runs, num_params + 1);
results_pso = zeros(num_runs, num_params + 1);
5 target_kpi = [82.4, 77.53, 58.23, 52.1, 31, 34.7, 32.8, 35.3];
7 | 1b = [0.0001, 0, 0, 0.0001, 0];
8 \text{ ub} = [0.9, 0.9, 0.9, 0.9, 0.9];
10 for run = 1:num_runs
      fprintf('Run %d:\n', run);
11
12
      opts = optimoptions('ga', 'Display', 'off', 'MaxGenerations', 500, 'PopulationSize',
13
          5000);
      [optimal_ga, error_ga] = ga(@(x) compute_error(x, models, target_kpi, poly_degree),
    num_params, [], [], [], lb, ub, [], opts);
14
      results_ga(run, :) = [optimal_ga, error_ga];
15
16
      opts_pso = optimoptions('particleswarm', 'Display', 'off', 'SwarmSize', 50, '
17
           MaxIterations', 100):
       [optimal_pso, error_pso] = particleswarm(@(x) compute_error(x, models, target_kpi,
           poly_degree), num_params, lb, ub, opts_pso);
      results_pso(run, :) = [optimal_pso, error_pso];
19
20 end
21
22 fprintf('\nComparison of GA Results:\n');
23 disp(array2table(results_ga, 'VariableNames', [arrayfun(@(x) sprintf('Param_%d', x), 1:
      num_params, 'UniformOutput', false), {'Objective'}]));
25 fprintf('\nComparison of PSO Results:\n');
```

```
clear:
2 close all;
3 clc;
5 % Prompt user for direction input
6 prompt = 'Which direction? Enter 1 for Horizontal, 2 for Vertical, or 3 for cubic: ';
7 userInput = input(prompt);
9 if userInput == 1
10
     Direction = 'Horizontal';
11 elseif userInput == 2
     Direction = 'Vertical';
12
  elseif userInput == 3
     Direction = 'Cubic';
14
15 else
      error('Invalid input. Please enter 1 for Horizontal, 2 for Vertical, or 3 for cubic.');
16
17 end
19 % Specify the base folder where images are stored
20 Source_folder = 'C:\Users\LocalAdmin\Desktop\Calibration\Mixture\Mixture_v4\';
22 % List of repetition folders
23 repFolders = {'Rep1', 'Rep2', 'Rep3', 'Rep4'};
27 %****
28 %%%% Create output folder %%%%%
 Results_folder = fullfile(Source_folder, 'Results');
outputFolder = fullfile(Results_folder, ['Segregation_', Direction]);
31 if ~exist(outputFolder, 'dir')
32
     mkdir(outputFolder);
33 end
35 % Initialize output text file
outputFile = 'Pixel_ratio_pellets.txt';
37 fid = fopen(fullfile(outputFolder, outputFile), 'w');
39 % Define fixed width and precision for the output file
40 width = 10;
41 precision = 3;
42
43 % Define the number of sub-figures in horizontal and vertical directions
44 if strcmp(Direction, 'Horizontal')
      numHorizontalSubfigures = 6;
     numVerticalSubfigures = 1;
46
     \% fprintf(fid, '%-20s\t%-*s\n', 'Folder Name', width, 'RSD');
47
  elseif strcmp(Direction, 'Vertical')
48
     numHorizontalSubfigures = 1;
49
50
      numVerticalSubfigures = 3;
     % fprintf(fid, '%-20s\t%-*s\t%-*s\n', 'Folder Name', width, 'RSD');
51
52
      numHorizontalSubfigures = 6;
54
      numVerticalSubfigures = 3;
      % fprintf(fid, '%-20s\t%-*s\t%-*s\n', 'Folder Name', width, 'RSD');
55
56 end
57
fprintf(fid, '%-20s\t%-*s\n', 'Folder Name', width, 'RSD');
60 % Process each repetition folder
for repIdx = 1:numel(repFolders)
repFolder = repFolders{repIdx};
```

```
imagePath = fullfile(Source_folder, repFolder, 'HeapEdited_RGB.png');
63
64
      % Check if the .png image exists in the folder
65
      if ~isfile(imagePath)
          fprintf('Image not found in %s, skipping.\n', repFolder);
67
68
           continue; % Skip this folder if the file doesn't exist
69
70
71
      % Read the image
      MixRGB = imread(imagePath);
72
73
75 % If image has 4 channels (RGBA), strip alpha
      if size(MixRGB, 3) == 4
76
          MixRGB = MixRGB(:, :, 1:3);
77
78
79
80
      imshow(MixRGB);
81
82
      MixRGB = imread(imagePath);
83
84
85 if isempty (MixRGB)
      error('Image could not be read or is empty: %s', imagePath);
86
87
  end
88
89 disp(['Trying to read: ', imagePath]);
      91
92
93
       [PelletBW, PelletM] = Mask_Pellet_v2(MixRGB);
      imwrite(PelletBW, fullfile(outputFolder, strcat("Pellet_BW_", repFolder, '.png')));
94
95
      96
      [SinterBW, SinterM] = Mask_Sinter_v2(MixRGB);
97
      imwrite(SinterBW, fullfile(outputFolder, strcat("Sinter_BW_", repFolder, '.png')));
98
99
      100
      101
                                              *************
102
      \mbox{\ensuremath{\mbox{\%}}} Get the size of the binary image
103
       [Height, Width] = size(SinterBW);
104
105
106
      % Calculate the size of each sub-figure
      subfigureHeight = floor(Height / numVerticalSubfigures);
107
      subfigureWidth = floor(Width / numHorizontalSubfigures);
108
      % Initialize an array to store the counts
110
      counts_sinter = zeros(numVerticalSubfigures, numHorizontalSubfigures);
111
112
      % Initialize figure
113
      figure('visible', 'off');
114
115
      % Loop through each sub-figure
116
      for i = 1:numVerticalSubfigures
          for j = 1:numHorizontalSubfigures
118
119
               \mbox{\ensuremath{\mbox{\%}}} Define the coordinates of the sub-figure
               startY = (i - 1) * subfigureHeight + 1;
120
              endY = min(i * subfigureHeight, Height);
startX = (j - 1) * subfigureWidth + 1;
121
122
               endX = min(j * subfigureWidth, Width);
123
124
               % Extract the sub-image
125
               subImage = SinterBW(startY:endY, startX:endX);
126
127
               % Plot the sub-image in a subplot
128
               {\tt subplot} ({\tt numVerticalSubfigures} \ , \ {\tt numHorizontalSubfigures} \ , \ (i\mbox{-}1) \ *
129
                   numHorizontalSubfigures + j);
               imshow(subImage);
130
131
              \% Count the number of true pixels in the sub-image
```

```
counts_sinter(i, j) = sum(subImage(:));
133
                     end
134
135
             end
136
             % Save the figure
137
138
              saveas(gcf, fullfile(outputFolder, strcat('subfigures_sinter_', repFolder, '.jpg')));
139
             140
             141
142
             \mbox{\ensuremath{\mbox{\ensuremath{\mbox{\ensuremath{\mbox{\ensuremath{\mbox{\ensuremath{\mbox{\ensuremath{\mbox{\ensuremath{\mbox{\ensuremath{\mbox{\ensuremath{\mbox{\ensuremath{\mbox{\ensuremath{\mbox{\ensuremath{\mbox{\ensuremath{\mbox{\ensuremath{\mbox{\ensuremath{\mbox{\ensuremath{\mbox{\ensuremath{\mbox{\ensuremath{\mbox{\ensuremath{\mbox{\ensuremath{\mbox{\ensuremath{\mbox{\ensuremath{\mbox{\ensuremath{\mbox{\ensuremath{\mbox{\ensuremath{\mbox{\ensuremath{\mbox{\ensuremath{\mbox{\ensuremath{\mbox{\ensuremath{\mbox{\ensuremath{\mbox{\ensuremath{\mbox{\ensuremath{\mbox{\ensuremath{\mbox{\ensuremath{\mbox{\ensuremath{\mbox{\ensuremath{\mbox{\ensuremath{\mbox{\ensuremath{\mbox{\ensuremath{\mbox{\ensuremath{\mbox{\ensuremath{\mbox{\ensuremath{\mbox{\ensuremath{\mbox{\ensuremath{\mbox{\ensuremath{\mbox{\ensuremath{\mbox{\ensuremath{\mbox{\ensuremath{\mbox{\ensuremath{\mbox{\ensuremath{\mbox{\ensuremath{\mbox{\ensuremath{\mbox{\ensuremath{\mbox{\ensuremath{\mbox{\ensuremath{\mbox{\ensuremath}\ensuremath}\ensuremath}\ensuremath}\ensuremath}\ensuremath}\ensuremath}\ensuremath}\ensuremath}\ensuremath}\ensuremath}\ensuremath}\ensuremath}\ensuremath}\ensuremath}\ensuremath}\ensuremath}\ensuremath}\ensuremath}\ensuremath}\ensuremath}\ensuremath}\ensuremath}\ensuremath}\ensuremath}\ensuremath}\ensuremath}\ensuremath}\ensuremath}\ensuremath}\ensuremath}\ensuremath}\ensuremath}\ensuremath}\ensuremath}\ensuremath}\ensuremath}\ensuremath}\ensuremath}\ensuremath}\ensuremath}\ensuremath}\ensuremath}\ensuremath}\ensuremath}\ensuremath}\ensuremath}\ensuremath}\ensuremath}\ensuremath}\ensuremath}\ensuremath}\ensuremath}\ensuremath}\ensuremath}\ensuremath}\ensuremath}\ensuremath}\ensuremath}\ensuremath}\ensuremath}\ensuremath}\ensuremath}\ensuremath}\ensuremath}\ensuremath}\ensuremath}\ensuremath}\ensuremath}\ensuremath}\ensuremath}\ensuremath}\ensuremath}\ensuremath}\ensuremath}\ensuremath}\ensuremath}\ensuremath}\ensuremath}\ensuremath}\ensuremath}\ensuremath}\ensuremath}\ensuremath}\ensuremath}\ensuremath}\ensuremath}\ens
143
144
              [Height, Width] = size(PelletBW);
145
             % Calculate the size of each sub-figure
146
              subfigureHeight = floor(Height / numVerticalSubfigures);
147
             subfigureWidth = floor(Width / numHorizontalSubfigures);
148
149
150
             % Initialize an array to store the counts
             counts_pellet = zeros(numVerticalSubfigures, numHorizontalSubfigures);
151
             % Initialize figure
153
             figure('visible', 'off');
154
155
             % Loop through each sub-figure
156
             for i = 1:numVerticalSubfigures
157
158
                     for j = 1:numHorizontalSubfigures
159
                              \mbox{\ensuremath{\mbox{\%}}} Define the coordinates of the sub-figure
                              startY = (i - 1) * subfigureHeight + 1;
160
                              endY = min(i * subfigureHeight, Height);
161
                              startX = (j - 1) * subfigureWidth + 1;
162
163
                              endX = min(j * subfigureWidth, Width);
164
165
                              \% Extract the sub-image
                              subImage = PelletBW(startY:endY, startX:endX);
166
167
                              \mbox{\ensuremath{\mbox{\%}}} Plot the sub-image in a subplot
                              subplot(numVerticalSubfigures, numHorizontalSubfigures, (i-1) *
169
                                      numHorizontalSubfigures + j);
                              imshow(subImage);
171
                              \% Count the number of true pixels in the sub-image
172
173
                              counts_pellet(i, j) = sum(subImage(:));
                      end
174
175
             end
176
             % Save the figure
177
             saveas(gcf, fullfile(outputFolder, strcat('subfigures_pellet_', repFolder, '.png')));
178
179
ratios = nan(numVerticalSubfigures, numHorizontalSubfigures); % Initialize with NaNs
181
     for i = 1:numVerticalSubfigures
182
             for j = 1:numHorizontalSubfigures
183
                      denominator = counts_sinter(i, j) + counts_pellet(i, j);
184
                     if denominator > 0
185
                              ratios(i, j) = counts_pellet(i, j) / denominator;
                      end
187
188
             end
189 end
190
     valid_ratios = ratios(~isnan(ratios));
191
192 if ~isempty(valid_ratios)
             mean_ratios = mean(valid_ratios);
193
             std_ratios = std(valid_ratios);
194
             RSD = std_ratios / mean_ratios;
195
196
     else
             RSD = NaN;
197
     end
198
199
200
             % For Horizontal or Cubic, output RSD
201
          fprintf(fid, '%-20s\t%-*.*f\n', [repFolder, ' (RSD)'], width, precision, RSD);
```



Results CCD and RSM

(This page is left intentionally blank)

E.1. Results CCD 86

E.1. Results CCD

Run	C_{pp}	μ_{r-pp}	μ_{s-pp}	C_{pg}	μ_{s-pg}
1	0.2608693	0.260798	0.260798	0.260869	0.260798
2	0.2608693	0.260798	0.260798	0.260869	0.639202
3	0.2608693	0.260798	0.260798	0.639231	0.260798
4	0.2608693	0.260798	0.260798	0.639231	0.639202
5	0.2608693	0.260798	0.639202	0.260869	0.260798
6	0.2608693	0.260798	0.639202	0.260869	0.639202
7	0.2608693	0.260798	0.639202	0.639231	0.260798
8	0.2608693	0.260798	0.639202	0.639231	0.639202
9	0.2608693	0.639202	0.260798	0.260869	0.260798
10	0.2608693	0.639202	0.260798	0.260869	0.639202
11	0.2608693	0.639202	0.260798	0.639231	0.260798
12	0.2608693	0.639202	0.260798	0.639231	0.639202
13	0.2608693	0.639202	0.639202	0.260869	0.260798
14	0.2608693	0.639202	0.639202	0.260869	0.639202
15	0.2608693	0.639202	0.639202	0.639231	0.260798
16	0.2608693	0.639202	0.639202	0.639231	0.639202
17	0.6392307	0.260798	0.260798	0.260869	0.260798
18	0.6392307	0.260798	0.260798	0.260869	0.639202
19	0.6392307	0.260798	0.260798	0.639231	0.260798
20	0.6392307	0.260798	0.260798	0.639231	0.639202
21	0.6392307	0.260798	0.639202	0.260869	0.260798
22	0.6392307	0.260798	0.639202	0.260869	0.639202
23	0.6392307	0.260798	0.639202	0.639231	0.260798
24	0.6392307	0.260798	0.639202	0.639231	0.639202
25	0.6392307	0.639202	0.260798	0.260869	0.260798
26	0.6392307	0.639202	0.260798	0.260869	0.639202
27	0.6392307	0.639202	0.260798	0.639231	0.260798
28	0.6392307	0.639202	0.260798	0.639231	0.639202
29	0.6392307	0.639202	0.639202	0.260869	0.260798
30	0.6392307	0.639202	0.639202	0.260869	0.639202
31	0.6392307	0.639202	0.639202	0.639231	0.260798
32	0.6392307	0.639202	0.639202	0.639231	0.639202
33	0.0001	0.45	0.45	0.45005	0.45
34	0.9	0.45	0.45	0.45005	0.45
35	0.45005	0	0.45	0.45005	0.45
36	0.45005	0.9	0.45	0.45005	0.45
37	0.45005	0.45	0	0.45005	0.45
38	0.45005	0.45	0.9	0.45005	0.45
39	0.45005	0.45	0.45	0.0001	0.45
40	0.45005	0.45	0.45	0.9	0.45
41	0.45005	0.45	0.45	0.45005	0
42	0.45005	0.45	0.45	0.45005	0.9
43	0.45005	0.45	0.45	0.45005	0.45
44	0.45005	0.45	0.45	0.45005	0.45
45	0.45005	0.45	0.45	0.45005	0.45
46	0.45005	0.45	0.45	0.45005	0.45
47	0.45005	0.45	0.45	0.45005	0.45
• •	3			22000	

Table E.1: Input parameter values for CCD

E.1. Results CCD 87

Run	Time +3	M_h	M_I	M_r	HighX	HighY	0.25Y	0.5Y	0.75Y
1	6.45	36.68015	94.01253	45.6913	626	321	399.25	371	335.75
2	7.58	40.56808	86.43811	49.35311	587.5	300.5	359	327.25	317.5
3	6.45	37.13583	93.38976	45.66619	614.5	320.5	398.75	363	334.75
4	7.58	40.69089	85.30302	49.24754	608.5	305.75	357.25	321.75	327.25
5	6.89	40.92542	88.58243	46.87409	546.5	286.25	358	308	313
6	8.09	44.66442	81.70815	49.98505	482.75	253.5	324.25	266	305.25
7	6.90	41.01399	89.05329	46.1574	576.25	286.25	363	309	316.75
8	8.07	44.78455	82.06709	48.56278	476.5	257.75	333	262.75	302.25
9	6.59	40.80903	93.2345	42.34343	632.75	290.5	368.5	327	314.25
10	7.68	44.45355	87.04547	44.86426	522.5	271.25	334.5	288.75	304
11	6.62	40.96381	94.32931	40.87765	594.75	296.5	376.25	336.5	311
12	7.70	44.49632	85.77401	45.15074	524.75	277	328	289.25	298.5
13	7.43	49.84414	83.3522	43.18652	501.5	201.25	296.75	210.75	247.75
14	8.55	53.27353	75.72827	47.37756	476.75	164.25	246.5	173.25	244
15	7.47	50.24528	83.7251	42.24707	489.5	200.5	292.75	211.5	255.75
16	8.55	53.16328	75.07804	47.2197	472.25	169.5	263.75	177.75	241.25
17	6.43	35.76399	90.31018	50.28574	633	327	402.75	377.5	337.75
18	7.58	39.11967	82.33834	54.8536	525.25	316.75	370.5	341.75	343
19	6.45	35.71481	88.65436	51.58316	645.5	339.25	404.75	380.25	346.25
20	7.57	39.18475	80.61357	54.60616	529.25	322.75	365	336.75	347.75
21	6.86	40.56241	85.74752	50.05134	568.25	288.5	359.5	319.5	314.25
22	7.99	43.98508	78.96905	53.3807	443.5	264.25	328.5	276.5	314.75
23	6.85	40.68909	85.00901	50.3328	510.25	300.5	361.5	317.25	325.25
24	7.94	44.5189	77.34351	53.05047	532.5	272.75	323.75	280.25	308
25	6.59	39.10674	89.21604	48.04464	596.25	312.5	379.25	344.5	327.75
26	7.70	42.00348	80.62535	53.70718	509.25	299.75	344	305.75	325.75
27	6.59	39.10798	89.23658	47.59931	596	316.5	385.25	347.25	329.5
28	7.66	42.07947	80.14214	52.49904	529.5	299.25	351.25	313.75	324.5
29	7.28	48.894	78.50738	48.96004	464	214.75	300.5	223	269.25
30	8.43	51.9976	72.8187	51.50185	501.25	186.5	277.75	199.5	254
31	7.27	49.01394	78.52692	48.40921	500.75	227.75	304.5	235.5	276.75
32	8.29	51.59355	72.57155	50.73755	482	191.25	277.75	203.75	269
33	7.50	47.5254	86.87821	41.97218	523	237.5	309	249.75	274.75
34	7.28	37.57443	77.09311	61.19166	500.25	333.75	385.25	351.25	358.25
35	6.84	32.85769	85.74917	57.7025	635	370.5	408.25	409	379.25
36	7.76	53.17426	77.81742	45.33966	497	189.25	270	200	246
37	6.28	23.70403	80.31799	71.4959	703.25	460.5	493	500.25	469.5
38	7.82	48.0105	81.19631	47.13049	490	220.75	310	231.5	269
39	7.45	46.3087	83.61504	46.45573	502	238.5	310.25	259	291.75
40	7.47	46.56074	84.04358	44.35102	553	251.5	324.5	257.75	289
41	5.60	41.21905	75.669	59.13641	502	298.25	358.25	308.75	331.25
42	8.99	49.68634	71.34851	55.07318	466.5	218.5	285.5	225.5	282
43	7.46	46.1905	86.18969	43.95401	534.25	250.75	322.5	262	282
44	7.48	46.30918	85.85627	44.1812	508	249.25	324	264.25	285.75
45	7.49	46.63257	83.9534	45.7633	521.5	244.75	327	254	280.75
46	7.49	46.68384	84.06608	45.59198	537.75	246.25	323.75	253.75	281
47	7.46	46.53896	84.61121	45.20596	525.5	241	326	261.75	285

Table E.2: Results CCD of pellet. The input parameters are displayed in the previous table.

E.1. Results CCD 88

Run	Time +3	PeakX	PeakY	M-heap	M-left	M-right	0.25Y	0.5Y	0.75Y
1	5.723333	610.5	325	37.86236	75.60987	36.52563	395.75	387.25	334
2	6.315	579.75	297.75	40.84144	82.04778	27.10528	387	343.5	318.5
3	5.715	593.75	318.5	38.42059	77.96515	33.58133	410	369.25	328
4	6.32	575.25	299.75	41.09753	81.43499	27.18243	383.75	337.25	318
5	6.175	568	279.25	41.84885	75.33801	32.81353	355.25	307.25	304.25
6	6.98	510.75	252.75	45.18698	74.58308	30.22053	338.75	261.25	297.25
7	6.19	550.5	289	41.37694	73.8439	34.72725	357.25	310.75	313.25
8	6.995	522.25	255.25	45.17105	73.51231	31.00657	335.25	271.25	297.5
9	5.845	619.5	306.25	39.68603	78.05972	32.25304	387.5	354.75	313.25
10	6.48	567.25	276.75	42.73814	83.09411	24.15421	373.5	308.5	304.5
11	5.83	635.75	307.5	39.41071	78.6637	31.8902	383.75	358	318.25
12	6.485	580.5	281.75	42.65491	81.34524	25.73893	365.75	313.25	302
13	6.383333	515	228	46.50189	73.79153	29.70144	318.6667	253	265.6667
14	7.206667	507.3333	206.3333	48.96552	71.14055	29.87743	301.3333	217	265
15	6.3775	477	229.25	46.50213	72.80169	30.65563	311.6667	238.5	277
16	7.23	478	204.25	49.37879	71.76559	28.5404	305	216.5	265.5
17	5.72	637.75	319.25	38.07514	77.46079	34.43902	409.25	376.75	328.5
18	6.385	581.75	308.5	40.89826	80.98641	28.082	381	339.5	319
19	5.72	644.5	322	37.88226	78.65275	33.40428	402.75	390.5	328.75
20	6.34	587	306	41.03083	79.07933	29.52863	382.25	341.5	329.25
21	6.186667	530.25	286.25	42.24012	71.49637	36.22754	357.75	313.75	312.5
22	6.98	477	249.75	45.80338	74.60394	29.52386	339.75	264	303.25
23	6.16	558	283	42.43465	74.9372	32.55311	344.75	312.75	307.75
24	6.9725	517.25	257.5	45.49859	72.83626	31.32476	330.25	268.75	300.5
25	5.84	602	308.75	39.01468	79.15118	31.81379	386.25	362.5	317
26	6.466667	568.75	287	42.12993	80.98399	26.85712	377	316.25	307.25
27	5.8625	623	308.75	39.60846	79.41717	30.89963	388.25	351.25	319.5
28	9.303333	564.5	287	42.19508	80.11359	27.36886	372.25	320.25	309.5
29	6.3275	500	232	46.8388	70.91749	32.2088	335.75	239	284.5
30	7.19	483.75	215.5	49.4481	68.83597	31.65264	304.25	221.25	265.75
31	6.3375	510.5	233	46.24977	70.74005	32.92569	337	254.25	279.75
32	7.175	491.25	208.75	49.67364	71.56681	28.37448	308.5	224.25	263.75
33	6.45	540.6667	243.6667	46.20383	73.09346	30.68875	342.6667	266	277
34	6.425	530	268.5	45.03356	71.66356	32.95549	342.25	289.75	293.5
35	6.19	565	311.75	39.98262	80.19888	29.80303	396.5	350	328.75
36	6.63	514.5	217	48.90558	72.07197	29.01189	312.75	239.75	259
37	5.566667	641.25	424.75	28.45555	72.52367	48.90715	472	480.5	426.75
38	6.846667	507.6667	245.6667	44.98039	72.00209	32.95565	332	266.3333	288.3333
39	6.43	540	259.5	45.50506	74.64499	29.84353	328.5	290	290.5
40	6.4475	562	252	45.77776	75.13847	28.57529	340.5	275	285.25
41	5.1525	507	306	41.32419	56.55238	52.09474	359	319.25	332.5
42	7.255	506.5	236.5	47.93706	64.93363	36.97124	316.75	248	282.5
43	6.42	542.5	255.75	45.68792	75.03282	29.26132	349.25	285.25	288
44	6.466667	568.5	264.25	45.37045	76.33119	28.2719	348.25	280	283
45	6.455	557.5	259.25	45.39721	77.58587	27.00266	347.75	281.25	283.25
46	6.455	512.25	252.25	46.07919	75.34051	28.56153	343.25	272.25	282.25
47	6.449	545.2	257.88	45.63	76.08	28.24	347.13	279.69	283.2

 Table E.3: Results CCD of sinter. The input parameters are the same as pellet.

E.2. Polynomials

E.2. Polynomials

Pellet	Time	M heap	M left	M right	X peak	Y peak	0.25Y	0.5Y	0.75Y
Constant	43.118	14.373	87.827	71.835	93.68	47.743	54.577	63.233	48.576
P1	7.5632	12.663	-5.8712	-4.3645	-11.116	-14.337	-5.1764	-17.213	-10.073
P2	8.1241	21.6	15.838	-37.22	-36.188	-12.093	-12.053	-26.655	-13.936
P3	27.416	49.403	7.462	-55.09	-73.115	-37.819	-39.55	-56.634	-34.748
P4	2.4892	0.9383	-3.4368	7.664	-6.8941	2.7301	3.4109	-2.2578	0.26415
P5	41.381	16.175	25.734	-38.181	-17.755	-5.8483	-12.052	-17.001	-10.488
P1^2	-2.4413	-18.676	-5.5434	22.829	-5.539	17.513	9.9502	19.689	13.712
P2^2	-7.0086	-16.37	-6.5415	22.523	21.314	14.669	8.5899	21.66	11.302
P3^2	-19.169	-51.722	-11.609	61.003	36.438	44.669	38.899	51.969	39.45
P4^2	0.89253	0.5125	3.5631	-7.6893	2.3023	-2.5536	-3.0157	-1.1176	-1.044
P5^2	-7.3171	-4.3371	-47.403	50.097	-19.056	4.0519	-0.54587	3.2036	7.413
P1P2	-4.0597	-5.699	-4.412	10.115	9.3855	6.8172	8.2214	5.0347	7.0646
P1P3	-8.25	6.161	7.499	-13.245	12.223	-2.0008	-4.2635	1.1932	-5.2457
P1P4	-2.6195	-0.70387	-4.412	2.2518	10.172	3.107	-3.9147	2.4158	2.001
P1P5	-1.3532	-2.486	0.65584	0.30838	-1.6588	2.6701	0.058205	3.8124	3.6596
P2P3	22.915	33.801	-40.781	6.4996	0.26189	-40.557	-28.866	-38.251	-23.825
P2P4	-0.61121	-1.032	4.8267	-3.472	-9.3855	-0.96765	0.81486	5.1366	0.44381
P2P5	-3.623	-3.4524	-0.31973	4.3584	14.404	-2.3643	1.4695	4.1757	-0.16732
P3P4	-1.746	0.005922	3.264	-2.3457	2.8811	0.69118	1.3387	1.3824	-0.9531
P3P5	0.56754	-0.45501	6.8823	-5.7555	26.233	-10.134	4.5249	2.3425	-3.5719
P4P5	-2.7065	-0.74434	-5.0115	-1.2092	11.786	-0.66208	1.4697	-1.0622	1.055

Table E.4: Polynomial model for the pellet KPIs. P1, P2, P3, P4, and P5 stand for C_{pp} , μ_{r-pp} , μ_{s-pp} , C_{pg} , and μ_{s-pg} respectively.

Sinter	Time	M heap	M left	M right	X peak	Y peak	0.25Y	0.5Y	0.75Y
Constant	53.685	22.429	56.776	70.268	69.545	44.483	49.957	59.779	44.935
P1	-19.495	0.7622	8.9546	-9.0925	3.3208	0.9244	-0.33815	-1.4313	0.10166
P2	-18.168	7.9645	0.4826	-8.4843	2.8821	-2.5462	-10.474	-12.254	-4.9901
P3	56.422	46.138	16.714	-62.482	-28.706	-39.11	-35.892	-59.212	-36.346
P4	-21.592	2.0898	-4.7871	4.0941	-9.8772	1.7051	5.729	-6.7667	-0.66885
P5	1.9683	13.891	82.989	-96.025	-0.77411	-12.753	-0.16959	-18.368	-12.713
P1^2	2.9608	-1.931	-5.8737	7.0625	-1.029	-0.9699	5.1071	0.44799	0.43916
P2^2	1.6021	-7.731	12.68	-4.8633	1.1523	3.125	28.502	8.843	4.6983
P3^2	-8.4391	-45.885	-6.4434	52.045	18.292	38.104	-4.8322	47.629	36.139
P4^2	3.0225	-1.8188	6.54	-5.8426	6.7093	-1.1345	-3.1645	2.7325	1.7357
P5^2	-8.5831	-6.8099	-63.332	69.831	-15.144	6.52	6.7517	3.2874	11.427
P1P2	22.823	-2.3898	-4.0631	6.4337	-5.1802	2.2409	6.7517	0.85124	1.4915
P1P3	-27.349	4.4806	-7.3924	2.8688	-9.4146	-1.0768	1.9935	-0.37105	0.88034
P1P4	23.932	-0.22404	4.5746	-4.4505	15.702	-1.237	-1.7172	4.213	-1.4043
P1P5	25.195	-0.07937	-5.7769	5.7297	-7.4938	3.0703	-3.2304	0.45836	0.47291
P2P3	-19.955	19.789	-23.73	3.8517	-19.395	-22.93	-10.417	-21.41	-13.669
P2P4	25.443	0.1698	0.2651	-0.43269	-4.8746	-1.1204	0.53839	-0.41471	0.57477
P2P5	26.502	-1.7595	-7.4	9.178	8.8025	0.77112	1.1785	5.8707	-1.5641
P3P4	-24.38	-1.3991	1.7625	-0.42089	-2.1245	0.71301	-1.1641	2.4664	-0.38561
P3P5	-10.89	1.3156	-25.427	24.004	12.251	-3.3318	-1.2222	3.9502	-0.60381
P4P5	24.671	0.76048	-8.5721	6.057	2.5901	-0.0291	-0.77121	2.6847	-0.61842

Table E.5: Polynomial model for the sinter KPIs. P1, P2, P3, P4, and P5 stand for C_{pp} , μ_{r-pp} , μ_{s-pp} , C_{pg} , and μ_{s-pg} respectively.

F

Results

(This page is left intentionally blank)

Sim	run1	run2	run3	run4	Average	Stdev
1	NaN	5.72	5.72	5.73	5.723333	0.005774
2	6.33	6.31	6.3	6.32	6.315	0.01291
3	5.69	5.75	5.71	5.71	5.715	0.025166
4	6.33	NaN	6.31	NaN	6.32	0.014142
5	6.15	6.18	6.18	6.19	6.175	0.017321
6	6.98	NaN	6.96	7	6.98	0.02
7	6.18	6.17	6.21	6.2	6.19	0.018257
8	7	7	6.95	7.03	6.995	0.010257
9	5.83	, 5.85	5.88	5.82	5.845	0.033100
10	6.48	NaN	6.47	6.48	6.476667	0.020438
11		NaN		5.83		
	5.84		5.82		5.83	0.01
12	6.48	NaN	6.49	NaN	6.485	0.007071
13	6.36	6.37	NaN	6.42	6.383333	0.032146
14	7.22	7.18	NaN	7.22	7.206667	0.023094
15	6.35	6.36	6.41	6.39	6.3775	0.027538
16	7.18	7.25	7.24	7.25	7.23	0.033665
17	5.72	NaN	NaN	5.72	5.72	0
18	NaN	6.4	NaN	6.37	6.385	0.021213
19	5.71	5.74	5.72	5.71	5.72	0.014142
20	6.32	NaN	6.35	6.35	6.34	0.017321
21	6.18	6.16	NaN	6.22	6.186667	0.030551
22	NaN	6.99	6.99	6.96	6.98	0.017321
23	6.15	NaN	6.18	6.15	6.16	0.017321
24	6.99	6.98	6.96	6.96	6.9725	0.015
25	5.84	5.84	5.84	NaN	5.84	0
26	6.45	6.47	NaN	6.48	6.466667	0.015275
27	5.87	5.84	5.89	5.85	5.8625	0.022174
28	NaN	6.45	6.46	15	9.303333	4.933461
29	6.32	6.31	6.35	6.33	6.3275	0.017078
30	NaN	NaN	7.19	7.19	7.19	0
31	6.35	6.3	6.38	6.32	6.3375	0.035
32	7.16	7.14	7.22	7.18	7.175	0.034157
33	6.46	NaN	6.44	6.45	6.45	0.01
34	6.42	6.44	6.39	6.45	6.425	0.026458
35	6.19	6.19	6.19	NaN	6.19	0
36	6.63	6.64	6.65	6.6	6.63	0.021602
37	5.56	5.57	NaN	5.57	5.566667	0.005774
38	6.83	6.89	NaN	6.82	6.846667	0.037859
39	6.4	6.44	6.45	NaN	6.43	0.037033
40	6.42	6.46	6.46	6.45	6.4475	0.020430
41	5.15	5.16	5.15	5.15	5.1525	0.01693
42	7.26	7.26	7.23			0.003
				7.27	7.255	
43	6.45	NaN	6.39	NaN 6.45	6.42	0.042426
44	6.43	NaN	6.52	6.45	6.466667	0.047258
45	6.44	6.43	6.47	6.48	6.455	0.023805
46	6.46	6.45	NaN	NaN	6.455	0.007071
47	6.45	6.43	6.47	NaN	6.449	0.0185

Table F.1: Discharge time of sinter for the CCD. As can be seen in the last column the standard deviation is always very small, even though some simulations have one or two runs excluded.



Optimization results

G.1. Sensitivity of the Local Optimization

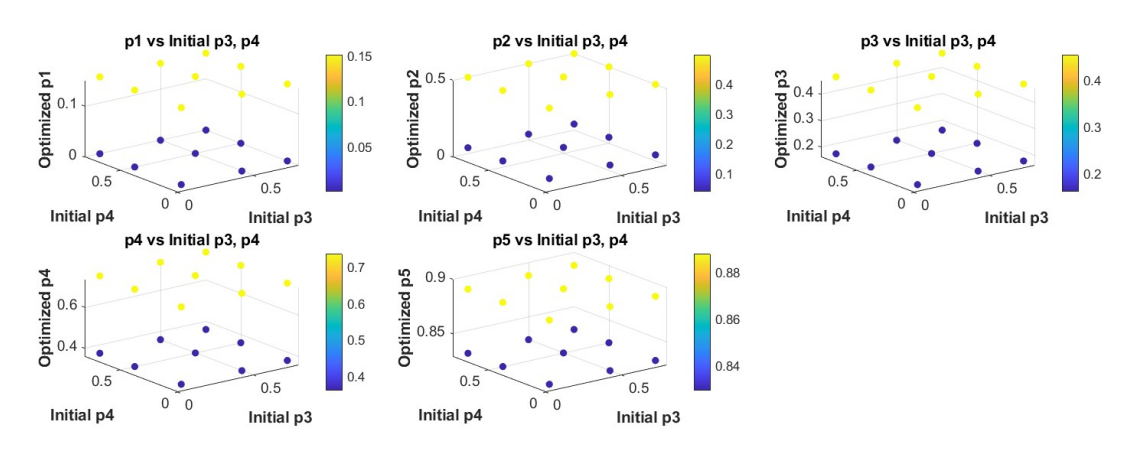


Figure G.1: Pellet parameter value, local optimization sensitivity to initial guess

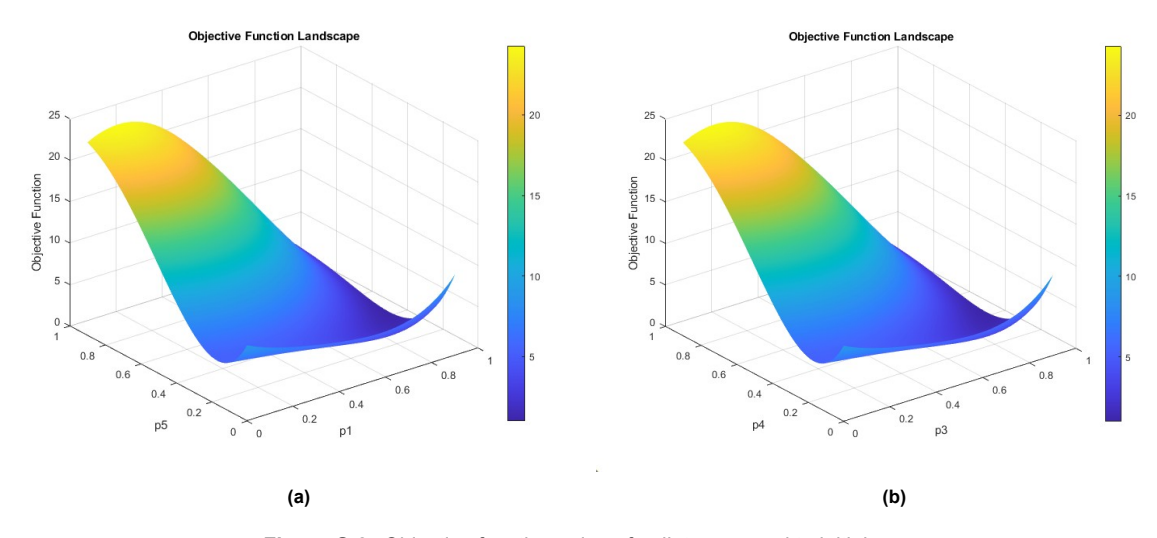


Figure G.2: Objective function value of pellet compared to initial guess

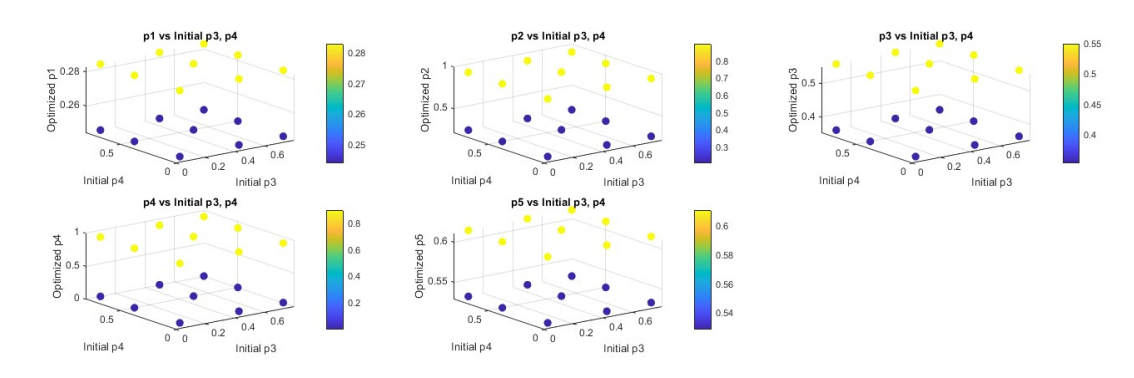


Figure G.3: Sinter parameter value, Local optimization sensitivity to initial guess

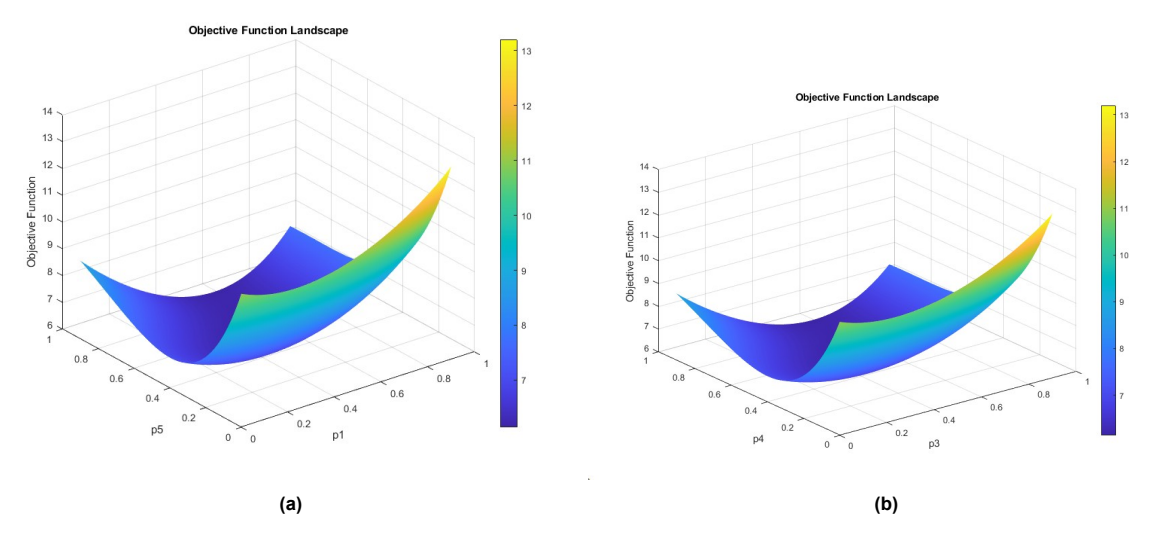


Figure G.4: Objective function value of sinter compared to initial guess

P1, P2, P3, P4, and P5 stand for $C_{pp},$ $\mu_{r-pp},$ $\mu_{s-pp},$ $C_{pg},$ and μ_{s-pg} respectively.

G.2. Results of PSO and GA: 5 smallest errors

Pellet	Error PSO	C_{pp}	μ_{r-pp}	μ_{s-pp}	C_{pg}	μ_{s-pg}
	0.0024213	0.070531	0.044578	0.46515	0.32915	0.83015
	0.0024213	0.068667	0.045248	0.46405	0.32898	0.83046
	0.0024214	0.067873	0.045663	0.46370	0.32911	0.83060
	0.0024214	0.073298	0.043637	0.46668	0.32911	0.83007
	0.0024215	0.072926	0.043858	0.46619	0.33083	0.83005
	'					
Pellet	Error GA	C_{pp}	μ_{r-pp}	μ_{s-pp}	C_{pg}	μ_{s-pg}
	0.0024215	0.075956	0.043131	0.46557	0.32932	0.83027
	0.0024213	0.071766	0.044308	0.46486	0.32899	0.83035
	0.0024225	0.066011	0.047165	0.45853	0.32860	0.83075
	0.0024237	0.052827	0.051262	0.45778	0.32878	0.83120
	0.0024286	0.104550	0.033843	0.48023	0.33575	0.82926
Sinter	Error PSO	C_{pp}	μ_{r-pp}	μ_{s-pp}	C_{pg}	μ_{s-pg}
Sinter	Error PSO 0.07769	C _{pp} 0.24333	μ_{r-pp} 0.9	$\frac{\mu_{s-pp}}{$ 0.35487	C _{pg} 0.9	$\frac{\mu_{s-pg}}{0.51373}$
Sinter						
Sinter	0.07769	0.24333	0.9	0.35487	0.9	0.51373
Sinter	0.07769 0.07769	0.24333 0.24326	0.9 0.9	0.35487 0.35486	0.9 0.9	0.51373 0.51374
Sinter	0.07769 0.07769 0.07769	0.24333 0.24326 0.24327	0.9 0.9 0.9	0.35487 0.35486 0.35486	0.9 0.9 0.9	0.51373 0.51374 0.51376
	0.07769 0.07769 0.07769 0.07769	0.24333 0.24326 0.24327 0.24337 0.24333	0.9 0.9 0.9 0.9	0.35487 0.35486 0.35486 0.35488	0.9 0.9 0.9 0.9 0.9	0.51373 0.51374 0.51376 0.51375
Sinter	0.07769 0.07769 0.07769 0.07769	0.24333 0.24326 0.24327 0.24337 0.24333	0.9 0.9 0.9 0.9	0.35487 0.35486 0.35486 0.35488	0.9 0.9 0.9 0.9 0.9	0.51373 0.51374 0.51376 0.51375 0.51374 μ_{s-pg}
	0.07769 0.07769 0.07769 0.07769 0.07769	0.24333 0.24326 0.24327 0.24337	0.9 0.9 0.9 0.9	0.35487 0.35486 0.35486 0.35488 0.35487	0.9 0.9 0.9 0.9	0.51373 0.51374 0.51376 0.51375 0.51374
	0.07769 0.07769 0.07769 0.07769 0.07769	$egin{array}{c} 0.24333 \ 0.24326 \ 0.24327 \ 0.24337 \ 0.24333 \ C_{pp} \ \end{array}$	0.9 0.9 0.9 0.9 0.9 μ_{r-pp}	0.35487 0.35486 0.35486 0.35488 0.35487 μ_{s-pp}	$0.9 \\ 0.9 \\ 0.9 \\ 0.9 \\ 0.9 \\ C_{pg}$	0.51373 0.51374 0.51376 0.51375 0.51374 μ_{s-pg}
	0.07769 0.07769 0.07769 0.07769 0.07769 Error GA 0.07769	0.24333 0.24326 0.24327 0.24337 0.24333 C_{pp} 0.24346	0.9 0.9 0.9 0.9 0.9 0.9	$\begin{array}{c} 0.35487 \\ 0.35486 \\ 0.35486 \\ 0.35488 \\ 0.35487 \\ \\ \mu_{s-pp} \\ 0.35488 \end{array}$	$0.9 \\ 0.9 \\ 0.9 \\ 0.9 \\ 0.9 \\ 0.9$	$\begin{array}{c} 0.51373 \\ 0.51374 \\ 0.51376 \\ 0.51375 \\ 0.51374 \\ \\ \mu_{s-pg} \\ 0.51367 \end{array}$
	0.07769 0.07769 0.07769 0.07769 0.07769 Error GA 0.07769 0.077691	0.24333 0.24326 0.24327 0.24337 0.24333 C_{pp} 0.24346 0.24413	0.9 0.9 0.9 0.9 0.9 μ_{r-pp} 0.9 0.9	$\begin{array}{c} 0.35487 \\ 0.35486 \\ 0.35486 \\ 0.35488 \\ 0.35487 \\ \\ \mu_{s-pp} \\ \\ 0.35488 \\ 0.35515 \\ \end{array}$	0.9 0.9 0.9 0.9 0.9 0.9 0.9	$\begin{array}{c} 0.51373 \\ 0.51374 \\ 0.51376 \\ 0.51375 \\ 0.51374 \\ \\ \mu_{s-pg} \\ 0.51367 \\ 0.51319 \\ \end{array}$
	0.07769 0.07769 0.07769 0.07769 0.07769 Error GA 0.07769 0.077691 0.077691	$\begin{array}{c} 0.24333 \\ 0.24326 \\ 0.24327 \\ 0.24337 \\ 0.24333 \\ \\ C_{pp} \\ 0.24346 \\ 0.24413 \\ 0.24314 \\ \end{array}$	0.9 0.9 0.9 0.9 0.9 0.9 0.9 0.9 0.9 0.9	$\begin{array}{c} 0.35487 \\ 0.35486 \\ 0.35486 \\ 0.35488 \\ 0.35487 \\ \\ \mu_{s-pp} \\ 0.35488 \\ 0.35515 \\ 0.35501 \\ \end{array}$	$egin{array}{c} 0.9 \\ 0.9 \\ 0.9 \\ 0.9 \\ 0.9 \\ \hline C_{pg} \\ 0.9 \\ 0.9 \\ 0.9 \\ \hline \end{array}$	$\begin{array}{c} 0.51373 \\ 0.51374 \\ 0.51376 \\ 0.51375 \\ 0.51374 \\ \\ \mu_{s-pg} \\ 0.51367 \\ 0.51319 \\ 0.51414 \\ \end{array}$

Table G.1: Five best results per optimizer per material and their corresponding input parameter values.



Results of optimal parameter inputs

H.1. At 4.665 m

	Exp Pellet	Sim Pellet	Dev (%)	Exp Sinter	Sim Sinter	Dev (%)
Time [s]	5.24 ± 0.34	5.21 ± 0.04	0.48	4.6191 ± 0.72	3.61 ± 0	21.85
M-heap [kg]	40.63 ± 0.52	38.52 ± 0.28	5.20	42.58 ± 0.78	47.01 ± 0.41	10.40
M-left [kg]	77.53 ± 8.08	77.23 ± 1.00	0.38	86.74 ± 3.55	76.3 ± 2.07	12.04
M-right [kg]	58.23 ± 8.2	60.59 ± 1.16	4.06	20.68 ± 3.82	26.2 ± 2.46	26.7
PeakX [px]	503 ± 46.76	486.25 ± 122.19	3.33	486.6 ± 107.72	538 ± 28.48	10.46
PeakY [px]	319 ± 8.96	328.00 ± 11.40	2.82	251.2 ± 139.27	240 ± 13.78	4.65
0.25Y [px]	354 ± 16.91	362.50 ± 8.37	2.40	345.2 ± 150.32	333 ± 13.78	3.67
0.5Y [px]	336 ± 21.7	340.25 ± 6.15	1.26	266.2 ± 72.16	269 ± 10.11	0.86
0.75Y [px]	360 ± 24.47	355.00 ± 4.31	1.39	294.4 ± 125.19	265 ± 11.02	9.99

Table H.1: Comparison of experimental and simulation KPIs. Mean values are presented with 95% confidence intervals, and deviations between experimental and simulation means are indicated.

H.2. Validation

Pellet	3m Exp	3m Sim	Dev (%)	1m Exp	1m Sim	Dev (%)
Time [s]	5.24 ± 0.34	5.21 ± 0.01	0.67	5.24 ± 0.34	5.23 ± 0.00	0.19
M-heap [kg]	42.33 ± 1.37	39.34 ± 0.47	7.07	45.53 ± 1.12	42.03 ± 0.14	7.69
M-left [kg]	76.95 ± 1.43	77.59 ± 2.02	0.83	69.35 ± 2.94	70.37 ± 0.30	1.48
M-right [kg]	57.12 ± 1.43	59.46 ± 2.00	4.10	61.52 ± 3.23	64.00 ± 0.44	4.03
PeakX [px]	416 ± 85.94	481.25 ± 101.78	15.69	447 ± 49.51	459.50 ± 50.53	2.80
PeakY [px]	301.33 ± 10.9	314.50 ± 5.44	4.37	253 ± 11.55	278.00 ± 3.67	9.88
0.25Y [px]	352 ± 6.75	357.50 ± 4.77	1.56	330.67 ± 23.25	343.00 ± 18.37	3.73
0.5Y [px]	308.33 ± 14.31	326.25 ± 3.01	5.81	263.67 ± 9.4	288.00 ± 12.86	9.23
0.75Y [px]	346 ± 6.75	349.75 ± 11.79	1.08	$\textbf{338} \pm \textbf{7.23}$	344.50 ± 13.78	1.92

Table H.2: Validation of the optimal parameter set with different heights of the hopper; experimental and simulation data of pellet

H.3. Mixture

Sinter	3m Exp	3m Sim	Dev (%)	1m Exp	1m Sim	Dev (%)
Time [s]	4.62 ± 0.72	3.59 ± 0.07	22.29	4.62 ± 0.72	3.62 ± 0.04	27.62
M-heap [kg]	43.6 ± 0.32	47.46 ± 0.56	8.86	45.84 ± 0.56	51.44 ± 0.99	10.89
M-left [kg]	76.97 ± 4.48	72.04 ± 3.02	6.4	59.5 ± 7.15	55.95 ± 2.96	6.35
M-right [kg]	29.43 ± 4.56	30.34 ± 3.12	3.1	44.66 ± 7.19	42.61 ± 3.85	4.81
PeakX [px]	477 ± 47.89	507 ± 157.51	6.4	452 ± 12.4	417 ± 37.51	7.9
PeakY [px]	243 ± 9.82	228 ± 5.17	6.3	191 ± 33.54	185 ± 7.58	12.24
0.25Y [px]	338 ± 13.82	327 ± 10.04	3.04	301 ± 14.11	286 ± 25.13	5.35
0.5Y [px]	254 ± 12.65	242 ± 15.18	4.74	190 ± 9.17	166 ± 12.91	12.63
0.75Y [px]	309 ± 15.69	$\textbf{273} \pm \textbf{7.59}$	11.6	310 ± 14.46	266 ± 22.08	14.25

Table H.3: Validation of the optimal parameter set with different heights of the hopper; experimental and simulation data of

H.3. Mixture

KPI	Exp Mixture	Sim Mixture	Dev (%)
Time [s]	4.4 ± 0.39	4.22 ± 0.08	4.17
M-heap [kg]	41.96 ± 0.52	44.92 ± 0.50	7.06
M-left [kg]	82.71 ± 4.86	74.81 ± 1.48	9.55
M-right [kg]	35.35 ± 5.09	40.12 ± 1.12	13.49
PeakX [px]	514.4 ± 29.23	492.00 ± 40.82	4.35
PeakY [px]	284.2 ± 3.09	262.00 ± 8.91	7.81
0.25Y [px]	361.6 ± 14.09	339.25 ± 12.07	6.18
0.5Y [px]	305.8 ± 10.87	282.00 ± 6.62	7.78
0.75Y [px]	330 ± 11.45	301.50 ± 9.94	8.64

Table H.4: Mean values with a 95% CI of the resulting KPIs of the simulations with the chosen DEM parameters for the mixture of sinter and pellet.

Results of Processed Heaps of the Mixture

I.1. Experimental runs

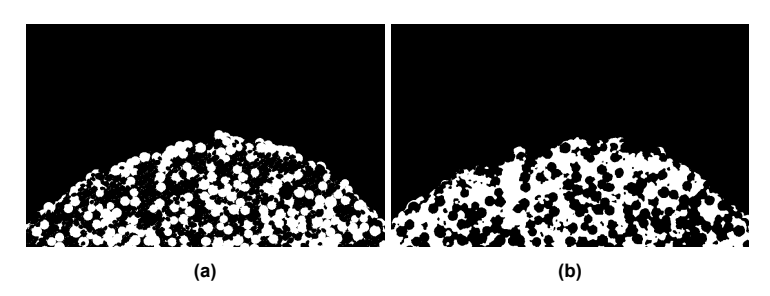


Figure I.1: Run 1, a) pellet, b) sinter.

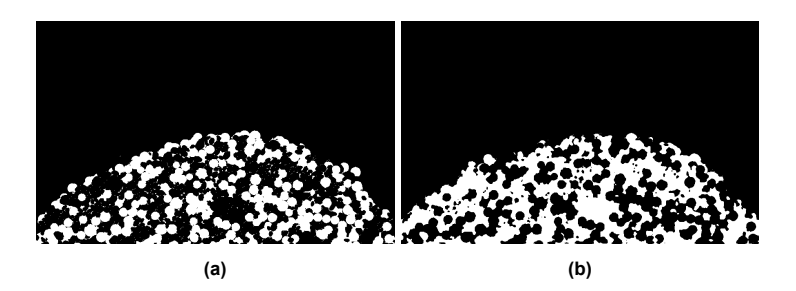


Figure I.2: Run 2, a) pellet, b) sinter.

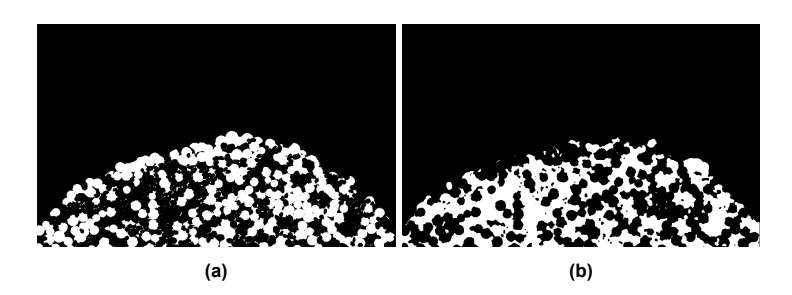


Figure I.3: Run 3, a) pellet, b) sinter.

I.2. Simulation runs

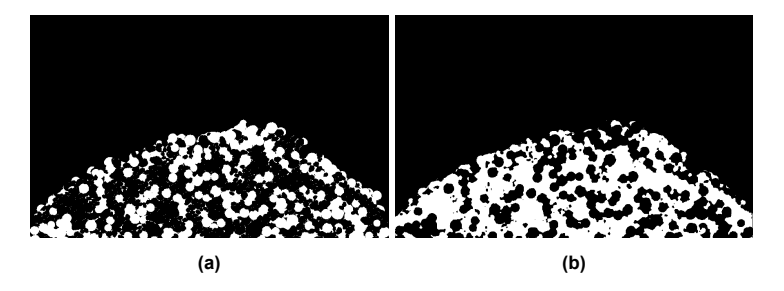


Figure I.4: Run 4, a) pellet, b) sinter.

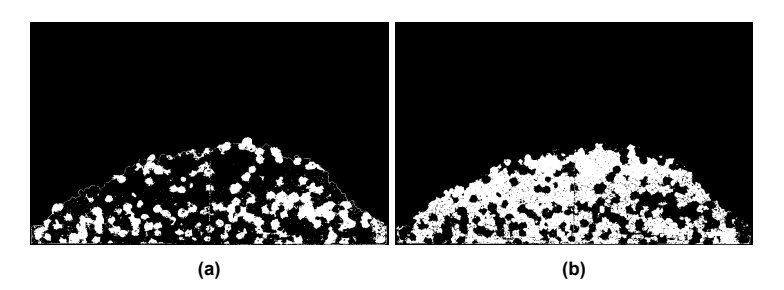


Figure I.5: Run 5, a) pellet, b) sinter.

I.2. Simulation runs

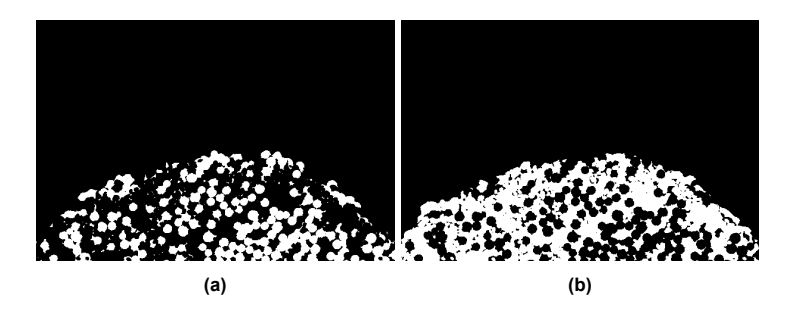


Figure I.6: Run 1, a) pellet, b) sinter.

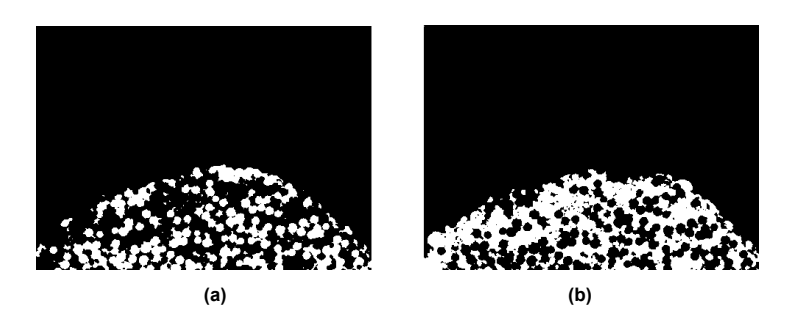


Figure I.7: Run 2, a) pellet, b) sinter.

I.2. Simulation runs

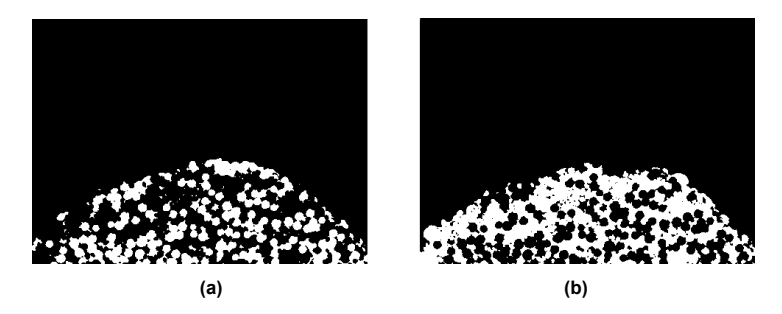


Figure I.8: Run 3, a) pellet, b) sinter.

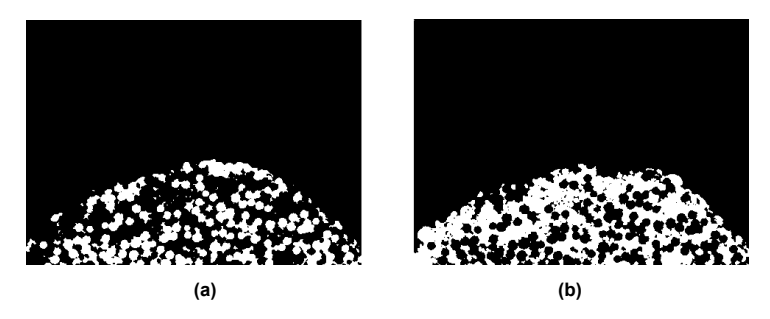


Figure I.9: Run 4, a) pellet, b) sinter.